Polyoxometalate catalysts for the selective transformation of lignocellulosic biomass: Lignin depolymerization and furan derivative valorization

Peixuan Zhang, Peng Lei, Jie Li, Weijie Geng, Yingnan Chi*, Changwen Hu

Key Laboratory of Cluster Science Ministry of Education, School of Chemistry and Chemical Engineering, Beijing Institute of Technology, Beijing 100081, China

Received: 2 February 2026; Revised: 13 March 2026; Accepted: 31 March 2026

*Address correspondence to chiyingnan7887@bit.edu.cn

Cite This: Polyoxometalates, 2026, 5, 9140130 https://doi.org/10.26599/POM.2026.9140130

Abstract: Lignocellulosic biomass, consisting of lignin, cellulose, and hemicellulose, represents a major renewable resource, and its efficient utilization is central to green and sustainable chemistry. Polyoxometalates (POMs) have emerged as versatile catalysts for biomass valorization owing to their tunable Brønsted acidity/basicity, redox properties, and unique electron/proton storage capability. This review provides a comprehensive overview of recent advances in POM-catalyzed lignocellulosic biomass conversion, with particular emphasis on lignin depolymerization and the selective conversion of hemicellulose- and cellulose-derived platform molecules, namely furfural (FF) and 5-hydroxymethylfurfural (HMF). For lignin depolymerization, the catalytic roles of different POM families are systematically discussed. For the valorization of FF and HMF, particular attention is devoted to their selective oxidative and reductive transformations. This review encompasses a broad range of POM catalysts, including classical POMs and their cation-modified derivatives, supported POM materials, and structurally novel POM architectures, and highlights how their intrinsic properties govern reaction pathways, product selectivity, and reaction mechanisms under thermal, photocatalytic, and electrocatalytic conditions. Finally, current challenges and future opportunities for biomass valorization using POM-based catalytic systems are discussed.

Keywords: polyoxometalate catalysis, lignocellulosic biomass valorization, lignin depolymerization, furfural, 5-hydroxymethylfurfural

1 Introduction

In recent years, the excessive consumption of fossil fuels has not only triggered a global energy crisis but has also disrupted the carbon balance of ecosystems, leading to severe environmental problems. In this context, there is an urgent need to develop renewable energy sources as alternatives to fossil fuels. Biomass energy represents an important class of renewable energy, owing to its abundant reserves, low cost, and wide availability. Among various forms of biomass energy, lignocellulosic biomass accounts for the largest proportion (reaching up to 75%) and holds great potential as a feedstock for the synthesis of high-value-added chemicals and liquid fuel.[1] It is primarily composed of cellulose (40-50%), hemicellulose (15-25%), and lignin (20-25%), resulting in a highly integrated and mechanically robust hierarchical structure.[2,3]

Lignin is primarily a 3D cross-linked polymer formed by the connection of phenylpropane units via C−O bonds and C−C bonds, featuring a variety of active functional groups and complex linkage patterns, including β-O-4, β-β, β-5, β-1, α-O-4, 4-O-5, and 5-5 linkages.[4-7]The selective cleavage of C–O and C–C bonds is widely recognized as an effective strategy for

lignin valorization, enabling the production of valuable aromatic compounds. Among the linkages in lignin, the β-O-4 accounts for the highest proportion (approximately 46-60%), with a bond dissociation energy of around 54-72 kcal/mol. From the perspective of bond energy, when β-O-4 bonds break, other linkages with lower dissociation energies also undergo cleavage.[5,8,9] Consequently, the cleavage of β-O-4 bonds has emerged as the key step in lignin depolymerization. Due to the structural and compositional complexity of natural lignin, model compounds are commonly employed in fundamental studies. Representative examples include 2-phenoxy-1-phenylethanol (PP-ol), 2-phenoxy-1-phenylethanone (PP-one), guaiacylglycerol-β-guaiacyl ether (GG), and veratrylglycerol-β-guaiacyl ether (VG) (Scheme 1(a)). Investigating the cleavage of these model compounds enables a deeper understanding of the cleavage pathway and catalytic mechanism, thereby providing theoretical support for the development of high-performance catalysts. To date, several strategies have been developed to promote the cleavage of C–O and/or C–C bonds in β-O-4 linkages, including pyrolysis[10-13], acid-catalyzed depolymerization[14-17], base-catalyzed depolymerization[18-20], reductive catalytic depolymerization[21-23], and oxidative catalytic depolymerization[9,24-29]. During the depolymerization of lignin, catalysts play a vital role in governing bond cleavage efficiency and product selectivity.

Cellulose and hemicellulose can be hydrolyzed into glucose and xylose, respectively, which can subsequently undergo dehydration to generate biomass-derived furfural molecules: 5-hydroxymethylfurfural (HMF) and furfural (FF). HMF is primarily produced from the dehydration of glucose derived from cellulose, whereas FF is mainly formed via the conversion of xylose from hemicellulose. While the catalytic conversion of cellulose and hemicellulose into biomass-derived furan molecules is now relatively well established,[30-35] recent research has increasingly focused on their subsequent transformation into value-added chemicals. FF and HMF contain abundant functional groups, including aldehyde groups, furan rings, and/or hydroxyl groups, which can be converted into value-added products through reduction, oxidation, ring-opening, and other reactions (Scheme 1(b)-(c)).[36-40] The resulting products find applications in fuels, pharmaceuticals, fragrances, pigments, and various other fields. Accordingly, the valorization of FF and HMF has gradually become a central aspect of biomass utilization.

Polyoxometalates (POMs) are nanoscale anionic clusters composed of multiple early transition-metal ions (such as Mo, W, V, Nb, and Ta) linked through shared oxygen atoms.[41,42] The development of POMs chemistry spans nearly two centuries. Since Berzelius first synthesized ammonium 12-molybdophosphate in 1826, a wide variety of POM structures have been discovered, including classic Keggin, Wells-Dawson, Lindqvist, Anderson, etc.[43] POMs not only possess unique Brønsted acidity/basicity and redox activity but also exhibit highly tunable compositions and electronic structures, enabling precise modulation of their catalytic properties at the atomic and molecular levels.[44-46] In addition, some Lewis acidic metal centers can be deliberately incorporated into the POM framework, allowing POMs to serve as Lewis acid catalysts.[47-49] Moreover, POMs can undergo rapid and reversible multi-electron transfer, often accompanied by proton transfer, and therefore act as electron/proton reservoirs in photocatalysis[50-53] and electrocatalysis[54-56]. These distinctive features and advantages have driven the application of POMs from conventional thermocatalysis to photocatalysis and electrocatalysis.

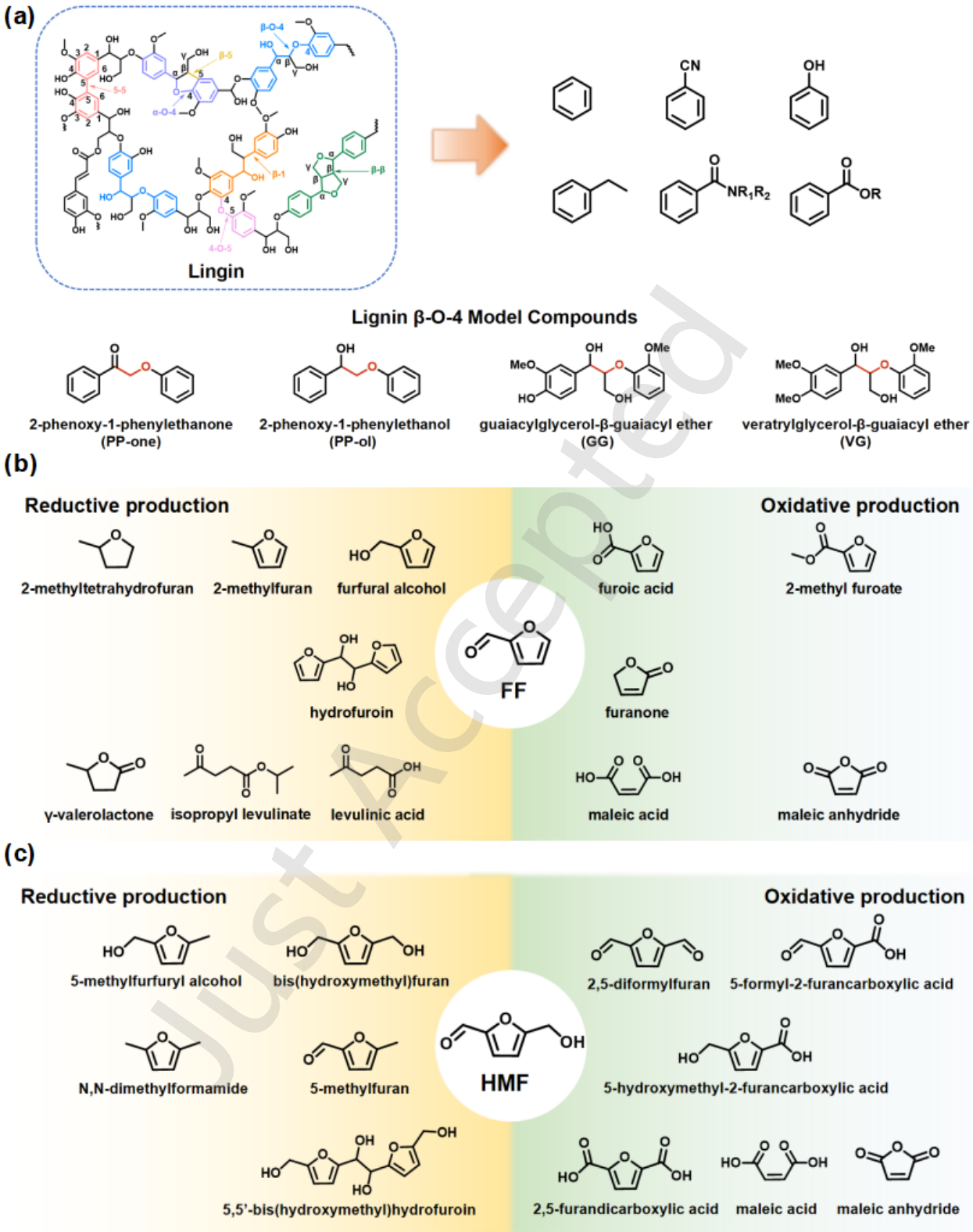

Scheme 1 (a) Partial structural schematic of lignin, its main linkages, conversion products, and commonly used lignin β-O-4 model compounds. Common reductive and oxidative production of FF (b) and HMF (c).

Recently, POM catalysts have demonstrated remarkable activity in biomass conversion by leveraging their tunable Brønsted acidity and oxidizing properties. Reported POM-based catalysts can be broadly classified into three categories: (i) classical POMs and their cation-modified derivatives; (ii) supported POM

catalysts; and (iii) structurally novel crystalline POM catalysts. Among these systems, some directly utilize the intrinsic catalytic properties of POMs, including the Brønsted acidity of Keggin-type $XM_{12}O_{40}$ (M = Mo, W; X = Si, P)[57-60], the oxidative activity of vanadium-substituted polyoxomolybdates[61-64] and polyoxovanadates[65-67], and the basicity of polyoxoniobates[68-70]. In contrast, other systems integrate POMs with additional active sites (e.g., Cu, and Co)[49,71,72], thereby cooperatively enhancing biomass conversion. Moreover, POM-catalyzed biomass valorization is undergoing a transition from thermally driven catalysis toward light- and electricity-driven catalytic systems.

In recent years, several reviews have highlighted the use of POMs in biomass conversion. In 2021, Yan and co-workers published the first comprehensive review on POM-based catalysts in biorefineries, covering diverse biomass feedstocks (e.g., lignin, husk, corn stover, beech wood, cellulose, starch, glycogen) and their derivatives (e.g., fructose, glucose, xylan, HMF, levulinic acid, glycerol).[73] They focused on the preparation of POM-based catalysts, as well as the application of POMs and metal-POM composites in the production of high-value products. The subsequent review focused specifically on lignin, summarizing studies related to its separation, depolymerization, and upgrading using POM catalysts.[74,75] In 2012, Wang *et al.* overviewed the advances in the application of polyoxometalates for the conversion of cellulose and its model compound cellobiose to platform chemicals.[76] Additionally, Wei and Liu provided a comprehensive review on POM-catalyzed synthesis of furan derivatives using biomass as the feedstock.[77] More recently, Lv and co-workers focused on POM-based photocatalytic systems[78], while Lu and Yu reviewed biomass conversion over POM@MOF composites[79]. This review provides a comprehensive overview of recent advances in POM-catalyzed lignocellulosic biomass conversion, with particular emphasis on lignin depolymerization and the selective transformation of biomass-derived platform molecules, including FF and HMF, a topic that has not yet been systematically reviewed for POM-based catalytic system. This review also summarizes the design and synthesis of POM-based catalysts, their catalytic performance, and, in particular, emphasizes the structure-activity relationships and underlying reaction mechanisms.

2 Depolymerization of Lignin

In lignin depolymerization studies, some investigations are conducted directly using natural lignin, whereas others use structurally similar model compounds, such as PP-ol and PP-one. The use of model compounds simplifies the reaction system, thereby enabling clearer elucidation of the depolymerization process and deeper understanding of the catalytic mechanisms. POMs have been extensively investigated in both model compound systems and natural lignin catalytic depolymerization, leading to a series of significant advances. To date, several reviews have summarized the research progress of POMs in lignin depolymerization,[74,75] and this review mainly focuses on the relevant research advances in the past five years. POM-catalyzed lignin depolymerization is dominated by oxidative pathways and the following sections summarize these studies according to the type of POM catalysts.

2.1 Polyoxomolybdate-Catalyzed Lignin Depolymerization

2.1.1 Thermocatalytic Depolymerization

Vanadium-substituted polyoxomolybdates are widely used to promote thermocatalytic lignin depolymerization, owing to their excellent oxidative properties and tunable Brønsted acidity. Such depolymerization reactions are generally conducted at elevated temperatures with high-pressure molecular oxygen as the oxidant. Keggin-type $H_5PMo_{10}V_2O_{40}$ and $H_5PMo_9V_3O_{40}$[80-82] are among the most commonly used clusters and their catalytic role has been well established in the previous reviews[74,75].

To enable the reuse of POM catalysts, a series of POM-based ionic liquids have been developed. Wang and co-workers chose Wells-Dawson-type $H_6V_2Mo_{18}O_{62}$ ($H_6V_2Mo_{18}$), which was subsequently modified by betaine (Bet) to yield $BetH_5V_2Mo_{18}O_{62}$ (Fig. 1(a)).[63] Interestingly, $BetH_5V_2Mo_{18}O_{62}$ functions as a homogeneous catalyst at temperatures above 80 °C and can be easily recovered by simply lowering the reaction

temperature back to room temperature. The catalyst (0.015 mmol) achieved a PP-ol conversion of 92.9%, with yields of phenol and acetophenone reaching 86.3% and 77.2%, respectively (140 °C, 0.8 MPa O_2). After 10 cycles of reuse, the conversion of pp-ol remains at 87.4%. Mechanistic investigations indicate that the catalyst donates protons and electrons to convert O_2 into HOO• active species, which selectively oxidize the *α*–OH group of PP-ol to a carbonyl group (Fig. 1(b)). Then, the catalytic activity was

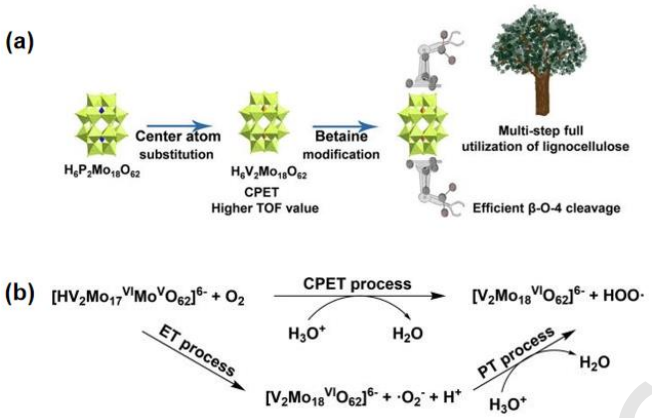

Fig. 1 (a) Application of $BetH_5V_2Mo_{18}O_{62}$ in PP-ol conversion and (b) reaction process. Adapted with permission from Ref. [63], Copyright 2022 American Chemical Society.

further improved by using $NLLH_5V_2Mo_{18}O_{62}$ (NLL = N-lauroyl-L-lysine).[83] Under the reaction conditions of 130 °C and 1.0 MPa O_2, a PP-ol conversion of 96.8% was achieved, with selectivity of 91.2% for phenol and 83.3% for acetophenone ($n_{PP\text{-}ol}$:$n_{catalyst}$ = 5:1). In Lv's group, a recoverable POM-ionic liquid catalyst was synthesized by reacting $PMo_{10}V_2$ with 1-methyl-3-(4-sulfobutyl)-1H-imidazolium zwitterions (Fig. 2).[84] Under 0.1 MPa O_2 at 130 °C for 12 h, this catalyst (0.03 mmol) achieved a 100% conversion of PP-ol, with benzaldehyde and phenol yields of 96% and 80%, respectively. After 5 cycles, the catalyst retains its structural integrity.

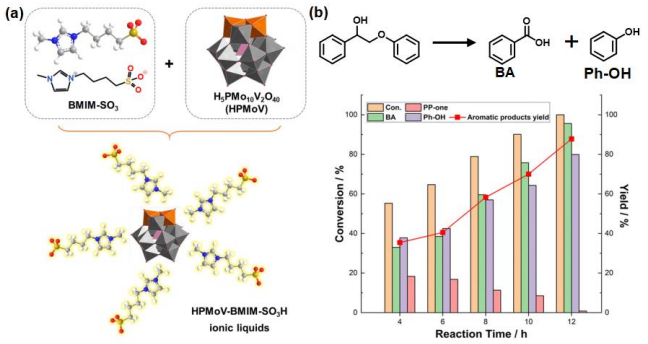

Fig. 2 (a) Assembly schematic of POM-ionic liquid. (b) Depolymerization performance of PP-ol at different time intervals. Adapted with permission from Ref. [84], Copyright 2023 The Royal Society of Chemistry.

In addition to Keggin- or Wells-Dawson-type POMs, an Anderson-type $(NH_4)_4[CuMo_6O_{24}H_6]$ was used by Hou and co-workers to catalyze the oxidative cleavage of PP-ol.[72] The catalyst (30 mg) afforded a PP-ol conversion of 95% and the primary products included phenol (yield: 89%), benzoic acid, and acetophenone. Notably, the catalyst exhibited remarkable stability, maintaining reliable performance over 10 cycles. In the oxidative depolymerization of birch lignin, the catalyst achieved an 83% conversion of birch lignin with a combined yield of dimeric and monomeric products of 53.4%.

To enhance practical application value, numerous studies have directly adopted natural lignin as the reaction substrate.[85-93] Deng *et al.* reported an oxidative catalytic fractionation and depolymerization of lignin through a one-pot two-step approach using $H_3PMo_{12}O_{40}$ (PMo_{12}) as the only catalyst.[85] The POM enabled 96% extraction of stabilized lignin from lignocellulosic sawdust at 100 °C. Subsequent heating to 140 °C converted 74.0 wt% of lignin (based on Klason lignin) into lignin-derived chemicals, including 45.9 wt% aromatic monomers. An and Wei synthesized a series of polyoxometalate ionic liquids (POM-ILs) for the oxidative depolymerization of alkali lignin.[86] PMo_{12} was demonstrated to be an effective catalyst for various lignins, delivering aromatic yields up to 23.8 wt%.[89,90] Furthermore, Fe incorporation and Cs^+ modification of PMo_{12} enabled its application as a heterogeneous catalyst, maintaining comparable monomer yields while confirming the efficient depolymerization of lignin macromolecules.[91]

2.1.2 Photocatalytic and Electrocatalytic Depolymerization

Compared with traditional thermocatalysis, photocatalysis and electrocatalysis operate under mild conditions and are more environmentally benign, thereby attracting extensive research attention in the field of lignin depolymerization. Cho *et al.* selected the giant Keplerate-type Mo_{132} for the depolymerization of PP-ol (Fig. 3).[94] Under irradiation with a 300 W xenon lamp for 6 h, the selectivity of phenyl formate reached 97.8% (Mo_{132}: 1 mol% vs. PP-ol). The post-reaction catalyst can regain its activity after heat treatment, demonstrating potential recyclability. Zhao *et al.* fabricated a Z-scheme heterojunction photocatalyst $CdS/PMo_{10}V_2/g\text{-}C_3N_4$ via a hydrothermal method.[95] Using alkaline lignin as the reaction substrate, the total yield of vanillin and vanillic acid reached 32.7 mg per gram of lignin under irradiation with a 300 W xenon lamp. Recently, Duan, Shi, and Sun immobilized $H_4PMo_{11}VO_{40}$ onto $g\text{-}C_3N_4$ and combined it with a choline chloride/p-toluenesulfonic acid deep eutectic solvent.[64] Under xenon-lamp rradiation at 80 °C, larch lignin was selectively converted into a single monophenolic product, 1-(4-hydroxy-3-methoxyphenyl)butan-1-one, with an 11% yield.

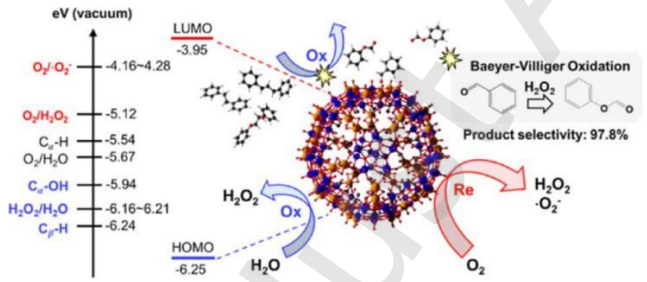

Fig. 3 Mo_{132} for the depolymerization of PP-ol under irradiation using H_2O_2 as the oxidant. Adapted with permission from Ref. [94], Copyright 2023 American Chemical Society.

Electrocatalysis enables the oxidative depolymerization of lignin while producing hydrogen, thereby achieving the full utilization of lignin. Wang's group employed PMo_{12} (0.1 mol/L) as the anolyte and conducted the reaction in an adiabatic reactor at 80 °C for 3 h.[96] Under these conditions, the corn straw degradation rate reached as high as 63.48%, the cathodic Faraday efficiency for hydrogen production peaked at 94.54%. Subsequently, using lignin as the substrate and 0.1 mol/L PMo_{12} as the anolyte, they achieved a lignin degradation conversion of 96.81% with a hydrogen Faradaic efficiency of 95.93%.[97] Similarly, Zhang and Liu used a $FeCl_3$-PMo_{12} catalytic system for biomass degradation and hydrogen production.[98]

In 2022, Ryu and co-workers proposed a photoelectrochemical cell system integrating a perovskite photocathode with lignocellulosic biomass, enabling efficient bias-free solar hydrogen production while achieving the valorization of biomass (Fig. 4).[99] In this system, lignocellulosic biomass serves as an alternative electron source, and PMo_{12} acts as a soluble catalyst as well as an electron/proton mediator. Through the redox reaction of PMo_{12} driven by biomass oxidation, electron extraction and storage are realized. The cathode (perovskite photocathode) is immersed in an acidic electrolyte (0.5 mol/L H_2SO_4) for hydrogen evolution, while the anode (carbon nanotube paper) is immersed in an electrolyte containing reduced PMo_{12}, which provides electrons through the reoxidation of PMo_{12} without the need for external bias. The system operates cyclically: at night, biomass reduces PMo_{12} at 60 °C (for 12 h); during the daytime, under illumination, the reoxidation of PMo_{12} and hydrogen evolution occur (for 12 h). This system exhibits excellent performance: 50.6% of lignin is converted into high-value-added products, and the Faradaic efficiency for H_2 production is close to 100%.

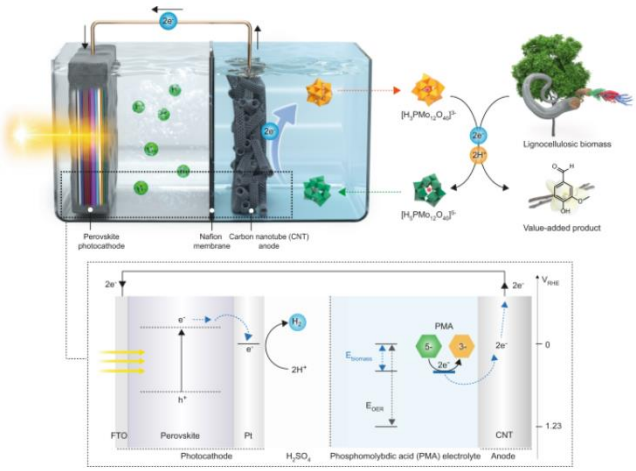

Fig. 4 Perovskite photocathode integrated with Pt and PMo_{12} as an electron extraction system coupled to achieve bias-free hydrogen evolution from biomass. Adapted with permission from Ref. [99], Copyright 2022 Springer Nature.

2.2 Polyoxotungstate-Catalyzed Lignin Depolymerization

2.2.1 Thermocatalytic Depolymerization

Fu *et al.* synthesized 3D hierarchical flower-like bimetallic nitride nanosheets (SiW_{12}@Pd/Co-ZIF-NS) via a Pd/Co-ZIF template and $H_4SiW_{12}O_{40}$-induced phase transformation (Fig. 5(a)).[58] This catalyst (100 mg) efficiently promoted the transfer hydrogenolysis of β-O-4 model compound (phenethyl phenyl ether), achieving 100% conversion with 87% ethylbenzene and 93% phenol yields using isopropanol as solvent and hydrogen donor (Fig. 5(b)). The catalyst can be recycled 4 times while maintaining structural stability. It also exhibited high activity for C–O bond cleavage in lignin dimers and the depolymerization of natural lignin.

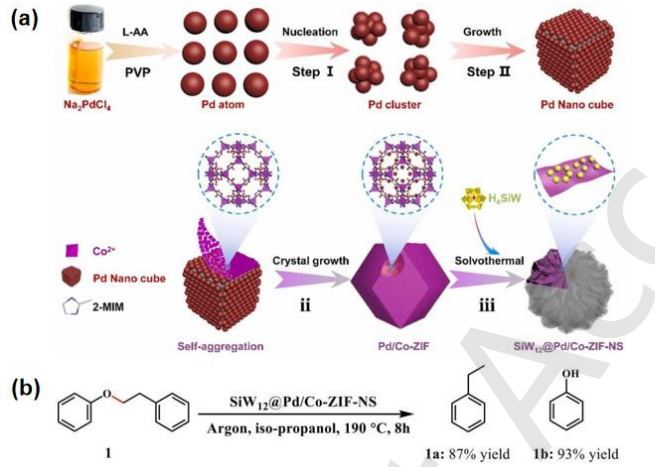

Fig. 5 (a) Synthesis process of SiW_{12}@Pd/Co-ZIF-NS. (b) Catalytic cleavage of the C−O linkage in β-O-4 lignin model dimers. Adapted with permission from Ref. [58], Copyright 2023 Elsevier B.V.

A series of vanadium-doped Wells-Dawson-type catalysts, $H_{6+x}P_2W_{18-x}V_xO_{62}$ (x=1, 2, 3, 4), were used to promote the oxidative depolymerization of larch lignin in Shi's group.[100] Total acidity decreased with increasing vanadium content. Among these, $H_9P_2W_{15}V_3O_{62}$ exhibited the best performance, achieving 11.42% aromatic monomer yield at 170 °C, 3 h, and 1 MPa O_2 with selective cleavage of C_α–C_β bonds in lignin side chains. The excellent activity is attributed to a balance between moderate oxidation and acidity. Subsequently, Shi and Xu constructed a bifunctional catalyst $Ni_{0.75}Co_{0.75}$@$CsPMo_{12}$ by doping bimetallic Ni and Co onto Keggin-type POMs.[101] Under optimized conditions (190 °C, 3 h, 1.5 MPa O_2), this catalyst efficiently depolymerized pine lignin into vanillin and methyl vanillate, with selectivities of 57.8% and 27.3%, respectively.

2.2.2 Photocatalytic Depolymerization

Yang and Lv developed a Ni_9P_3/CdS photocatalyst by combining $K_5Na_{11}[Ni_9(OH)_3(H_2O)_6(HPO_4)_2(PW_9O_{34})_3]$•$55H_2O$ (Ni_9P_3) with CdS quantum dots for the selective hydrogenolysis of lignin β-O-4 model compounds (Fig. 6).[102] Under 450 nm LED irradiation for 8-10 h, this photocatalytic system achieved 95% conversion with >93% selectivity toward various phenols and ketones ($n_{catalyst}$:$n_{PP\text{-}one}$ = 1:100). The POM/CdS system exhibits satisfactory stability and can be reused over several cycles. On the basis of experimental results and spectroscopic analyses, a tentative reaction mechanism has been proposed, indicating that the surface-adsorbed hydrogen species formed on Ni_9P_3 are essential for the activation and subsequent cleavage of the C_β–O bond. In contrast to the predominantly explored oxidative depolymerization strategies, this work establishes a POM-catalyzed hydrogenolytic depolymerization pathway, broadening the scope of lignin valorization under mild and noble-metal-free conditions.

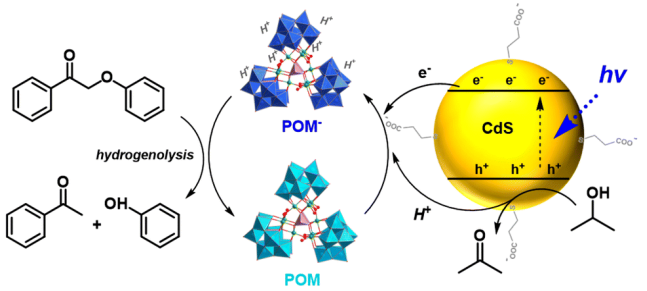

Fig. 6 Proposed mechanism for photocatalytic hydrogenolysis of PP-ol. Adapted with permission from Ref. [102], Copyright 2023 The Royal Society of Chemistry.

Liu's group achieved the cleavage of C–C bonds in PP-ol by supporting $K_7P_2W_{17}VO_{62}$ ($P_2W_{17}V$) on TiO_2 (Fig. 7).[103] Under UV light, 98.8% of PP-ol was converted and the primary products were benzaldehyde and phenol (10 mg $P_2W_{17}V$). In addition, the catalyst boasts the advantages of easy separation and recyclability. Mechanistic studies revealed that PP-ol undergoes C_α–C_β bond cleavage predominantly through a C_β-centered radical pathway with photogenerated electrons and $O_2^{\bullet-}$

as the active species. In the same group, a multifunctional photocatalyst, Cu/$P_2W_{17}V/TiO_2$, was fabricated for selective and tunable lignin depolymerization (Fig. 8).[104] Using PP-ol or β-O-4 lignin model compounds, bond cleavage selectivity can be controlled by reaction time: short irradiation favors C_β–O scission, while prolonged irradiation promotes C_α–C_β cleavage, yielding aromatic aldehydes and phenols. In this system, Cu enhances charge transfer and facilitates C_β–O cleavage, whereas $P_2W_{17}V$, with acidic, basic, and redox sites, accelerates electron transfer to O_2 and drives C_α–C_β bond cleavage. Alkaline lignin can also be photocatalytically converted to vanillin. This work demonstrates the first example of regulating C_α–C_β versus C_β–O bond scission simply through temporal control, highlighting the potential of trifunctional photocatalysts for producing valuable lignin-derived chemicals.

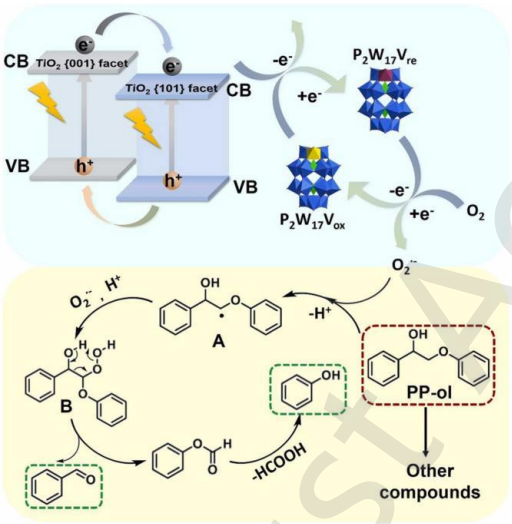

Fig. 7 Preliminary mechanism for the photocatalytic conversion of PP-ol to benzaldehyde and phenol. Adapted with permission from Ref. [103], Copyright 2023 Elsevier Ltd.

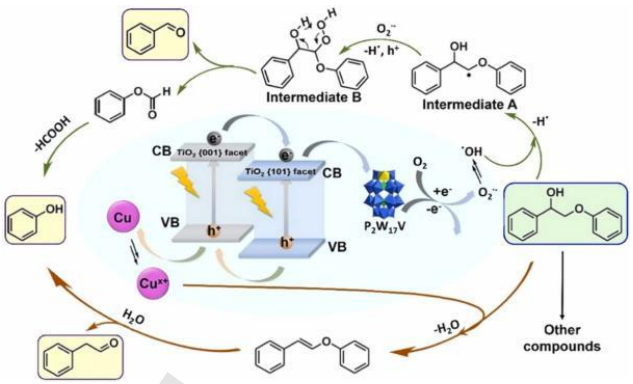

Fig. 8 Preliminary mechanism for the photocatalytic conversion of PP-ol catalyzed by Cu/$P_2W_{17}V/TiO_2$. Adapted with permission from Ref. [104], Copyright 2024 Elsevier B.V.

Distinct from conventional POM-based catalysts, Xuan and Cronin reported a novel high-nuclearity polyoxotungstate, $K_4Na_{10}H_2[Cu_9(OH)(C_9H_7N_3O_2)_9(H_2O)_{22}][H_{16}P_8W_{64}O_{236}]$ (P_8W_{64}), for lignin depolymerization.[105] In this structure, both sides of the P_8W_{48} cavity are capped with W_8 units, leading to the formation of P_8W_{64}, which are further connected by Cu-triazole-benzoate complexes into layered structures (Fig. 9(a)). Upon exfoliation, the resulting ultrathin nanosheets exhibited highly selective C_α–C_β bond cleavage of β-1 lignin model compounds under 400 nm LED irradiation, achieving up to 99% conversion (P_8W_{64}: 0.5 mol% vs. PP-ol). For the 1,2-diphenylethanol (a lignin model), the combined yield of benzaldehyde and benzoic acid reached 79%. Mechanistic studies reveal that the P_8W_{48} clusters serve as photoactive centers, where photogenerated electrons reduce O_2 to superoxide radicals ($O_2^{\bullet-}$) and holes abstract C_β–H to form carbon-centered radicals, cooperatively enabling selective C_α–C_β bond scission (Fig. 9(b)).

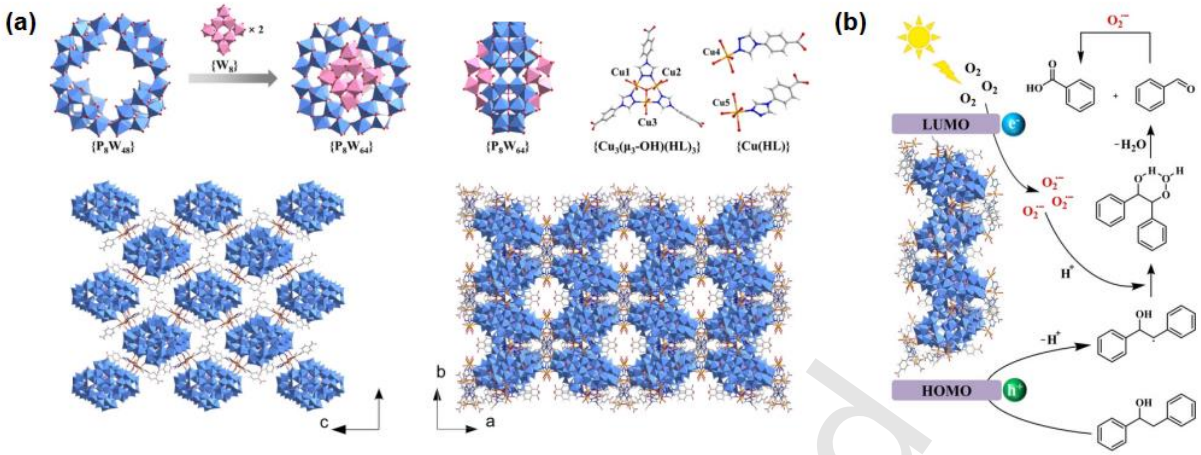

Fig. 9 (a) Structural schematic of P_8W_{64}. (b) Proposed mechanism for the photocatalytic depolymerization of 1,2-diphenylethanol. Adapted with permission from Ref. [105], Copyright 2024 Wiley-VCH GmbH.

2.3 Polyoxovanadate-Catalyzed Lignin Depolymerization

Although V-substituted polyoxomolybdates and polyoxotungstates have been widely explored for the oxidative depolymerization of lignin and its model compounds, examples employing polyoxovanadate catalysts remain very rare. Liu *et al.* successfully synthesized $[Cu^{I}(bbi)]_2\{[Cu^{I}(bbi)]_2V^{IV}_2V^{V}_8O_{26}\}\cdot 2H_2O$ (NENU-MV-5, bbi = 1,1'-(1,4-butanediyl)bis(imidazole)) under hydrothermal conditions.[65] This compound features a 3D supramolecular architecture, constructed through electrostatic assembly of one-dimensional cationic chains $[Cu(bbi)]^+$ and 2D anionic layers $\{[Cu(bbi)]_2V_{10}O_{26}\}^{2-}$ (Fig. 10(a)). In catalytic tests using PP-ol, NENU-MV-5 (0.01 mmol) achieved >99% conversion, yielding phenol (60%), benzoic acid (9.5%), and methyl benzoate (90%) at 100 °C under 0.4 MPa O_2 for 12 h. After 5 cycles, the catalyst remains catalytically stable with its structure intact.

The catalyst incorporates two types of active sites—mixed-valence V^{V}–O–V^{IV} moieties and Cu(I) centers—which act synergistically to drive the catalytic reaction (Fig. 10(b)). The reaction mechanism proceeds in two key steps. Initially, V^{IV} species adsorb and activate O_2 to $^{\bullet}O_2^{-}$, which then combine with H^+ provided by methanol to HOO$^{\bullet}$. Concurrently, V^{V} centers form a stable five-membered ring with β-O-4 alcohol, activating the C_α–H bond. The HOO$^{\bullet}$ radicals subsequently abstract hydrogen atoms from the activated C_α–H bonds, oxidizing β-O-4 alcohol to β-O-4 ketone—a process identified as the rate-determining step. Following this oxidation, Cu(I) sites react with O_2 to form Cu(II)-OO$^{\bullet}$ species, which catalyze the cleavage of the C_α–C_β bond in β-O-4 ketone, yielding benzoic acid and phenyl formate. The phenyl formate further undergoes decarboxylation to produce phenol and CO_2.

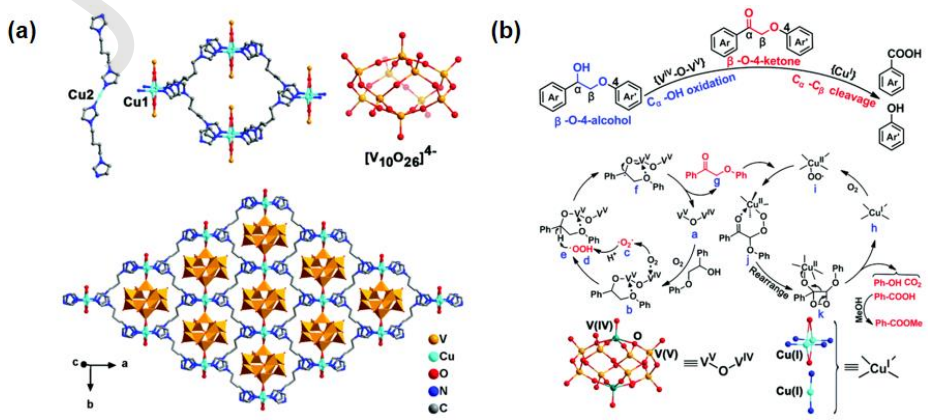

Fig. 10 (a) The structure of NENU-MV-5. (b) Proposed catalytic mechanism of NENU-MV-5 toward PP-ol. Adapted with permission from Ref. [65], Copyright 2020 The Royal Society of Chemistry.

2.4 Polyoxoniobate-Catalyzed Lignin Depolymerization

Polyoxoniobates possess significantly higher negative charge densities than their Mo/W analogues, owing to the lower oxidation state of Nb(V) relative to Mo(VI) and W(VI). This high negative charge density endows the surface oxygen atoms with pronounced Brønsted basicity. Among known POMs, Lindqvist-type $\{Nb_6O_{19}\}$ cluster exhibits the highest negative charge density[106] and has been used as a base catalyst in the hydrolysis of chemical warfare agents, Knoevenagel condensation, and CO_2 fixation.[107-114]

Previous studies have shown that the C_β–H bond of β-O-4 ketones can be activated by inorganic or organic bases (e.g., NaOH, KOH, Cs_2CO_3, K_2CO_3, pyridine)[115,9], however, the requirement for excess corrosive bases and their poor recyclability severely limits industrial applicability. In this context, we used a catalytic amount of the solid base, $K_7HNb_6O_{19}$ (KNb_6), combined with copper-modified graphitic carbon nitride (Cu/C_3N_4), to catalyze the oxidative cleavage of the β-O-4 ketone model, PP-one (Fig. 11(a)).[68] Under relatively mild conditions (80 °C, 0.5 MPa O_2), the reaction achieved 96% PP-one conversion, with phenol obtained in 90% yield and an overall aromatic monomer yield of 90%, giving a high selectivity of 94% toward aromatic products. Moreover, the catalytic activity was well maintained after five cycles (Fig. 11(b)).

Kinetic isotope experiments display that C_β–H activation is the rate-determining step. CO_2-TPD analysis shows that KNb_6 possesses weak basic sites and the uniquely basic surface oxygen atoms of KNb_6 contribute to the activation of the C_β–H bond of PP-one (Figs. 11(c)-11(e)). Mechanistically, the terminal oxygen (O_t) and bridging oxygen (O_β) on the surface of KNb_6 synergistically activated the C_β–H bond of PP-one through hydrogen bonding interactions, facilitating the insertion of molecular oxygen to form hydroperoxide intermediates (Fig. 11(f)). Subsequently, Cu/C_3N_4 catalyzed the selective cleavage of the C_α–C_β bond in the intermediates, generating benzoic acid and phenyl formate. Phenyl formate further underwent decarboxylation to produce phenol, while benzoic acid reacted with methanol via esterification to form methyl benzoate. In addition, the catalysts were also active for the oxidative cleavages of oxidized organosolv lignin.

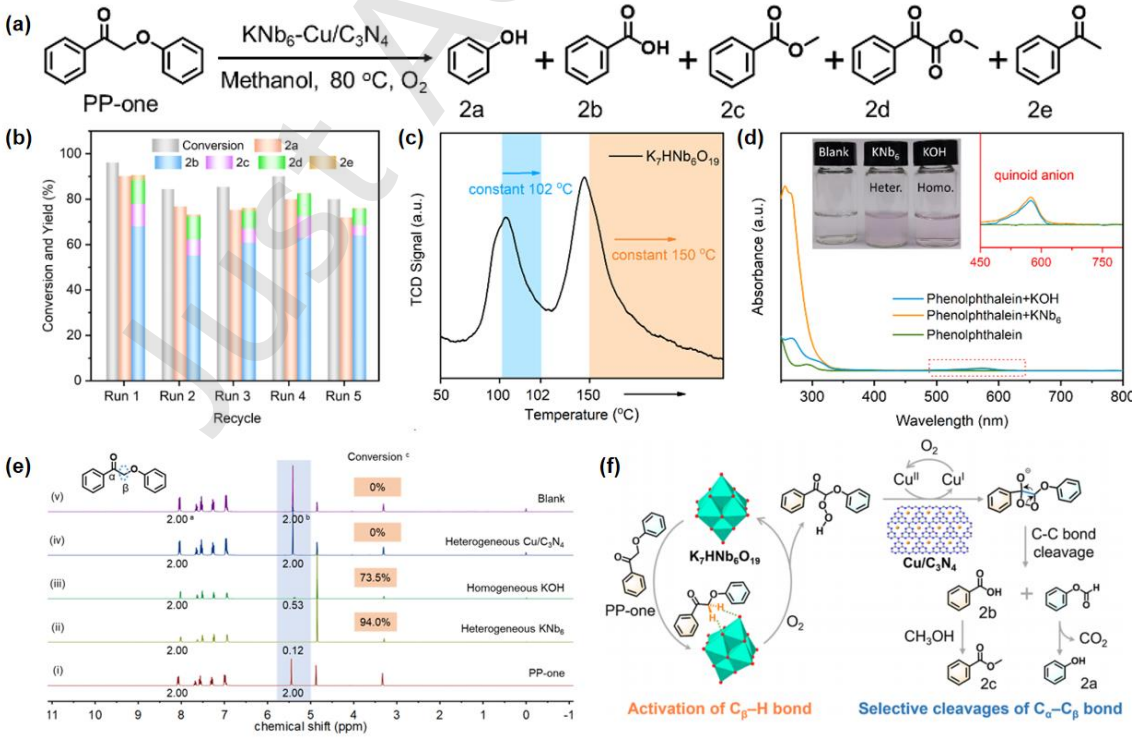

Fig. 11 (a) Cleavage reaction of PP-one by KNb_6-Cu/C_3N_4. (b) Recyclability test. (c) CO_2-TPD of KNb_6 (d) Absorption spectra of phenolphthalein. (e) hydrogen−deuterium exchange reactions. (f) Possible reaction mechanism. Adapted with permission from Ref. [68], Copyright 2023 American Chemical Society.

Compared with the β-O-4 ketone model PP-one, the β-O-4 alcohol model PP-ol more closely resembles natural lignin. So we combined KNb_6 with cobalt-cobalt oxide (Co-CoO_x) supported on N-doped carbon ($CoMA/C_{900}$) (Fig. 12).[69] The $CoMA/C_{900}$ catalyst was synthesized via the high-temperature calcination of cobalt acetate, melamine, and activated carbon. Under mild conditions (100 °C, 0.2 MPa O_2), PP-ol was nearly fully converted within 3 h, yielding primarily phenol (99%) and methyl benzoate (98%).

In the first step, the hydroxyl group of PP-ol interacts with the basic surface oxygen atoms of KNb_6, while Co^0 in $CoMA/C_{900}$ activates O_2 to form $^{\bullet}O_2^-$ radicals (confirmed by EPR), which react with MeOH to generate HOO$^{\bullet}$ species. PP-ol is then oxidized by HOO$^{\bullet}$ to form the PP-one intermediate, identified as the rate-determining step. In the second step, the C_β–H bond of PP-one is activated by KNb_6 and oxidized by reactive oxygen species, leading to preferential C_β–O bond cleavage and formation of phenol and methyl benzoylformate. Finally, methyl benzoylformate undergoes C_α–C_β bond cleavage via methanol attack, producing methyl benzoate and methyl formate, with the latter being oxidized and decarboxylated to regenerate MeOH and release CO_2. Importantly, KNb_6 and $CoMA/C_{900}$ work synergistically in all three steps. Furthermore, this catalytic system was extended to other β-O-4 alcohol analogs and birch lignin, exhibiting efficient depolymerization activity across all tested substrates.

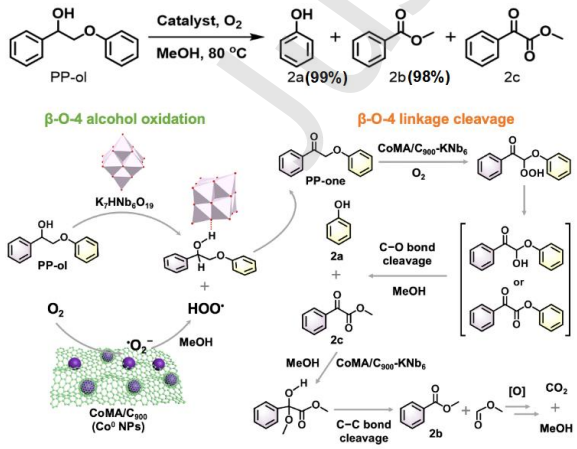

Fig. 12 Possible cleavage mechanism of PP-ol catalyzed by KNb_6-$CoMA/C_{900}$. Adapted with permission from Ref. [69], Copyright 2025 The Royal Society of Chemistry.

Lignin depolymerization usually produces aromatics containing only C, H, and O. Introducing nitrogen sources during β-O-4 cleavage allows the synthesis of high-value nitrogen-containing aromatics. Therefore, the catalytic performance of KNb_6 was explored for PP-one depolymerization using $NH_2OH{\bullet}H_2O$ as the nitrogen source. Under mild conditions (120 °C, 10 min), near-complete conversion was achieved, affording phenol (93%) and benzonitrile (73%) (KNb_6: 0.2 eq. PP-one). KNb_6 also maintained its basicity and activity over multiple catalytic cycles.

Interestingly, the catalytic activity of Lindqvist-type hexaniobates is strongly influenced by their alkali metal counter-cations. Four hexaniobate catalysts ($LiNb_6$, $NaNb_6$, KNb_6, and $CsNb_6$) were evaluated, revealing a catalytic activity trend of $KNb_6 \approx CsNb_6 > NaNb_6 > LiNb_6$ (Fig. 13(b)). Density functional theory (DFT) calculations further indicate that the bridging oxygen atoms carry higher negative charge density than terminal oxygen atoms, and the average surface oxygen charge density of $CsNb_6$ is highest(Fig. 13(c)).

PP-one^{oxime}, formed via oximation with $NH_2OH{\bullet}H_2O$, acts as a key intermediate in the catalytic pathway. The DFT calculations reveal a four-step reaction pathway for the KNb_6-catalyzed cleavage of the PP-one^{oxime} intermediate. i) Hydrogen migration. The bridging oxygen of $\{H_aNb_6O_{19}\}$ interacts with the C_β–H of PP-one^{oxime}, transferring H_β to the cluster and H_a to the substrate nitrogen, forming an alkenyl hydroxylamine intermediate, confirmed by *in situ* FT-IR spectroscopy. ii) Hydroxyl migration. A water molecule attacks the C=C bond accompanied by N–OH cleavage to generate an imine intermediate. iii) C_β–O bond cleavage. The cluster activates the C_β–OH group and protonates phenolic oxygen, promoting C_β–O bond cleavage to form phenol and imine aldehyde, detected by GC-MS. iv) C_α–C_β bond cleavage. Basic oxygen atoms in KNb_6 mediate proton transfer, enabling C_α–C_β cleavage to produce benzonitrile and formaldehyde (Fig. 13(d)). During the reaction, KNb_6 serves as a recyclable inorganic proton shuttle: its basic surface oxygen atoms accept protons from the substrate, while adjacent protonated −OH groups donate protons,

enabling the key steps of PP-one^{oxime} cleavage. KNb_6 also shows high activity toward various lignin β-O-4 ketone models and oxidized birch lignin.

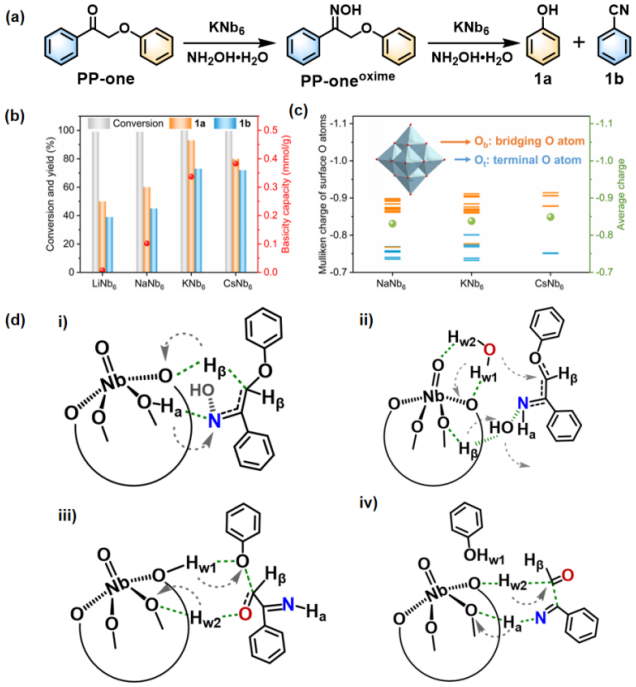

Fig. 13 (a) Cleavage of PP-one to yield phenol and benzonitrile with $NH_2OH•H_2O$. The influence by alkali metal counter-cations on (b) catalytic performance and (c) charge density distribution of bridging and terminal surface O atoms. (d) The proton shuttle role of KNb_6 in the cleavage of PP-one^{oxime} intermediate. Adapted with permission from Ref. [70], Copyright 2026 American Chemical Society.

In summary, lignin depolymerization is influenced by multiple factors. For thermocatalytic processes, reaction temperature, pressure, and time play crucial roles. Increasing temperature and pressure generally promotes the reaction. Typically, the reaction temperature ranges from 90 to 190 °C, while the pressure does not exceed 1.2 MPa. In photocatalytic systems, parameters such as the light source (e.g., Xe lamps, UV light, or LEDs) and reaction temperature are key factors affecting catalytic performance.

Regarding the choice of POM catalysts for thermocatalysis, polyoxoniobates usually operate under the mildest reaction conditions, followed by polyoxovanadates and polyoxomolybdates, while polyoxotungstates generally require the most demanding conditions. This trend can be attributed to the special alkalinity of hexaniobate, which can readily activate C−H bond under milder conditions. In contrast, polyoxovanadates and polyoxomolybdates promote lignin depolymerization mainly by their excellent oxidative activity. As polyoxotungstates possess relatively weak oxidative ability; higher temperatures and pressures are usually required in thermocatalytic system. As a result, they are more commonly employed in photocatalytic systems, where their excellent electron-transfer capability can be effectively utilized.

From the perspective of catalyst architecture, Keggin-type POMs are more widely employed than Wells-Dawson and Anderson types. This arises from their excellent stability, tunable acidity and redox properties. In addition, the design of the reactor is also crucial for achieving efficient lignin depolymerization. For example, Ryu et al. developed a home-made two-compartment H-type photoelectrochemical (PEC) reactor featuring a “cathode-anode separated design”. On the cathode side, a perovskite photoelectrode is employed to harvest solar energy for proton splitting and hydrogen evolution, while the anode side achieves the oxidative depolymerization of lignin mediated by PMo_{12}.

3 Oxidation of FF and HMF

The oxidation of FF and HMF has been extensively investigated, with particular emphasis on HMF. These oxidation processes can afford dialdehydes, monocarboxylic acids, and even dicarboxylic acids, as well as their corresponding esters, all of which have broad applications. In the oxidative transformation of HMF, catalysts play a key role in regulating substrate conversion and product selectivity. Among them, POM-based catalysts have attracted considerable attention owing to their intrinsic Brønsted acidity and excellent redox properties.

3.1 Oxidation of FF

3.1.1 The Production of 2-methyl furoate

2-Methyl furoate holds significant application value in the fine chemical, fragrance, and flavor industries. It is typically synthesized via the esterification reaction following the oxidation of FF under acid conditions (Scheme 2).[116] POMs possess Brønsted acidity and strong oxidation properties,

making them applicable to this reaction. However, common Keggin-type POMs are highly soluble in water, which hampers their recyclability. To overcome this limitation, a range of strategies has been developed. Rodrigues *et al.* synthesized $Cu_2SiW_{12}O_{40}$ via metal ion exchange method.[117] Using hydrogen peroxide as the oxidant, the conversion rate of FF reached 98% with 79% selectivity for 2-methyl furoate. Subsequently, $Cu_1H_1PW_{12}O_{40}$ was immobilized on montmorillonite K-10, yielding the composite catalyst Cu-PW_{12}/K-10.[118] Employing tert-butyl hydroperoxide (TBHP) as the oxidant, the reaction was conducted at 120 ℃ after 5 h, achieving a FF conversion of 91% and an exceptional 100% selectivity toward 2-methyl furoate. In this catalytic system, the Brønsted acidity of PW_{12} and the intrinsic acidity of montmorillonite K-10 synergistically facilitated the condensation reaction between furfural and methanol. Meanwhile, Cu^{2+} cations promote activation of TBHP, thereby generating reactive oxygen species that drive the oxidative esterification process.

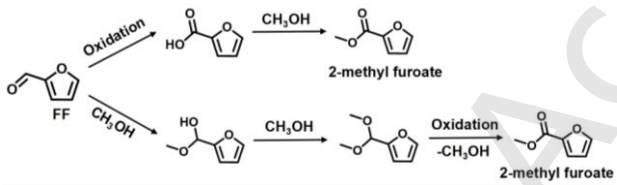

Scheme 2 The conversion of FF to 2-methyl furoate.

3.1.2 The Production of Maleic acid and Maleic anhydride

Currently, researches on POM-catalyzed oxidation of FF remain relatively limited, with most studies focusing on the production of maleic acid and maleic anhydride (Scheme 3). These two compounds have broad applications in resins, lubricant additives, plasticizers, agricultural chemicals, and other fields.[119] The synthesis of maleic acid and maleic anhydride requires catalysts with strong oxidative capability, a property intrinsically associated with POMs.

In 2011, Yin *et al.* used PMo_{12} to catalyze the aerobic oxidation of FF. Under the reaction conditions of 110 ℃, 2 MPa O_2 for 14 h, the conversion of FF reached 50.3% with a maleic acid yield of 34.5%.[119] The reaction follows a pathway in which the furan ring undergoes opening before decarboxylation, ultimately yielding maleic acid. Subsequently, they employed PMo_{12} in combination with copper nitrate for this oxidation, and the synergistic catalytic system improved FF conversion to 95.2% and maleic acid yield to 49.2% under the conditions of 98 ℃, 2 MPa O_2, and 14 h.[120] Specifically, Cu^{2+} serves as the redox-active center, abstracting electrons from FF to generate Cu^{+}. The presence of PMo_{12} facilitates the oxidative regeneration of Cu^{+} back to Cu^{2+}. The combination of $PMo_{10}V_2$ with $Cu(CF_3SO_3)_2$ and PMo_{12} with copper acetate have also been explored.[121,122]

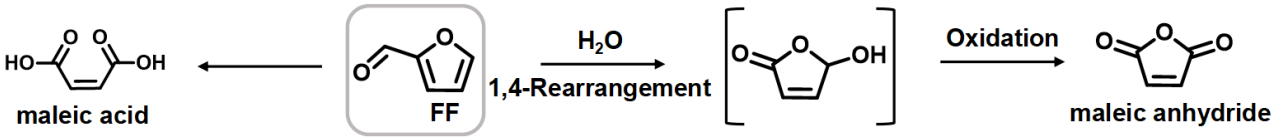

Scheme 3 The conversion of FF to maleic acid and maleic anhydride.

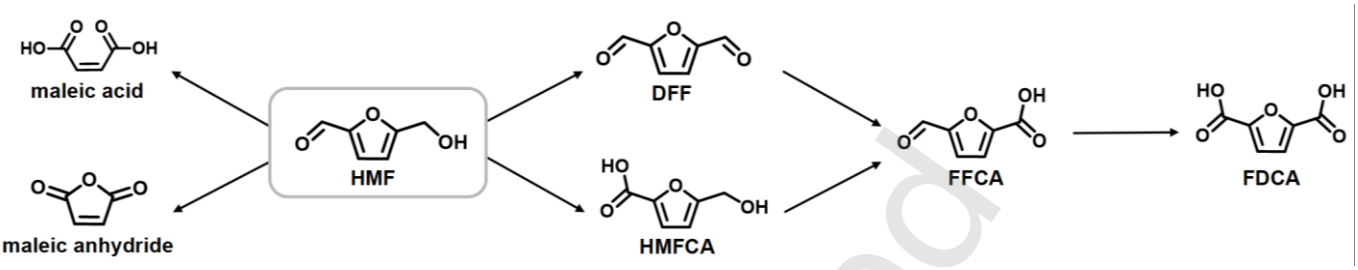

Scheme 4 The oxidation of HMF to different products.

Besides, FF can be directly oxidized to produce formic acid. Albert *et al.* synthesized vanadium-substituted Anderson-Evans-type tungstotellurates, $NaTeV_xW_{6-x}$ (x = 1, 2, 3).[123] Among these catalysts, $NaTeV_3W_3$ exhibited the optimal performance, achieving a FF conversion of 98.4% and directly producing formic acid with a yield of 33.2%. In 2024, They selected $H_4[PVMo_{11}O_{40}]$ as the catalyst, achieving a FF conversion of 69.3%, along with maleic acid and formic acid yields of 22.6% and 14.7%, respectively.[124]

3.2 Oxidation of HMF

HMF can be selectively oxidized into several valuable chemical intermediates, including 2,5-diformylfuran (DFF), 5-hydroxymethyl-2-furancarboxylic acid (HMFCA), 2,5-furandicarboxylic acid (FDCA), 5-formyl-2-furancarboxylic acid (FFCA), maleic anhydride and maleic acid (Scheme 4).[125] In the following, the discussion is structured according to the type of product formed, with a focus on POM-based catalyst design, catalytic performance, and reaction mechanism. Molecular oxygen, a green and cost-effective oxidant, is mainly used for HMF oxidation.

3.2.1 The Production of 2,5-diformylfuran

Due to its chemical versatility, DFF finds applications in the preparation of pesticides, fluorescent compounds[126], novel polymeric materials[127], and ligands[128]. HMF contains an aldehyde and a hydroxyl group, and selective oxidation of the hydroxyl group while avoiding oxidation of the aldehyde is a key challenge in DFF preparation. This underscores the importance of rational catalyst design. To date, Mo- and V-containing POMs have been extensively investigated in the selective oxidation of HMF to DFF, owing to their excellent redox properties compared to their W- and Nb-based counterparts. Therefore, we will present the content in the order of polyoxomolybdates, vanadium-containing molybdates, and finally polyoxovanadates.

Gao *et al.* used a Keplerate-type $[(NH_4)_{42}[Mo^{VI}_{72}Mo^{V}_{60}O_{372}(CH_3COO)_{30}(H_2O)_{72}]$ (Mo_{132}) for oxidation of HMF to DFF (Fig. 14).[129] The presence of both Mo^{6+} and Mo^{5+} in Mo_{132} endows it with outstanding catalytic activity, achieving 99.2% HMF conversion and 100% DFF selectivity under both atmospheric and anaerobic conditions. More importantly, after five consecutive catalytic cycles, the catalyst retained high catalytic activity. The reaction mechanism was investigated by CV, XPS, and DRIFTS. First, the –OH of HMF adsorbs onto the Mo_{132}, preventing the –CHO from accessing the active sites and thus affording 100% selectivity to DFF. Subsequently, two hydrogen atoms from O–H and C–H bonds transfer to the terminal oxygen of Mo_{132}, with a new C=O bond formed and Mo^{6+} reduced to Mo^{5+}. Finally, O_2 reoxidizes the catalyst, regenerating its activity for successive catalytic cycles.

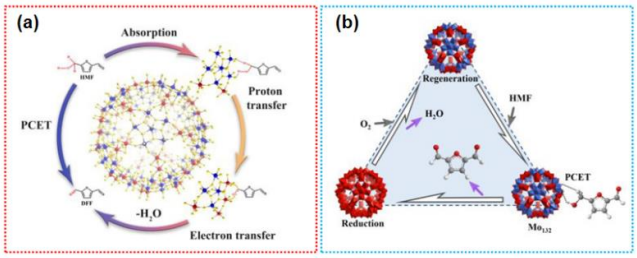

Fig. 14 (a) Possible reactive sites in Mo_{132}-catalyzed HMF oxidation. (b) Proposed mechanism for the selective oxidation of HMF to DFF. Adapted with permission from Ref. [129], Copyright 2022 Elsevier B.V.

In the presence of the $[PMo_{12}O_{40}]^{3-}$, the oxidation of HMF to DFF proceeds through a multi-step process.[130] Initially, one HMF molecule is oxidized to DFF by $[PMo_{12}O_{40}]^{3-}$ and the POM is reduced to $[H_2PMo_{12}O_{40}]^{-}$. Molecular oxygen is then incorporated, forming a peroxide intermediate ($[PMo_{12}O_{41}]^{3-}$), which subsequently oxidizes a second HMF molecule to DFF, thereby regenerating the original $[PMo_{12}O_{40}]^{3-}$ species. In each oxidation event, two key bond cleavages occur: the O–H bond of the hydroxyl group and the C–H bond of the methylene group in HMF.

Subsequently, several PMo_{12}-based catalysts have been reported. Hu *et al.* fabricated bifunctional catalysts by supporting PMo_{12} on polyaniline (PAN) or formyl-functionalized PAN (F-PAN).[131] Huang *et al.* synthesized a zeolite-like crystalline catalyst, $[La(H_2O)_3Cl_{0.5}(pdc)][La(H_2O)_4(pdc)]\}_2[PMo_{12}O_{40}]$ $\cdot 2H_2O$ (PZF-1) (H_2pdc = pyridine-2,6-dicarboxylate) through hydrothermal reaction.[132] In this structure, La centers are connected by pdc ligands into a 3D zeolite-like framework, while $[PMo_{12}O_{40}]^{3-}$ anions interact with the framework by electrostatic and hydrogen-bonding interactions.

Moreover, further studies revealed that partial substitution of Mo atoms by V in Keggin-type clusters can further enhance their catalytic performance, owing to the superior redox properties of V. Therefore, Keggin-type $PMo_{10}V_2$ and PMo_4V_8 have been widely employed in the selective oxidation of HMF to DFF.

Wang *et al.* immobilized $PMo_{10}V_2$ on various support materials for catalyst recycling. In 2018, $PMo_{10}V_2$ was encapsulated into the mesopores of silica nanofibers, resulting in the successful fabrication of $PMo_{10}V_2/SiO_2$.[133] In the above case, $PMo_{10}V_2$ interacts with the support by hydrogen bonding interaction, leading to POM leaching.[134] To address the issue, they functionalized the silica surface with $–NH_2R$ groups. Upon protonation of the $–NH_2$ groups to $–NH_3^+$, strong electrostatic interactions enable stable immobilization of POMs, resulting in $PMo_{10}V_2/SiO_2–NH_2$ nanofiber catalysts. Subsequently, surface-modified CeO_2 (surf-CeO_2) was used as support due to its high oxygen release capacity.[135] Furthermore, $PMo_{10}V_2$ was immobilized on chitosan nanofiber, forming $PMo_{10}V_2$/chitosan nanofiber.[136] Later, they loaded $PMo_{10}V_2$ onto layered double hydroxides (LDHs), leading to an enhancement in catalytic activity.[137]

The spindle-shaped Fe_3O_4/C, obtained from the pyrolysis of the metal-organic framework MIL-88A(Fe), was used by Gao's group to combine with Keplerate-type POM ($Mo_{72}V_{30}$). $Mo_{72}V_{30}$@Fe_3O_4/C achieved nearly complete conversion of HMF with 100% selectivity toward DFF after 4 h (120 °C, 0.4 MPa O_2).[138] Compared with $Mo_{72}V_{30}$, Keggin-type POMs are attractive due to their straightforward and easily scalable synthesis. In this system, Fe_3O_4/C and Co_3O_4/C facilitate the adsorption of HMF molecules, while $PMo_{10}V_2$ acts as the primary catalytic center (Fig. 15).[139] Together, these effects enhance HMF conversion efficiency and suppress the over-oxidation of DFF. Among them, $PMo_{10}V_2$@Fe_3O_4/C achieved a 99.1% conversion of HMF and nearly 100% selectivity for DFF. After 10 cycles of reuse, the HMF conversion remains as high as 92%, while the DFF selectivity still stays close to 100%.

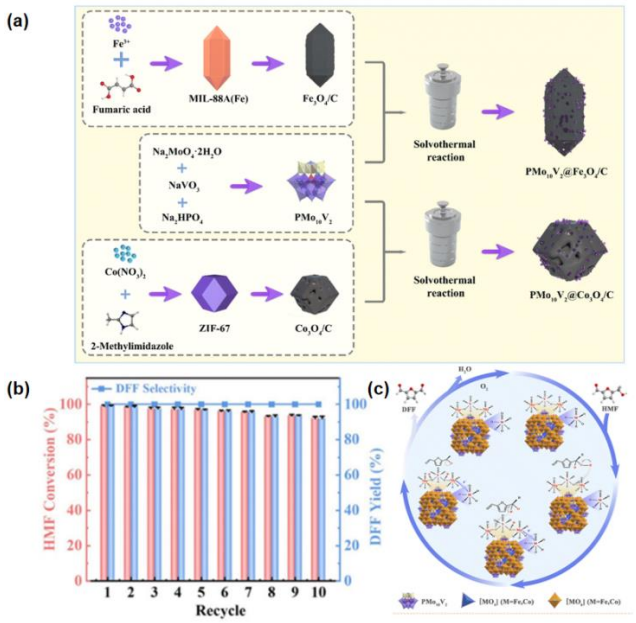

Fig. 15 (a) The synthesis process for the catalysts. (b) Cycling tests of $PMo_{10}V_2$@Fe_3O_4/C (c) The proposed mechanism of HMF to DFF. Adapted with permission from Ref. [138], Copyright 2023 The Royal Society of Chemistry.

Hydroxyapatite (HAP) possesses abundant ion-exchange sites, enabling effective interaction with charged species, and exhibits intrinsic basicity that promotes the dehydrogenative oxidation of HMF. Based on this, Wang *et al.* prepared PMo_4V_8/HAP catalysts via ion exchange of hydroxyl groups on HAP with $\{PMo_4V_8O_{40}\}$ (PMo_4V_8).[140] In 2023, by immobilizing PMo_4V_8 onto alkyl and alkyl-amino functionalized silica nanoparticles, a Pickering interfacial catalyst, $PMo_4V_8/SiO_2(C_8/C_8NH_2)$, was successfully fabricated.[141]

In addition to $PMo_{10}V_2$ and PMo_4V_8, other molybdovanadophosphate has also been utilized as an effective catalyst for the oxidation of HMF to DFF. Zhong *et al.* developed a series of bifunctional and recyclable catalysts based on acidic cesium salts of molybdovanadophosphoric POMs (CsMVP-POMs) by proton exchange reaction, which enabled the conversion of HMF to DFF using oxygen as the oxidant.[143] By comparing various CsMVP-POMs, it was found that the vanadium content has a significantly influence on their catalytic performance. Among them, the CsMVP-POMs catalyst with the highest V/Mo ratio exhibited the strongest redox activity, indicating that vanadium effectively promotes the conversion of HMF to DFF[142]. Similar trend was also observed by Zhizhina and co-workers.

In addition to the supported catalysts mentioned above, several crystalline POM catalysts with novel structure have been reported successively. In 2021, we reported three discrete imidazole-functionalized Mo−V POMs, $HPMo_8V^{IV}_4O_{40}(V^VO)_2[(V^{IV}O)(IM)_4]_2$ (IM = 1-methylimidazole, 1-ethylimidazole, or 1-propylimidazole), which contains a bi-capped pseudo-Keggin $\{HPMo_8V_4O_{40}(VO)_2\}$ modified by two imidazole-functionalized $\{(VO)(IM)_4\}$.[62] Notably, three different types of vanadium centers are present in this cluster, including substituted V species in the pseudo-Keggin $\{PMo_8V_4\}$, capped $\{VO\}$ units, and organic-functionalized $\{(VO)(IM)_4\}$ groups (Fig. 16(a)). These clusters as heterogeneous catalysts were active for the oxidation of HMF to DFF. Using atmospheric O_2 as oxidant, 95% of HMF was converted with 95% selectivity for DFF after 4 h at 100 °C.

To understand the role of each component in the catalyst, two crystalline catalysts, $[NH_4]_4[HPMo_8V^{IV}_4O_{40}(V^VO)_2]$ and $(V^{IV}O)(mIM)_4SO_4$, were synthesized and used in the catalytic transformation. The former exhibited high conversion but low selectivity, whereas the latter showed high selectivity but lower conversion (Fig. 16(b)). Taken together, these results demonstrate that $[HPMo_8V_4O_{40}(VO)_2]^{4-}$ anion is primarily responsible for the efficient conversion of HMF, while the imidazole-functionalized V groups $[(VO)(1\text{-}mIM)_4]^{2+}$ play a key role in achieving high selectivity toward DFF (Fig. 16(c)). Under anaerobic conditions, HMF can be oxidized by an imidazole-functionalized Mo–V POM, achieving a conversion of maximum 44%, accompanied by the reduction of Mo^{VI} and V^V to Mo^V and V^{IV}, respectively. These observations indicate that both Mo and V centers within the cluster participate in the oxidation process. Upon the introduction of O_2, the conversion of HMF is further enhanced, and the reduced POM is reoxidized, thereby recovering its oxidative capability.

Recently, we synthesized a multi-ligand functionalized polyoxovanadate,

$V_6O_6(OCH_3)_4(mIM)_6(C_6H_5PO_3)_4$ (mIM = 1-methylimidazole).[144] The cluster features two $\{V_2O_6(OCH_3)_2\}$ units linked through four phenylphosphonate ligands to construct a $\{V_4O_4(OCH_3)_4(PhPO_3)_4\}$ unit, which is subsequently decorated on both sides with two $\{VO_3(mIM)_3\}$ (Fig. 17(a)). In this reaction, V plays a pivotal role (Fig. 17(b)). O_2 first oxidizes P_4V_6 to generate V^{5+} from V^{4+}, forming the oxidized active species $P_4V_{6(ox)}$, accompanied by the partial removal of mIM ligands. Subsequently, HMF adsorbs onto the surface of $P_4V_{6(ox)}$, which then oxidizes HMF via a proton coupled electron transfer (PCET) pathway to produce DFF, while itself being reduced to $P_4V_{6(red)}$. Finally, $P_4V_{6(red)}$ is reoxidized by O_2, thereby completing the catalytic cycle.

Huang and co-workers synthesized the catalyst, $[Pd(eIM)_4][V_6O_{16}(eIM)_4]$ (eIM = 1-ethyl imidazole, IPP-1), by the electrostatic assembly of Pd-complex with polyoxovanadate cluster.[66] This catalyst also exhibits excellent performance after 12 h (Figs. 18(a)-18(b)). The oxidation process proceeds via two parallel pathways (Fig. 18(c)). The first pathway centers on the Pd site. HMF adsorbs onto the catalyst surface, where its hydroxyl group forms hydrogen bonds with the imidazole ligands and/or V=O units. Initially, the hydroxyl hydrogen atom of HMF is transferred to a bridging oxygen atom in $[V_6O_{16}(eIM)_4]^{2-}$, accompanied by electron transfer to Pd^{2+}. This leads to the formation of DFF while simultaneously reducing Pd^{2+} to Pd^0.

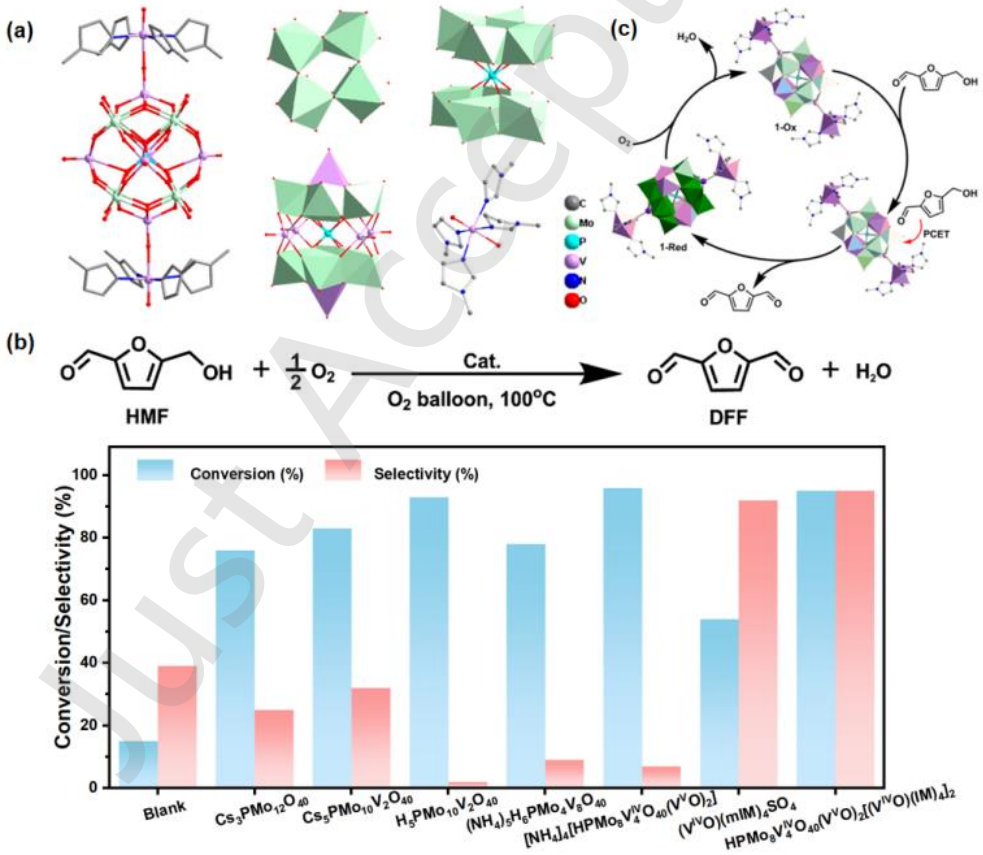

Fig. 16 (a) The structure of the catalyst . (b) Selective oxidation of HMF to DFF with various catalysts. (c) Mechanism of selective oxidation of HMF. Adapted with permission from Ref. [62], Copyright 2021 American Chemical Society.

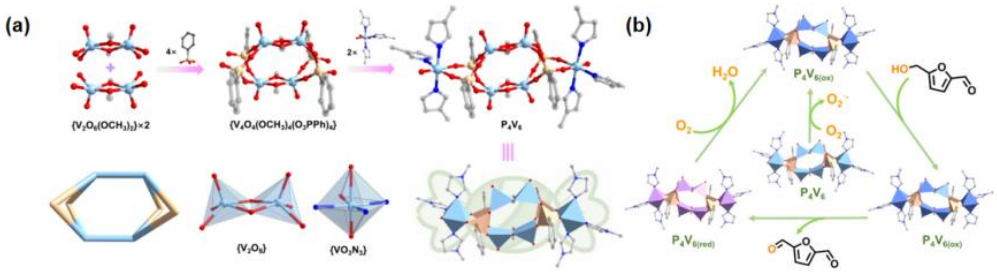

Fig. 17 (a) The sructure of P_4V_6. (b) Plausible mechanism of P_4V_6-mediated aerobic oxidation of HMF to DFF. Adapted with permission from Ref. [144], Copyright 2025 American Chemical Society.

Subsequently, Pd^0 is reoxidized by V^{5+}, which in turn is reduced to V^{4+}. Finally, V^{4+} is regenerated to V^{5+} by O_2, completing the catalytic cycle. The second pathway involves direct oxidation at the V center. Here, HMF is directly oxidized by the $[V_6O_{16}(eIM)_4]^{2-}$ anion via a PCET process, yielding DFF along with V^{4+} species. The V^{4+} species is then reoxidized to V^{5+} by O_2, thereby restoring the catalyst.

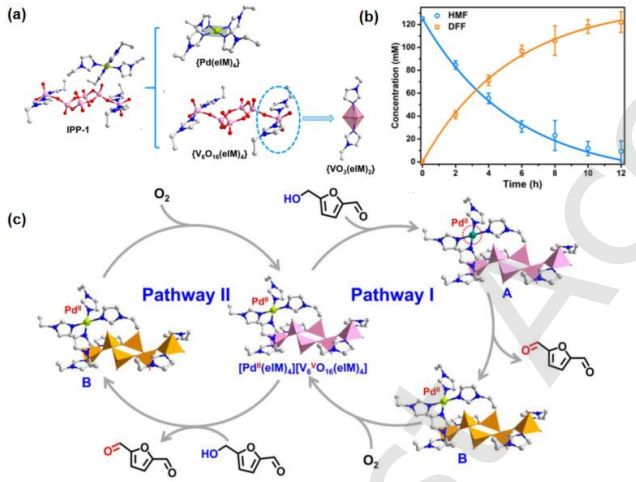

Fig. 18 (a) The structure of IPP-1. (b) Concentration variations of HMF and DFF with reaction time. (c) Plausible mechanism of HMF oxidation. Adapted with permission from Ref. [66], Copyright 2023 Elsevier Inc.

The catalytic performances of three representative polyoxovanadates, $HK_5(V_{10}O_{28})\cdot 20H_2O$ (V_{10}), $K_7[V_{15}O_{36}(CO_3)]\cdot nH_2O$ (V_{15}), and $K_{10}[V_{34}O_{82}]\cdot 20H_2O$ (V_{34}), have been systematically investigated by Gao *et al.*[67] V_{10} contains vanadium exclusively in the +5 oxidation state, V_{15} comprises seven V^{4+} and eight V^{5+} centers, and V_{34} consists of sixteen V^{4+} and eighteen V^{5+} centers (Fig. 19 (a)). Among these clusters, V_{34} exhibited the highest catalytic activity, indicating that the presence of mixed-valence V^{4+}/V^{5+} sites facilitates electron transfer between the catalyst and the substrate. Then, V_{34} was immobilized on a porous Fe_3O_4-doped carbon support obtained from carbonized MIL-88. Confining V_{34} within the pores of Fe_3O_4/C not only restricts active-site aggregation and substrate over-oxidation but also enables convenient magnetic recovery of the catalyst owing to the intrinsic magnetic properties of the Fe_3O_4/C support. Under 0.4 MPa O_2 at 110 °C, the resulting composite catalyst affords nearly quantitative HMF conversion with an almost 100% yield of DFF (Fig. 19(b)-19(c)).

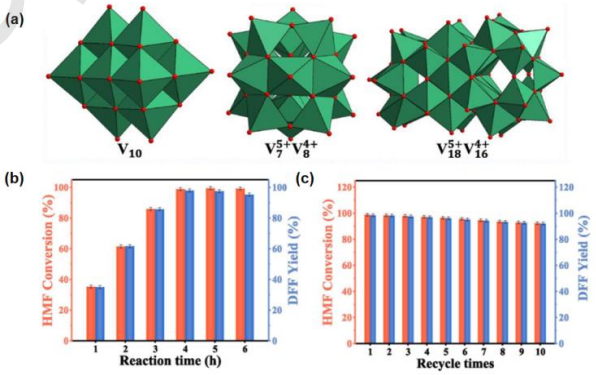

Fig. 19 (a) Polyhedral presentations of V_{10}, V_{15}, V_{34}. (b) HMF conversion and DFF yield at different reaction times. (c) Recycling tests for V_{34}-catalyzed HMF oxidation. Adapted with permission from Ref. [67], Copyright 2025 Elsevier Ltd.

While the aforementioned studies focus on thermocatalysis, the application of POMs in the electrocatalytic oxidation of HMF remains largely unexplored. In Lv's group, a robust Ru_4/PEI-rGO composite catalyst was fabricated by immobilizing $Rb_8K_2[Ru_4(\mu\text{-}O)_4(\mu\text{-}OH)_2(H_2O)_4(\gamma\text{-}SiW_{10}O_{36})_2]\cdot 25H_2O$ (Ru_4) on polyethyleneimine-functionalized reduced graphene oxide (PEI-rGO) (Fig. 20).[145] This architecture promotes efficient interfacial charge transfer and improved accessibility of active sites. Under an applied potential of 0.94 V (vs. Ag/AgCl) in a pH 6 HAc/NaAc buffer solution, electrolysis for 6 h

resulted in a 50.8% conversion of HMF with 66.2% selectivity toward DFF. However, with the addition of 2,2,6,6-tetramethylpiperidinyloxyl (TEMPO), the conversion of HMF surges to 99.7%, while the selectivity toward DFF drops to 0 with furanic carboxylic acids as the main product. The mechanistic investigation reveals that the sandwiched Ru centers in POM can shuttle between different oxidation states, thereby facilitating the conversion of HMF to DFF.

3.2.2 The Production of 5-formyl-2-furancarboxylic acid

FFCA is one of the intermediates in the production of FDCA, with promising applications as a chemical intermediate in drug synthesis, biomaterials, and other fields.[146] To obtain HMFCA, which contains –CHO and –COOH groups, two synthetic approaches have been established. In the first approach, the $–CH_2OH$ group in HMF is initially oxidized to –CHO to form

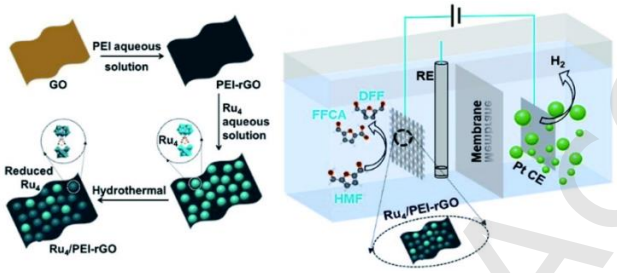

Fig. 20 Illustrations of Ru_4/PEI-rGO preparation pathway and electrocatalytic HMF conversion integrated with hydrogen production system. Adapted with permission from Ref. [145], Copyright 2022 The Royal Society of Chemistry.

DFF, followed by further oxidation of one aldehyde group to –COOH. In the alternative pathway, the native –CHO group in HMF is first oxidized to –COOH to yield HMFCA, after which the $–CH_2OH$ group is selectively oxidized to –CHO.

Lv and co-workers reported the use of Anderson-type $Na_3H_6FeMo_6O_{24}•5H_2O$ for the oxidation of HMF to FFCA.[147] In this system, Mo centers act as the primary catalytic active sites, with DFF inferred as a key reaction intermediate. Under optimal reaction conditions, the yield of the target product FFCA reached up to 75% at 100 °C under atmospheric O_2 over 8 h. Subsequently, the same group examined the catalytic performance of an Anderson-type POMs, $(NH_4)_3H_6CoMo_6O_{24}$ ($CoMo_6$), for FFCA formation (Fig. 21).[71] When conducted in deep eutectic solvents (DESs) at 130 °C for 8 h, the $CoMo_6$-based system enabled nearly complete conversion of HMF, affording a maximum FFCA yield of up to 97%. Notably, in contrast to their earlier study, HMFCA rather than DFF was identified as the key reaction intermediate in this process.

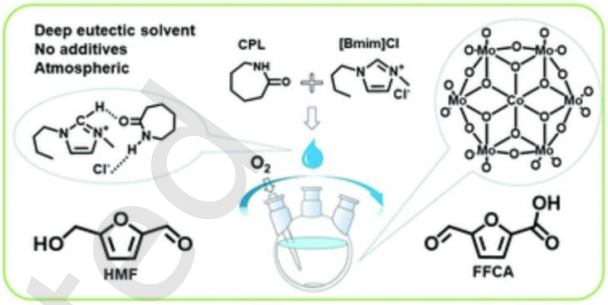

Fig. 21 $CoMo_6$ for the catalytic conversion of HMF to FFCA. Adapted with permission from Ref. [71], Copyright 2022 The Royal Society of Chemistry.

3.2.3 The Production of 5-hydroxymethyl-2-furan carboxylic acid

HMFCA serves as a pivotal intermediate in the synthesis of FDCA. Currently, research focusing on the conversion of HMF to HMFCA remains limited. Additionally, a prominent challenge lies in the cumbersome purification of HMFCA under alkaline reaction conditions.[148,149] Based on this, Zhang *et al.* developed a heterogeneous Ru/$CsPW_{12}$ catalyst through an impregnation method, wherein cesium-substituted tungstophosphate ($CsPW_{12}$) was supported on $RuCl_3•xH_2O$ followed by reduction with H_2.[150] Under optimized reaction conditions (130 °C, 6 h), a remarkable HMFCA yield (72.9%) was achieved.

3.2.4 The Production of 2,5-furandicarboxylic acid

As a critical building block, FDCA is employed to synthesize polyethylene furanoate (PEF), which serves as a viable substitute for petroleum-based polyethylene terephthalate in the plastics industry.[151] In FDCA production, several critical challenges remain, notably the difficulty of simultaneously activating both aldehyde and hydroxyl functionalities and achieving high selectivity toward FDCA. Compared with traditional aqueous solutions or organic solvents, imidazolium-based ILs exhibit superior solubility for furan derivatives, including HMF and FDCA. By

combining vanadium-substituted phosphomolybdic acid—possesses both Brønsted acidity and redox activity—with ILs, the issues can be effectively addressed.[152] The yield of FDCA can reach up to 89% after 6 h under the conditions of 140 ℃ and 1 MPa O_2. In this system, Mo/V bimetallic centers serve as the active sites to drive the oxidation reaction, while the ionic liquid activates HMF through hydrogen bonding interactions. Additionally, the ILs enhance the solubility of FDCA, thereby preventing aggregation of FDCA and suppressing side reactions under base-free conditions, ultimately enabling efficient and selective FDCA production.

Encapsulating POMs within MOFs represents a viable strategy to further enhance the stability of catalysts. Bhargava *et al.* encapsulated PMo_{12} into the Cu-BTC, successfully fabricating a PMo_{12}-Cu-BTC composite catalyst (Fig. 22(a)).[57] The catalyst enables the efficient conversion of HMF to FDCA under base-free and mild reaction conditions (120 ℃, 2 MPa O_2, 4 h), achieving an HMF conversion of 89.4% and an FDCA selectivity of 92.3%. In this composite system, PMo_{12} generates novel Cu–O–Mo synergistic sites via interfacial interactions with Cu-BTC (Fig. 22(b)-22(c)). Meanwhile, the porous structure of MOFs effectively inhibits the aggregation of PMo_{12} and contributes to the adsorption of HMF. This rational design effectively overcomes the intrinsic limitations of single-component catalysts, namely the relatively low catalytic activity of pristine MOFs and the susceptibility of POMs to leaching under catalytic conditions. The reaction pathway was elucidated by in situ ATR-IR spectroscopy through monitoring the evolution of key intermediates (DFF and FFCA). The formation of PMo_{12}-Cu-BTC interfacial synergistic sites was confirmed by EXAFS, while XANES disclosed the electronic state variations of Cu and Mo, supporting a charge-transfer mechanism. These experimental insights were further corroborated by theoretical calculations.

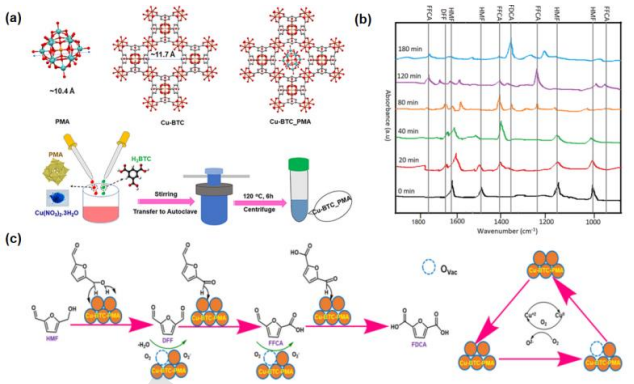

Fig. 22 (a) Structure and preparation process of PMo_{12}-Cu-BTC. (b) In situ ATR-IR spectra of HMF conversion reaction. (c) Plausible mechanistic pathway for HMF to FDCA. Adapted with permission from Ref. [57], Copyright 2023 American Chemical Society.

3.2.5 The Production of Maleic Acid and Maleic Anhydride

Maleic acid and maleic anhydride are a vital chemical raw material with high reactivity with extensive applications in synthetic resins, coatings, pharmaceuticals, pesticides and so on. Yin *et al.* developed a route for the preparation of maleic anhydride and maleic acid via the aerobic oxidation of HMF using vanadium-substituted POMs.[61] Among the catalysts, $PMo_{10}V_2$ exhibited the highest catalytic activity. When the reaction is conducted at 90 ℃ under 1 MPa O_2, the yield of maleic acid and maleic anhydride are 31.7% and 32.3%, respectively. A series of control experiments excluded the involvement of conventional oxidation intermediates—FDCA, DFF, FFCA, and HMFCA—in the reaction pathway. Mechanistic studies revealed that $PMo_{10}V_2$ triggers the reaction through an electron transfer-oxygen transfer (ET-OT) process, which cleaves the C–C bond between the hydroxymethyl group and the furan ring of HMF (Fig. 23). This is followed by a 1,4-rearrangement, hydrogen abstraction from the aldehyde group, and decarbonylation, ultimately yielding maleic anhydride, which can be further hydrolyzed to maleic acid under the reaction conditions.

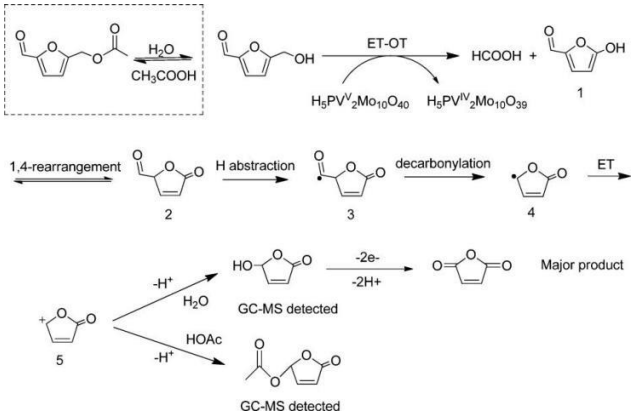

Fig. 23 Proposed mechanism for HMF oxidation mediated by $PMo_{10}V_2$. Adapted with permission from Ref. [61], Copyright 2015 American Chemical Society.

Recently, Lyu *et al.* fabricated a composite catalyst denoted as LCN/HPA-5 by loading $H_8[PV_5Mo_7O_{40}]$ (HPA-5) on nitrogen-deficient graphitic carbon nitride (LCN).[153] A photothermal catalytic strategy was employed for the selective oxidation of HMF, in which maleic anhydride was identified as the key intermediate and subsequently hydrolyzed to maleic acid. Under irradiation from a 300 W xenon lamp at 90 ℃ and 0.6 MPa O_2 for 4 h, a maleic acid yield of 50.8% was achieved.

Oxidation of HMF over POM-based catalysts has been predominantly investigated under thermocatalytic conditions, whereas photocatalytic oxidation remain largely underexplored. In this context, Lv and co-workers reported a photocatalytic HMF oxidation system employing $[W_{10}O_{32}]^{4-}$ as the catalyst with 2,2,6,6-tetramethylpiperidinyloxyl (TEMPO) as co-catalyst.[154] Under 365 nm light irradiation or 2 h, and the HMF conversion reached 88.0%, however, a mixture of furanic products was obtained, including DFF (yield: 14.0%), FDCA (yield: 7.7%), HMFCA (yield: 20.3%), and FFCA (yield: 28.2%). Under 365 nm irradiation, photoexcited $[W_{10}O_{32}]^{4-}$ activates TEMPO via a single-electron transfer (SET) process to generate $TEMPO^+$, which selectively oxidizes hydroxymethyl groups in HMF/HMFCA to form DFF and FFCA. Meanwhile, excited $[W_{10}O_{32}]^{4-}$ can directly promote oxidation of HMF intermediates, particularly the conversion of FFCA to FDCA. Both $[W_{10}O_{32}]^{4-}$ and TEMPO are regenerated by O_2 and hydrogen atom transfer (HAT) processes, enabling a photocatalytic cycle.

Table 1 Selective oxidation of HMF to DFF catalyzed by POMs.

Catalysts	Oxidant	Temp. (℃)	Time (h)	Conv. (%)	Yield (%)	TOF (h^{-1})	Ref.
$(NH_4)_6Mo_7O_{24}$	Air	130	6	36.7	25.7	61.17	[129]
$(NH_4)_{12}[Mo_{36}(NO)_4O_{108}(H_2O)_{16}]\cdot 33H_2O$	Air	130	6	87.4	87.4	145.67	
$(NH_4)_{42}[Mo^{VI}_{72}Mo^{V}_{60}O_{372}(CH_3COO)_{30}(H_2O)_{72}$	Air	130	6	99.2	99.2	165.33	
40-PMo_{12}/PAN	Air	160	4	97.2	94.0	17.91	[131]
40-PMo_{12}/F_3-PAN	Air	160	5	100.0	99.9	49.98	
$(H_2O)_3Cl_{0.5}(pdc)][La(H_2O)_4(pdc)]\}_2[PMo_{12}O_{40}]\cdot 2H_2O$	1.0 Mpa O_2	140	8	99	99	2.48	[132]
$[La(H_2O)_4(pdc)]_4[SiW_{12}O_{40}]\cdot 2H_2O$	1.2 Mpa O_2	140	8	90	90	2.25	
$H_5PMo_{10}V_2O_{40}$	1.0 Mpa O_2	120	8	99	50	1.46	[133]
$H_5PMo_{10}V_2O_{40}/SiO_2$	1.0 Mpa O_2	120	8	92.7	89.2	14.57	
$H_5PMo_{10}V_2O_{40}/SiO_2$-$NH_2$	1.0 Mpa O_2	120	8	93.2	90.0	11.43	[134]
$H_5PMo_{10}V_2O_{40}$@surf(4)/CeO_2[a]	1.0 Mpa O_2	120	6	100	95.3	12.28	[135]
$H_5PMo_{10}V_2O_{40}$/chitosan	0.8 Mpa O_2	120	6	96.2	94.1	15.57	[136]

Catalysts	Oxidant	Temp. (℃)	Time (h)	Conv. (%)	Yield (%)	TOF (h^{-1})	Ref.
$H_5PMo_{10}V_2O_{40}$@Mg_4Al-Surf	1.0 Mpa O_2	140	12	94.6	83.8	15.08	[137]
$Mo_{72}V_{30}$@Fe_3O_4/C	0.4 Mpa O_2	120	4	99.4	99.0	176.79	[138]
$H_5PMo_{10}V_2O_{40}$@Co_3O_4/C	1.4 Mpa O_2	130	6	98.7	~98.7	7.90	[139]
$H_5PMo_{10}V_2O_{40}$@Fe_3O_4/C	0.8 Mpa O_2	130	6	99.1	~99.1	18.00	
PMo_4V_8/HAP[b]	O_2	130	8	96.0	83.8	9.38	[140]
$PMo_4V_8/SiO_2(C_8/C_8NH_2)$[c]	O_2	130	10	81.8	73.7	6.81	[141]
$CsH_3PMo_{11}VO_{40}$	O_2	120	3	84	73	3.10	
$CsH_3PMo_{11}VO_{40}$	O_2	120	6	＞99	95	2.02	
$Cs_2H_2PMo_{11}VO_{40}$	O_2	120	3	82	75	3.19	
$Cs_2H_2PMo_{11}VO_{40}$	O_2	120	6	＞99	99	2.10	
$Cs_3HPMo_{11}VO_{40}$	O_2	120	3	78	71	3.02	[142]
$Cs_3HPMo_{11}VO_{40}$	O_2	120	6	＞99	＞99	2.10	
$CsH_4PMo_{10}V_2O_{40}$	O_2	120	3	88	82	1.70	
$CsH_4PMo_{10}V_2O_{40}$	O_2	120	6	＞99	＞99	1.03	
$Cs_3H_3PMo_9V_3O_{40}$	O_2	120	3	95	89	1.20	
$Cs_3H_3PMo_9V_3O_{40}$	O_2	120	6	＞99	81	0.55	
$H_7PMo_8V_4O_{40}$	Air	110	1.5	＞99	82.2	0.14	
$H_{10}P_3Mo_{18}V_7O_{84}$	Air	110	1.5	＞99	89.6	0.10	
$H_{17}P_3Mo_{16}V_{10}O_{89}$	Air	110	1.5	＞99	90.1	0,07	[143]
$Na_2H_5PMo_8V_4O_{40}$	Air	110	1.5	＞99	85.3	0.15	
$Co_2H_6P_3Mo_{18}V_7O_{84}$	Air	110	1.5	＞99	92.1	0.10	
$Cs_3PMo_{12}O_{40}$	O_2 balloon	100	4	76	19	0.52	
$Cs_5PMo_{10}V_2O_{40}$	O_2 balloon	100	4	83	27	0.73	
$H_5PMo_{10}V_2O_{40}$	O_2 balloon	100	4	93	2	0.51	
$(NH_4)_5H_6PMo_4V_8O_{40}$	O_2 balloon	100	4	78	7	1.93	[62]
$(NH_4)_4[HPMo_8V^{IV}_4O_{40}(V^{V}O)_2]$	O_2 balloon	100	4	96	7	1.85	
$HPMo_8V^{VI}_4O_{40}(V^{V}O)_2[(V^{IV}O)(IM)_4]_2{\cdot}4H_2O{\cdot}(IM)_8$	O_2 balloon	100	4	95	90	2.48	
$HPMo_8V^{VI}_4O_{40}(V^{V}O)_2[(V^{IV}O)(IM)_4]_2{\cdot}4H_2O{\cdot}(IM)_9$	O_2 balloon	100	4	94	89	2.46	
$HPMo_8V^{VI}_4O_{40}(V^{V}O)_2[(V^{IV}O)(IM)_4]_2{\cdot}(IM)_4$	O_2 balloon	100	4	92	87	2.40	[62]

Catalysts	Oxidant	Temp. (℃)	Time (h)	Conv. (%)	Yield (%)	TOF (h^{-1})	Ref.
$V_6O_6(OCH_3)_4(mIM)_6(C_6H_5PO_3)_4$	O_2 balloon	90	5	95	89	0.42	[144]
$[Pd(eIM)_4][V_6O_{16}(eIM)_4]$	O_2 balloon	90	12	93	91	13.7	
$[Pd(mIM)_4]_2(H_2V_{10}O_{28})\cdot 3H_2O$	O_2 balloon	90	12	68	41	2.43	[66]
$[Pd(mIM)_4]_2(V_4O_{12})\cdot 4H_2O$	O_2 balloon	90	12	76	54	3.21	
$HK_5(V_{10}O_{28})\cdot 20H_2O$	Air	130	6	92.1	90.9	0.01	
$K_7[V_{15}O_{36}(CO_3)]\cdot nH_2O$	Air	130	6	85.2	84.1	0.01	
$K_{10}[V_{34}O_{82}]\cdot 20H_2O$	Air	130	6	98.7	97.2	0.01	
$K_4[PW_{11}VO_{40}]\cdot 2H_2O$	Air	130	6	10.1	7.9	0.0009	[67]
$H_5[PW_{10}V_2O_{40}]\cdot 35H_2O$	Air	130	6	11.6	7.4	0.0008	
$H_6PW_9V_3O_{40}$	Air	130	6	16.1	3.9	0.0004	
$K_{10}[V_{34}O_{82}]\cdot 20H_2O@Fe_3O_4/C$	0.4 Mpa O_2	110	4	98.9	98.5	1.52	
Ru_4/PEI-rGO[d]	electricity	R. T.	6	50.8	33.6	0.56	[145]

[a] $H_5PMo_{10}V_2O_{40}$ (HPMoV) immobilized on nanofibers functionalized with C4 amino-surfactant.

[b] Hydroxyapatite (HAP) supported $(NH_4)_5H_6PMo_4V_8O_{40}$ (PMo_4V_8/HAP).

[c] $(NH_4)_5H_6PMo_4V_8O_{40}$($PMo_4V_8$) immobilized on alkyl/alkyl-amino grafted functionalized silica nanoparticles (Pickering catalyst).

[d] $Rb_8K_2[Ru_4(\mu\text{-}O)_4(\mu\text{-}OH)_2(H_2O)_4(\gamma\text{-}SiW_{10}O_{36})_2]\cdot 25H_2O$ (Ru_4) clusters uniformly deposited on PEI-functionalized reduced graphene oxide (PEI-rGO).

Table 2 Selective oxidation of HMF to FDCA catalyzed by POMs.

Catalysts	Oxidant	Temp. (℃)	Time (h)	Conv. (%)	Yield (%)	TOF (h^{-1})	Ref.
$H_3PMo_{12}O_{40}$	1.0 Mpa O_2	140	6	98.1	83.3	0.51	
$H_3PW_{12}O_{40}$	1.0 Mpa O_2	140	6	99.8	18.5	0.11	
$H_4SiMo_{12}O_{40}$	1.0 Mpa O_2	140	6	99.8	8.6	0.05	
$H_4SiW_{12}O_{40}$	1.0 Mpa O_2	140	6	99.7	38.4	0.23	
$HPMV_1$[a]	1.0 Mpa O_2	140	6	99.4	70.6	0.43	[152]
$HPMV_2$	1.0 Mpa O_2	140	6	99.7	68.8	0.42	
$HPMV_3$	1.0 Mpa O_2	140	6	99.8	45.0	0.27	
$HPMV_4$	1.0 Mpa O_2	140	6	99.8	23.8	0.14	
$HPMV_5$	1.0 Mpa O_2	140	6	99.4	44.6	0.27	
$HPMV_6$	1.0 Mpa O_2	140	6	99.4	88.8	0.54	
Cu-BTC_PMA[b]	2.0 Mpa O_2	120	5	89.4	82.5	-	[57]

[a] $HPMV_n$ (n=1~6) : V-substituted $H_3PMo_{12}O_{40}$ derivatives.

[b] PMA($H_3PMo_{12}O_{40}$) encapsulated in Cu-BTC MOFs (Cu-BTC_PMA).

The thermal oxidation of HMF has been extensively investigated, particularly for the production of DFF, primarily with molecular oxygen as the oxidant. Keggin-type polyoxomolybdates and their vanadium-containing derivatives and polyoxovanadates, are widely used. Typical reaction conditions involve temperatures of 90 ~ 160 °C and O_2 pressures ranging from ambient pressure (using an air balloon) to 2.0 MPa, with increasing efforts directed toward milder, ambient-pressure operations. For the oxidation of HMF and FF, molecular oxygen or air are the most commonly used oxidants. High-boiling-point solvents are generally preferred as reaction media, including dimethyl sulfoxide (DMSO), toluene, chlorobenzene, and deep eutectic solvents (DESs), which can effectively suppress solvent volatilization and thermal decomposition under reaction conditions. Mechanistically, HMF adsorbs onto the POM surface, where active sites such as Mo^{6+}/V^{5+} oxidize the hydroxyl group to a carbonyl and the reduced catalytic active centers are reoxidized by O_2. In some case, the heteroatom in POMs, such as Fe, Co, can further facilitate the regeneration of POM catalysts. Compared with DFF production, oxidative transformation of HMF into carboxylic acids remains less explored, and corresponding mechanistic understanding is quite limited. For FFCA formation, different POM systems show distinct pathways: in $(NH_4)_3H_6CoMo_6O_{24}$, the aldehyde is first oxidized to HMFCA, followed by hydroxyl oxidation to FFCA, whereas in $Na_3H_6FeMo_6O_{24} \cdot 5H_2O$, hydroxyl oxidation to DFF precedes nucleophilic addition and dehydrogenation to FFCA. FDCA formation generally proceeds through the DFF and FFCA intermediates, with Mo and V centers serving as the catalytic active sites for the stepwise oxidation.

4 Reduction of FF and HMF

This section focuses on the reductive transformations of FF and HMF catalyzed by POM-based systems. According to the nature of the hydrogen source, these reductive transformations can be classified into three categories, involving molecular hydrogen, alcohols (most commonly isopropanol), and, in electrocatalytic systems, water. Among them, the reductive conversion of FF using isopropanol as a hydrogen donor has been most extensively investigated. For each representative example, attention is paid to the preparation of the POM-based catalyst, the specific role of POMs in the catalytic process, the catalytic performance (conversion, product yield, and catalyst stability), as well as the catalytic mechanism.

4.1 Molecular hydrogen as reductant

Molecular hydrogen (H_2) is one of the most widely used hydrogen sources for the reduction of FF and HMF over metal-based catalysts.[37] However, studies involving POM-based catalytic systems remain rather limited, primarily because POMs themselves are generally incapable of directly activating H_2. Yadav *et al.* reported a bifunctional metal-acid catalyst, Pd-CsDTP/K-10, which can convert HMF into 2,5-dimethyl furan (DMF), a promising candidate for biofuel blending (Fig. 24).[155] The catalyst was fabricated by co-loading $Cs_{2.5}H_{0.5}PW_{12}O_{40}$ ($CsPW_{12}$) and Pd on montmorillonite K-10 clay, which achieves 98% HMF conversion, yielding 81% DMF under relatively mild conditions (90 °C, 1.0 MPa H_2, 2 h). Real-time analysis shows that the concentration of bis(hydroxymethyl)furan (BHMF) initially increased and then decreased as the reaction proceeds, while the concentration of DMF increases correspondingly, confirming BHMF as a reaction intermediate. Generally, the conversion of HMF to DMF proceeds via an initial hydrogenation to form BHMF, followed by the hydrogenolysis of BHMF to yield DMF. Compared with hydrogenation of HMF, the hydrogenolysis of BHMF is more challenging. It is found that homogeneous strong acid, such as HCl, can promote the hydrogenolysis of BHMF to DMF. In this catalytic system, Pd activates H_2 playing a pivotal role in the hydrogenation process, while $CsPW_{12}$ acting as a recyclable solid acid, enables the hydrogenolysis of BHMF to occur under mild conditions.

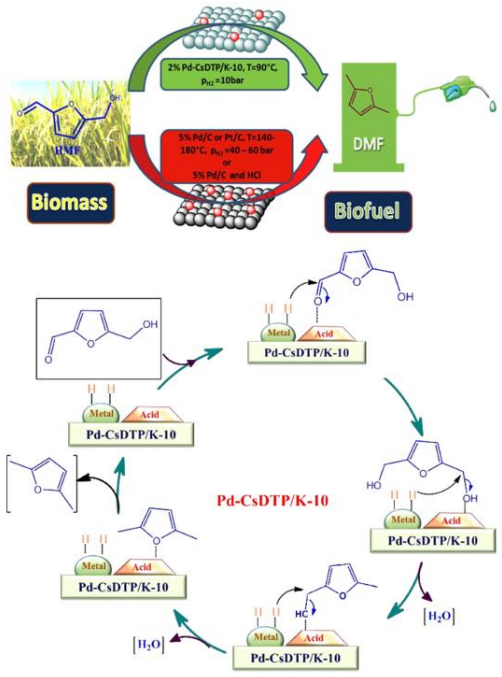

Fig. 24 Pd-CsDTP/K-10 for HMF conversion to DMF and its proposed reaction mechanism. Adapted with permission from Ref. [155], Copyright 2016 American Chemical Society.

4.2 Alcohols as Hydrogen Source

Alcohols are well-suited for the catalytic transfer hydrogenation (CTH) reaction mechanism. The hydrogen atoms on the α–C of alcohols have reduced electron density due to the electron-withdrawing effect of the hydroxyl group. These hydrogen atoms can be readily abstracted with the help of Lewis acid sites, forming H^- or hydrogen radicals that serve as transferable hydrogen species. Compared to H_2 as a hydrogen source, alcohols offer enhanced safety. Currently, isopropanol is widely utilized, primarily due to its structural symmetry and moderate steric hindrance. These properties not only ensure the ready removal of hydrogen atoms but also facilitate efficient interaction with the active sites of the catalyst.

4.2.1 Production of furfuryl alcohol

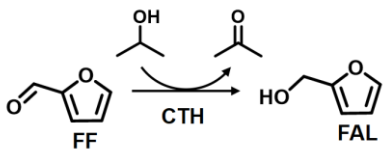

Scheme 5 The conversion of FF to FAL.

FF can be reduced to furfuryl alcohol (FAL) via CTH (Scheme 5). FAL is a key platform chemical derived from biomass, with applications spanning multiple fields including chemical engineering, materials science, and pharmaceuticals—such as the synthesis of high-value-added chemicals and solvents. Intrinsically, the CTH process is acid-base-driven reaction, and their catalytic performance depends on the synergistic cooperation between Lewis acid sites and Brønsted acid sites. Along this line, Fu *et al.* reported bimetallic cluster catalysts (yPOMs/UiO-66x), prepared by immobilizing POM clusters onto Zr-based metal-organic frameworks (UiO-66x) via a microwave-assisted approach (Fig. 25(a)).[156] At 40 °C, the reaction achieves a FAL yield of 96.0% with a selectivity of 98.1%. When the temperature is elevated to 80 °C, the yield and selectivity are further enhanced to 99.2% and 99.4%, respectively. Notably, the catalyst maintains exceptional catalytic performance even after six consecutive recycles. DFT calculations revealed that the synergistic W^{6+}–O^{2-}–Zr^{4+} acid-base sites facilitate the dissociation of the α–C(sp^3)–H bond in isopropanol and the subsequent transfer of hydrogen to the activated carbonyl group in FF (Fig. 25(b)).

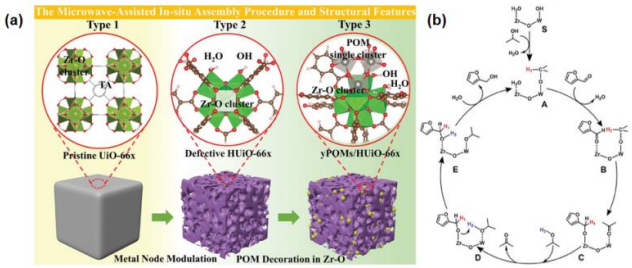

Fig. 25 (a) The structure of yPOMs/UiO-66x (Right). (b) Proposed reaction mechanism over POMs/Zr-MOFs. Adapted with permission from Ref. [156], Copyright 2024 Wiley-VCH GmbH.

4.2.2 Production of levulinic acid

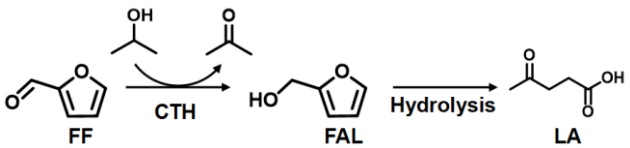

Scheme 6 The conversion of FF to LA.

As a pivotal platform chemical, LA bridges biomass resources and a wide range of high-value-added products. Usually, the transformation of FF to LA involves two cascade steps: (i) the

hydrogenation of FF to FAL, followed by (ii) the acid-catalyzed hydrolysis of FAL to yield LA (Scheme 6). This requires Lewis acid sites in step (i) and Brønsted acid sites in step (ii). By impregnating $H_3PW_{12}O_{40}$ on high surface area of SiO_2, Bokade *et al*. synthesized a bifunctional catalyst, $H_3PW_{12}O_{40}/SiO_2$, possessing both Lewis and Brønsted acid sites.[157] This catalyst enabled the one-pot cascade of FF to LA with a yield up to 51% at 170 ℃ for 12 h, with the alcohol solvent serving dual roles as both the reaction medium and the hydrogen source.

4.2.3 Production of isopropyl levulinate

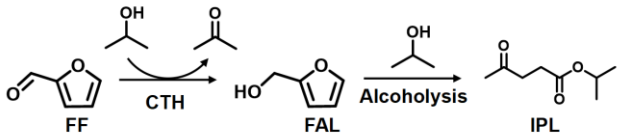

Scheme 7 The conversion of FF to IPL.

Starting from FF, isopropyl levulinate (IPL) can be obtained in one pot via the formation of LA followed by esterification (Scheme 7). IPL has broad applications, serving as a fuel oxygenate additive, a flavor enhancer, and a key precursor for the production of γ-valerolactone. In 2016, Fan *et al*. reported a metal-acid bi-functional catalyst Au-$H_4SiW_{12}O_{40}/ZrO_2$ for the conversion of FF to IPL.[158] First, $H_4SiW_{12}O_{40}$ is loaded onto the ZrO_2 support via impregnation method, followed by the deposition and reduction of Au onto $H_4SiW_{12}O_{40}/ZrO_2$ under ultrasound assistance, ultimately yielding the Au-$H_4SiW_{12}O_{40}/ZrO_2$ catalyst. Under the conditions of 120 ℃ and 0.1 MPa N_2 for 24 h, the yield of IPL reaches 80.2%. Additionally, the catalyst is also applicable to the reaction of FF with ethanol, 2-butanol, 1-propanol, and 1-butanol, demonstrating its excellent compatibility with various alcohols. In this reaction, Au exhibits extremely high selectivity towards the reduction of –CHO group in FF, effectively promoting the formation of FAL. Meanwhile, the presence of POMs facilitates the acid-catalyzed alcoholysis of FAL to produce IPL, while ZrO_2 serves as a support and plays a crucial role in regulating catalytic activity. In 2021, a series of bifunctional zirconia-zeolite-supported POMs (POMs = $[PW_{12}O_{40}]^{3-}$, $[PMo_{12}O_{40}]^{3-}$, $[SiW_{12}O_{40}]^{4-}$) catalysts with tunable Lewis and Brønsted acid sites were successfully fabricated via an in-situ synthesis strategy by He *et al*.[159] $H_3PMo_{12}O_{40}$/Zr-MCM-41 exhibits the optimal catalytic activity. Under the reaction conditions of 150 ℃ and 24 h, the FF conversion reaches 99.3%, with the IPL yield as high as 79.6%.

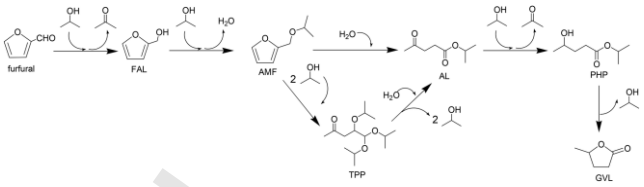

Fig. 26 Reaction pathway of FF conversion to IPL. Adapted with permission from Ref. [158], Copyright 2016 The Royal Society of Chemistry.

In above mentioned studies, catalysts have generally been constructed by immobilizing Brønsted-acidic POMs onto supports featuring Lewis acid sites. More recently, Guo *et al*. proposed an alternative catalyst design strategy, synthesizing a series of dual-acidic POMs, $M_xH_yPW_{12}O_{40}$ (M = Sn, Fe, Zn, Ni, Cu), via an ion-exchange method in which the Lewis-acidic metal centers directly interact with the polyanion clusters to form insoluble salts.[160] By allowing precise tuning of Lewis and Brønsted acid sites, $M_xH_yPW_{12}O_{40}$ catalysts address two major liminations of conventional supported systems: poor synergistic effects and the resultant low catalytic activity and selectivity, which stem from an inability to regulate Lewis and Brønsted acid properties in CTH-alcoholysis cascade reactions. In addition, the "pseudo liquid-phase" behavior of the POMs also contributes to the improvement of catalytic performance. Among the synthesized catalysts, $Sn_{0.25}H_2PW_{12}O_{40}$ exhibited the best catalytic activities, giving IPL yield up to 91.6% at 170 ºC for 120 min.

4.2.4 Production of γ-valerolactone

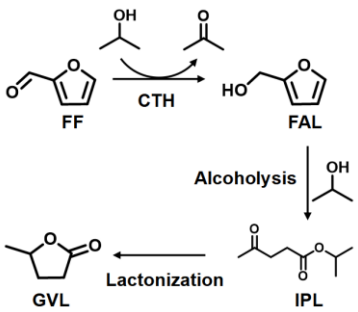

Scheme 8 The conversion of FF to GVL.

FF can also be converted to γ-valerolactone (GVL) through a multi-step cascade as shown in Scheme 8. GVL is a versatile molecule with a wide range of applications, serving as an illuminating liquid, a high-performance biofuel, and a promising fuel additive, as well as a key precursor for the synthesis of liquid alkanes and high-value biopolymers.[161] In 2019, Jae *et al.* successfully synthesized the PW_{12}/Zr-Beta catalyst by supporting $H_3PW_{12}O_{40}$ (PW_{12}) on Zr-Beta zeolite via the incipient wetness impregnation method.[162] The incorporation of PW_{12} significantly enhanced the catalyst's hydrolytic ring-opening capability. Moreover, PW_{12} and Zr active sites exhibited a synergistic effect, which remarkably accelerated the GVL formation rate from LA. As a result, the PW_{12}/Zr-Beta catalyst demonstrated exceptional performance in the one-pot conversion of FF to GVL. Eventually, a remarkable GVL yield of approximately 70% was achieved under mild reaction conditions (160 ºC, 24 h).

Later, Lingaiah *et al.* successfully fabricated the catalyst PW_{12}/ZrO_2-SBA-15 by dispersing PW_{12} onto ZrO_2-doped mesoporous silica SBA-15, which showed the high activity with complete conversion of FF and a GVL yield of 81% after 11 h at 170 ºC[163]. In addition, combining Zr-based MOFs with POMs is also a judicious choice. For instance, Unlu *et al.* supported PW_{12} on UiO-66. At 90 ºC, FF was completely converted with a GVL yield of up to 94.21%. More importantly, after 10 cycles of reuse, the catalyst retained a FF conversion of 96% and a GVL yield of 85%, showing negligible activity loss[164]. Similarly, Feng *et al.* confined PW_{12} within Zr-MOFs for the conversion of FF to GVL, achieving a GVL yield of 58.1%[165]. Recently, the bifunctional PW_{12}/Hf-SBA-15 (W/Hf = 0.37) catalyst was successfully fabricated via a sequential wet impregnation method by Xue *et al.*. Under the reaction conditions of 170 ºC for 4 h, the selectivity of GVL reached 73.5%. Specifically, Hf provides Lewis acid sites to mediate hydrogen transfer reactions, while PW_{12} acts as Brønsted acid sites to promote the ring-opening process. The synergistic effect between Lewis acid sites and Brønsted acid sites is the key for achieving high GVL selectivity[166].

Table 3 Catalytic conversion of FF to LA/AL/IPL/GVL by POM catalysts.

Catalyst	Product	Temp. (℃)	Time (h)	Conv. (%)	Yield (%)	TOF (h^{-1})	Ref.
50(wt.%)$H_3PW_{12}O_{40}/SiO_2$	LA	170	12	—	51	6.12	[157]
Au-$H_4SiW_{12}O_{40}/ZrO_2$	AL	120	24	100	80.2	1.51	[158]
$H_3PMo_{12}O_{40}$(20)/Zr-MCM-41[a]	IPL	150	24	99.3	79.6	1.05	[159]
$Sn_{0.25}H_2PW_{12}O_{40}$	IPL	170	2	95.4	91.6	1.90	[160]
$H_3PW_{12}O_{40}$/Zr-Beta[b]	GVL	160	24	100	68.0	0.49	[162]
$H_3PW_{12}O_{40}/ZrO_2$-SBA-15[c]	GVL	170	11	100	81	28.7	[163]
$H_3PW_{12}O_{40}$-UiO-66[d]	GVL	90	7	100	94.21	13.4	[164]
POMOF-PW[e]	GVL	160	23	—	58.1	1.46	[165]
$H_3PW_{12}O_{40}$/Hf-SBA-15_0.37 (W/Hf = 0.37)	GVL	170	4	100	73.5	353.8	[166]

[a]Zirconia and $H_3PMo_{12}O_{40}$ catalysts supported on zeolite fabricated via an in-situ approach.

[b]Zr-Beta: Zr-Beta zeolites.

[c]SBA-15: an ordered mesoporous neutral material with large surface area, widely employed as catalyst support in diverse reactions.

[d]UiO-66: the zirconium-based MOF.

[e]The postsynthetic functionalization of Zr-MOF via incorporation of $H_3PW_{12}O_{40}$.

4.2.5 Production of 5-hydroxymethylfurfuryl alcohol

Scheme 9 The conversion of FF to MFA.

The previous studies have focused on the reductive conversion of FF, whereas reports on the reduction of HMF are limited. Starting from HMF, 5-methylfurfuryl alcohol (MFA) can be obtained (Scheme 9). MFA serves as a versatile building block that enables the synthesis of diverse high-value materials, including flame-retardant composites. Additionally, it acts as a key intermediate in the production of bio-oil additives, flavor enhancers, and food preservatives. A lignin-MOF-based catalyst (Ni_3Co-MOF-LS) modified with silicotungstic acid (SiW_{12}) was fabricated, in which the Ni and Co metallic sites, coupled with the acidic sites of SiW_{12}, enabled complete HMF conversion (100%) and a high MFA yield of 86.5% (240 °C, 2 MPa N_2).[167] Both total acidity and the distribution of strong to medium–strong acid sites were essential for effective adsorption and desorption of reactants and intermediates.

4.3 Water as Proton Source in Electrocatalytic Reduction of FF and HMF

Conventional thermal hydrogenation generally requires harsh reaction conditions, such as elevated temperatures and high H_2 pressures, which result in high energy consumption and stringent equipment requirements. Moreover, the use of molecular hydrogen poses inherent safety concerns due to its flammability, including risks of leakage and explosion.[168] In addition, the high reaction temperatures often lead to undesired side reactions, decreasing the selectivity toward the target product.[169] Although alcohols can be employed as alternative hydrogen donors to avoid the direct use of molecular H_2, alcohol-based transfer hydrogenation often suffers from low hydrogen utilization efficiency, unavoidable by-product formation from alcohol oxidation, and increased energy and separation costs.

4.3.1 Fundamentals of Electrocatalytic Reduction Using Water as Proton Source

In contrast, electrocatalysis offers several

advantages over conventional thermocatalysis. Firstly,

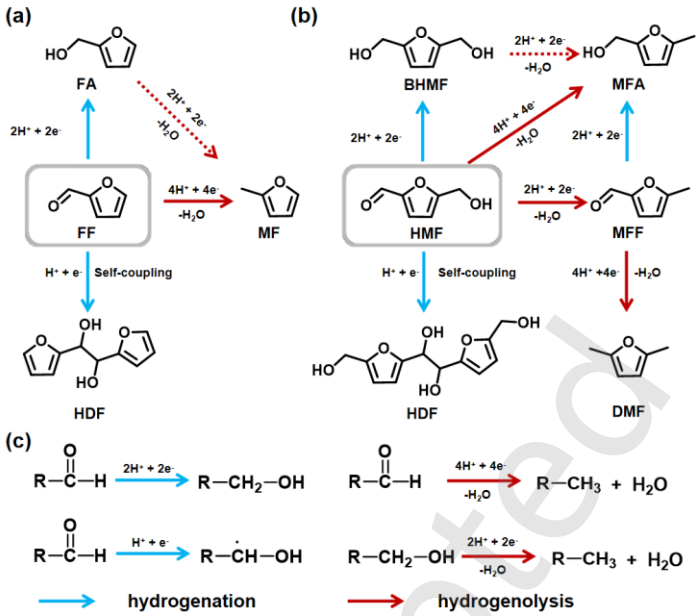

Scheme 10 The major pathways and products in the electrocatalytic reduction of FF and HMF.

electrocatalytic reactions generally proceed under mild conditions with lower energy consumption, thereby avoiding the harsh high-temperature and high-pressure environments required in traditional approaches. Additionally, the electrical energy driving electrocatalysis can be readily supplied by renewable sources, such as wind, solar, and tidal power, enhancing the overall sustainability of the process.[170] Furthermore, the use of water as a hydrogen source makes electrocatalysis both economically attractive and environmentally friendly.

The reduction of FF and HMF primarily involves C=O and C–O bonds and can proceed via hydrogenation, hydrogenolysis or dimerization pathways. Hydrogenation of the C=O bond adds hydrogen without cleaving the C–O bond, forming alcohols, whereas hydrogenolysis cleaves C–O, converting C=O or C–O into $–CH_3$. Dimerization involves C–C coupling of ketyl radicals generated during the reduction of HMF or FF, including reactions such as aldol condensation and hydroxyalkylation/alkylation (Scheme 10). The electroreduction of FF and HMF involves multiple parallel and competing reaction pathways, which often leads to low selectivity toward the desired reduction products. Moreover, because these reactions are typically carried out in aqueous media, the competing hydrogen evolution reaction (HER) is unavoidable, thereby diminishing the Faradaic efficiency. It has been demonstrated that electrocatalytic performance can be regulated by various factors, including electrolyte pH, applied potential, reactant concentration, electrolyte composition, and the nature of the catalyst. Among these parameters, the catalyst plays a particularly critical role in governing product selectivity.[171] In this context, the design of electrocatalysts becomes crucial for the enhancement of catalytic activities. Currently, research on the electrocatalytic reduction of FF and HMF has mainly focused on metal-based catalysts, especially Cu due to its relatively high HER overpotential. Given that the electroreduction of FF and HMF inherently involves both electron and proton transfer, integrating electron-proton storage units, POMs, with catalytically active Cu centers provides a promising new strategy for catalyst design.

4.3.2 Electroreductive C−C Coupling of Furfural to Hydrofuroin

Electrochemically driven C–C coupling of biomass-derived platform molecules, such as FF and HMF, offers an attractive approach for sustainable biofuel production. The reduction of FF via H^+/e^- transfer generates a ketyl radical intermediate, which

can undergo self-coupling to form hydrofuroin (HDF) or be further reduced through an additional H^+/e^- transfer to yield FAL. Previous investigations show that Cu and Pb are effective catalysts for converting FF into HDF, but high HDF selectivity relies on strongly alkaline conditions. Nevertheless, obtaining C–C coupled products in high yields under mild reaction conditions is still challenging.

Recently, we reported a highly efficient electrocatalyst, $[Cu(pz)]_3[PW_{12}O_{40}]$ (Cu-PW_{12}, pz = pyrazine), with well-defined structure, in which the Cu-pz complex serves as the redox-active catalytic center, while the Keggin-type $\{PW_{12}O_{40}\}$ functions as an electron reservoir (Fig. 27(a)).[49] Under neutral and ambient conditions, FF was converted almost completely (>99%) with high selectivity toward HDF, a key precursor for jet fuel (91.2%). The catalytic activity of Cu-PW_{12} far surpasses that of the Cu-pz complex, $CsPW_{12}$ alone, or their physical mixture, highlighting a synergistic catalysis effect between Cu center and PW_{12} (Fig. 27(b)). Importantly, the catalyst demonstrates excellent cycling stability, maintaining both activity and selectivity over multiple cycles (Fig. 27(c)).

A combination of experimental and computational approaches was employed to elucidate the reaction pathway and underlying mechanism. Initially, the radical scavenger 4-amino-2,2,6,6-tetramethylpiperidine-1-oxyl (4-NH_3-TEMPO) was introduced into the reaction system, and the formation of the furyl-TEMPO adduct, confirmed by GC-MS, directly demonstrated the involvement of radical intermediates (Fig. 27(d)). Electron paramagnetic resonance (EPR) experiments further validated the presence of ketyl radicals. Kinetic isotope effect (KIE) studies were then conducted to exclude the participation of the Volmer step. Electrolysis using D_2O instead of H_2O revealed that water is the primary hydrogen source, although the phosphate electrolyte (NaH_2PO_4/Na_2HPO_4) can also provide partial protons.

The addition of thiocyanate ions (SCN^-), which coordinate to and poison the Cu center, caused a significant decrease in FF conversion and HDF yield, demonstrating that Cu serves as the main active site for FF reduction (Fig. 27(e)). To clarify the role of POMs, a crystalline Cu-pz catalyst was synthesized. For Cu-pz alone, the rate-determining step is the HER, whereas incorporation of POMs alters the rate-determining step to the reduction of FF. The role of POMs was further elucidated by comparing the electrochemical properties of Cu-PW_{12} and Cu-pz, including electrochemical impedance spectroscopy (EIS), electrochemically active surface area (ECSA), Tafel slope, and cyclic voltammetry (CV) (Fig. 27(f)). POMs act as electron mediators, enhancing electron-transfer efficiency to promote furfural conversion, while simultaneously modulating the Cu(I)/Cu(0) redox potential to favor HDF formation.

Based on the above experiments, Cu LMM Auger XPS spectrum and density functional theory (DFT) calculations, a plausible electroreduction mechanism is proposed (Fig. 27(g)). PW_{12} and the Cu center in Cu-PW_{12} are sequentially reduced. The adsorbed FF is then reduced by Cu^0 to generate a ketyl radical, while Cu^0 is oxidized to Cu^I. The ketyl radical quickly detaches from the electrode and undergoes self-coupling in solution to form HDF.

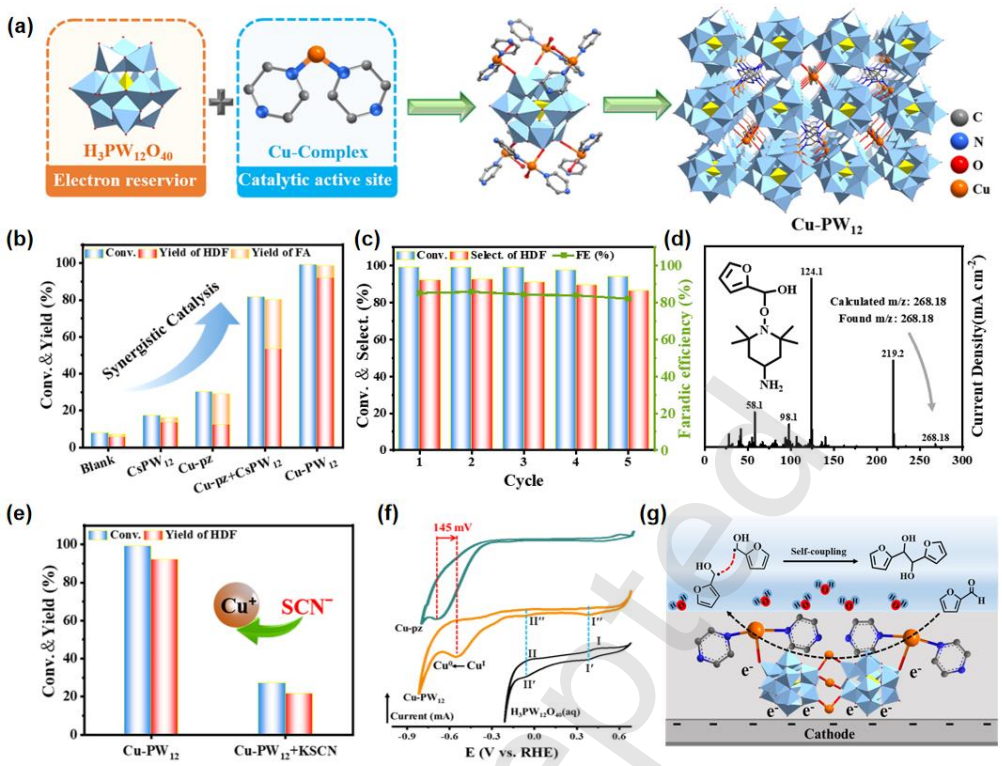

Fig. 27 (a) Fabrication of Cu-PW_{12}. (b) Electroreduction of FF over various catalysts. (c) Recycling test of FF electroreductive C–C coupling. (d) GC-MS spectrum of TEMPO. (e) FF reductive C–C coupling electrocatalytic activity with/without KSCN. (f) CV curves of PW_{12} solution (black), Cu-PW_{12} (orange) and Cu-pz (green). (g) Plausible mechanism of FF conversion to HDF. Adapted with permission from Ref. [49], Copyright American Chemical Society 2024.

4.3.3 Selective Electrocatalytic Hydrogenation of 5-Hydroxymethylfurfural

HMF can be reduced to a higher value product of BHMF by selective hydrogenation. This reaction proceeds via two hydrogenation steps. The initial step is through a hydrogen atom transfer (HAT) process involving surface-adsorbed H* species, leading to the formation of ketyl radical intermediates. However, when the catalyst surface cannot supply sufficient H^* species, the subsequent hydrogenation step is impeded. Instead, the coupling of ketyl radicals to form bis(hydroxymethyl)hydrofuroin (BHH) becomes the predominant reaction pathway. The key to mitigate the accumulation of ketyl radicals is to reduce the energy barrier for their hydrogenation.

Sun and co-workers achieved this by depositing PMo_{12} onto Cu nanowires, thereby constructing an efficient composite electrocatalyst (PMo_{12}/Cu) (Fig. 28(a)).[59] The catalyst exhibits excellent electrocatalytic activity for the hydrogenation of HMF to BHMF, achieving an HMF conversion of up to 93% and a BHMF selectivity of up to 97% under a high substrate concentration (1.0 M). To understand the role of PMo_{12} in the composite catalyst, Cu nanowires were prepared as a control catalyst. The introduction of PMo_{12} promotes the Volmer step, thereby accelerating the generation of surface-adsorbed H* species (Fig. 28(b)).

Mechanistic investigations combined with density functional theory calculations reveal that the PMo_{12}/Cu heterointerface functions as the active site for the electrocatalytic hydrogenation process (Fig. 28(c)). The enhanced electrocatalytic activity can be attributed to the stronger adsorption of water—the hydrogen source—on PMo_{12}/Cu compared with that on Cu nanowires. In addition, hydrogen bonding between the O atoms in the POM and the H atoms of water further stabilizes the adsorbed water molecules. Upon adsorption, water molecules dissociate, and the resulting H atoms preferentially bond with O atoms in the POM, forming Mo–O–H species. The formation of this Mo–O–H configuration effectively lowers the energy barrier for O–H bond dissociation, thereby

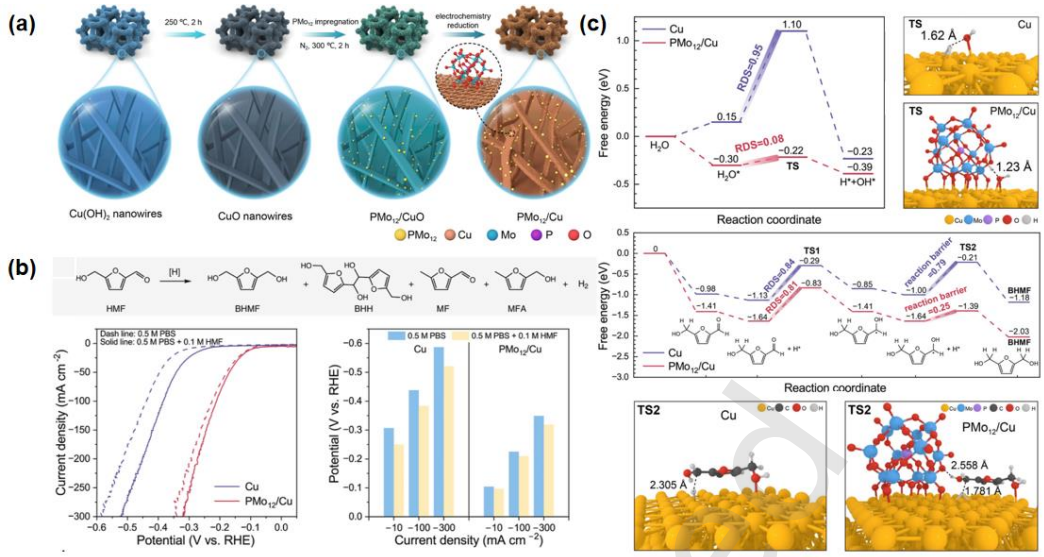

Fig. 28 (a) Synthesis process of PMo_{12}/Cu. (b) Linear sweep voltammetry (LSV) curves and applied potential vs. current density. (c) Theoretical calculation of the reaction. Adapted with permission from Ref. [59], Copyright 2024 American Chemical Society.

facilitating the Volmer step and promoting the generation of H^* species. For the hydrogenation of ketyl radicals, the ketyl radicals are adsorbed at the interface between PMo_{12} and Cu nanowires, where they are stabilized through hydrogen bonding with O atoms in the PMo_{12} lattice. Simultaneously, the proximity of H^* species to the Cu surface synergistically reduces the hydrogenation energy barrier.

Overall, due to the intrinsically weak reducing ability of POMs, additional active sites are generally required to facilitate the catalytic reduction of FF and HMF. To date, only one example using H_2 as the hydrogen source has been reported with Pd-$CsPW_{12}$/K-10, in which Pd activates H_2 to promote hydrogenation, while $CsPW_{12}$ facilitates the hydrogenolysis reaction through its Brønsted acidity. In the reductive conversion of HMF and FF, catalytic transfer hydrogenation with alcohols (mainly isopropanol) as the hydrogen donor has been most extensively investigated. In catalyst design, Lewis acidic centers are typically combined with Brønsted acidic POMs: the Lewis acid centers generate H^- or hydrogen radicals, while POMs promote subsequent reactions such as furan ring opening or esterification. Although the use of alcohols as hydrogen donors avoids the need for explosive H_2, these reactions generally require relatively high temperatures (90 ~ 170 °C), long reaction times, and suffer from relatively low atom economy. In contrast, electrocatalytic reduction with water as the hydrogen source offers several advantages, such as low cost, environmental benignity, and mild reaction conditions, and thus represents a highly promising strategy, although research in this area is still in its infancy. In terms of catalyst design, Cu typically serves as the catalytic active center, while POMs act as proton–electron sponges, playing a crucial role in facilitating electron transfer and activating water molecules.

In catalytic transfer hydrogenation, alcohols act as both the hydrogen source and the solvent, whereas in electrocatalytic reduction, water is typically used as the main solvent, with a small amount of organic solvent added to enhance substrate solubility. Current studies mainly focus on the reductive conversion of FF, while the reduction of HMF has been much less explored. This may be attributed to the fact that HMF contains both hydroxymethyl and aldehyde functional groups, which makes the reduction reactions more complex and difficult to control.

Etherification

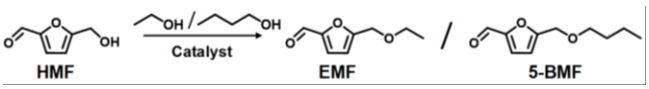

Scheme 11 The reaction process of HMF to EMF or 5-BMF.

Hydroxyl groups in HMF can react with alcohols to produce corresponding ethers, a process known as

etherification (Scheme 11). These ethers are considered promising biofuel candidates, including 5-ethoxymethylfurfural (EMF), 5-butoxymethylfurfural (5-BMF) and so on. POMs are frequently employed as catalysts for such etherification reactions[172] due to their strong acidity, environmental friendliness, and non-corrosive properties. Table 4 lists the currently reported POMs catalysts for the etherification of HMF and their catalytic performance. Among these catalysts, tungsten-based POMs are the most widely employed. The mechanism of the etherification reaction between HMF and ethanol, catalyzed by $[HPW_{12}O_{40}]^{2-}$ anion, was investigated by Yang *et al*. from a theoretical calculation perspective.[173] Their theoretical calculations revealed that the protons H^+ located on the[W−O_cH−W] and [W=O_dH] active sites play a crucial role in the etherification reaction of HMF with ethanol to form EMF.

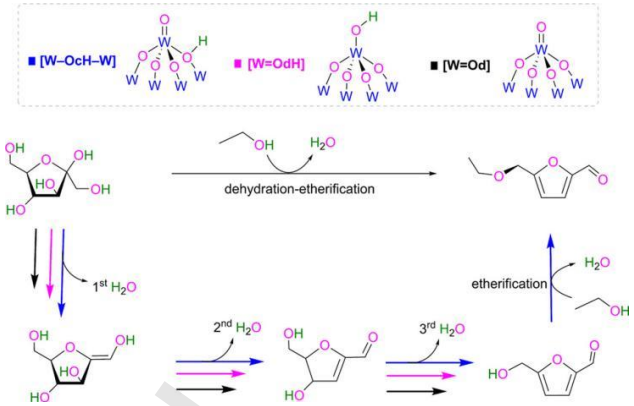

Fig. 29 Reaction routes for fructose conversion to EMF. Adapted with permission from Ref. [173], Copyright 2021 American Chemical Society.

Furfural acetals serve as feedstocks for various chemicals, including biofuel additives, fragrance ingredients, and solvents. The condensation reaction between FF and alcohols necessitates the involvement of acid catalysts, and POMs stand out as a promising option. Brusiquezi *et al.* fabricated Cs- and Co-doped Keggin-type POMs for this acetalization reaction, achieving remarkable catalytic performance.[174,175]

Table 4 Catalytic conversion of HMF to EMF/5-BMF by POM catalysts.

Catalysts	Product	Temp. (℃)	Time (h)	Conv. (%)	Yield (%)	TOF (h^{-1})	Ref.
$H_4SiW_{12}O_{40}$/MCM-41 nanospheresa[a]	EMF	90	4	92.0	77.4	20.87	[176]
Fe_3O_4@SiO_2-$H_3PW_{12}O_{40}$	EMF	100	11	97.9	83.6	1.15	[177]
30% wt.% K-10 clay-$H_3PW_{12}O_{40}$[b]	EMF	100	10	98.3	91.5	1.16	[178]
40 wt.% MCM-41-$H_3PW_{12}O_{40}$	EMF	100	24	96.1	83.4	5.00	[179]
$Ag_1H_2PW_{12}O_{40}$	EMF	100	10	94.4	88.7	5.21	[180]
$Cs_2H_2SiW_{12}O_{40}$	EMF	120	2.5	100	91	34.92	[181]
[Cu–BTC][$H_3PMo_{12}O_{40}$] (NENU-5)[c]	EMF	140	12	100	68.4	6.06	[182]
Pyridine-$H_3PW_{12}O_{40}$-1	EMF	80	24	97	90	1.84	[183]
30% TaTPA/SnO_2[d]	EMF	120	0.75	99.5	90.2	143.5	[184]
25 wt% $H_3PW_{12}O_{40}$/NbP[e]	EMF	120	1	95.2	89.0	128.2	[185]
$H_{14}[NaP_5W_{29}MoO_{110}]$ (12.5%)@SiO_2	5-BMF	100	1	89	73	1108	[186]
Fe_3O_4@SiO_2@KCC-1/Al_{10}/$H_3PW_{12}O_{40}$x[f]	EMF	120	1.5	99.5	93.1	99.3	[187]

[a]MCM-41 nanospheresa: Monodispersed mesoporous silica nanoparticles.[188]

[b]K-10 clay: a layered silicate mineral with a three-layer structural configuration.

[c][Cu–BTC][$H_3PMo_{12}O_{40}$] (NENU-5): a MOF-based compound (BTC = benzene-1,3,5-tricarboxylate).

[d]Modification of $H_3PW_{12}O_{40}$ via Ta ion exchange of protons and dispersion on SnO_2 support.

[e]NbP: mesoporous niobiumoxophosphate.

[f]Core-shell particles based on dendritic fibrous silica microspheres.

During the valorization of FF and HMF, especially in oxidation and etherification reactions, humins are generated as a byproduct. Humins are formed via complex interactions involving ether linkages, ester bonds, and other functional groups, and can be regarded as small molecular structural units based on various furan derivatives.[124] Prolonged reaction time, high temperatures, high substrate concentrations, and a large number of catalytically active sites all promote the formation of humins. Moreover, in recycling experiments, humins deposited on the catalyst surface block the access of FF and HMF to active sites, resulting in a slight decrease in controsubstrate conversion.[150] Therefore, appropriate l of reaction conditions is necessary to suppress side reactions.

6 Conclusions and outlooks

Recent progress in the POM-catalyzed valorization of lignin, FF and HMF, is summarized. POM catalysts possess significant intrinsic advantages: they feature designable structures and tunable compositions, exhibit dual properties of acidity, basicity and redox activity, and possess unique electron and proton storage and transfer capabilities. These characteristics enable POMs to adapt to various reaction systems such as thermal catalysis, photocatalysis, and electrocatalysis, providing a flexible catalytic solution for different types of biomass conversion reactions. Meanwhile, homogeneous and heterogeneous POM catalysts are compared in terms of stability, reusability and practical application. Homogeneous POMs show high activity but suffer from difficult recovery and metal leaching. Heterogeneous POM systems exhibit better stability and recyclability, although mass transfer and activity may be compromised. A rational balance between catalytic performance and durability is critical for biomass valorization.

For lignin depolymerization, the catalytic roles of different POM families, including polyoxomolybdates, polyoxotungstates, polyoxovanadates, and polyoxoniobates, are highlighted, with emphasis on cleavage pathways and catalytic mechanisms, particularly in systems studied using lignin model compounds. Current challenges in lignin depolymerization include the reliance on elevated temperatures and high oxygen pressures, as well as the fact that most mechanistic studies and evaluations of catalytic activity have been performed using lignin model compounds, leaving the activity toward complex natural lignin uncertain. In addition, some depolymerization processes, particularly for natural lignin, employ stoichiometric rather than truly catalytic amounts of homogeneous POMs, raising concerns about catalyst recovery and reusability. Most studies to date have focused on exploiting the intrinsic acidity, basicity, and oxidative properties of POMs under thermal conditions. Looking forward, the unique electron and proton storage and transfer capabilities of POMs could be harnessed in electrocatalytic or photocatalytic systems, enabling efficient bond cleavage under milder, greener conditions and improving carbon efficiency in lignin valorization.

For the oxidation of biomass-derived furan molecules, current studies have primarily focused on the oxidation of HMF, typically using molecular oxygen as the oxidant (from high to ambient pressures) under thermal conditions. Commonly employed POM catalysts include polyoxomolybdates, vanadium-substituted polyoxomolybdates, and polyoxovanadates. While satisfactory catalytic performance has been achieved for the selective oxidation of HMF, the range of reported oxidation products remains limited, mainly yielding DFF, whereas other valuable products such as HMFCA, FDCA, and FFCA have been less frequently reported. In the case of FF, oxidation predominantly produces maleic acid and maleic anhydride with relatively low yields, possibly due to overoxidation to CO_2. Although non-POM catalytic systems can produce additional oxidation products from FF, these transformations have not yet been demonstrated with POM catalysts. Furthermore, only a few studies have explored electrocatalytic or photocatalytic oxidation of HMF over POMs, and there is still considerable room for improvement in catalytic efficiency and

product selectivity under mild conditions.

For the reduction of biomass-derived furan molecules by POM catalysts, research has focused primarily on FF, with most studies relying on transfer hydrogenation using isopropanol as the hydrogen source. Direct hydrogenation using H_2 has been rarely reported, largely because POMs are generally incapable of activating molecular hydrogen. Electrocatalysis offers new opportunities for POM-catalyzed reduction of FF and HMF. Although electrocatalysis presents several advantages over thermocatalysis in the reduction of biomass-derived FF and HMF, research in electrocatalytic reduction—especially involving POM-based catalysts—remains at an early stage. Numerous challenges still need to be addressed. The first priority is to improve product selectivity and reaction efficiency while minimizing competing side reactions, such as HER, dimerization and over-reduction. Additionally, the rational design of catalytic active sites is critical for enhancing intrinsic activity. Beyond achieving high activity and stability, an effective catalyst should expose sufficient accessible sites to facilitate substrate adsorption. Moreover, due to the complexity of electrocatalytic reduction, elucidating the underlying reaction mechanisms continues to be challenging, particularly in tracking reactive intermediates. Advanced in situ and operando characterization methods play a key role in elucidating catalytic mechanisms. Finally, the product scope of electrocatalytic reduction remains relatively narrow compared to thermocatalysis. High-value products, such as furan, n-butanol, and n-butane, which are accessible via thermal routes, cannot yet be obtained through existing electrocatalytic methods. In this context, POMs owing to their unique electron–proton storage capability as well as their structurally designable and compositionally tunable nature, hold great promise for advancing the electrocatalytic reduction of biomass-derived molecules.

The core challenges for industrial application mainly include four aspects: i) how to achieve efficient recovery and reuse of homogeneous POMs to reduce the cost of industrial application; ii) developing high-efficiency POM-based catalysts suitable for natural biomass feedstocks to bridge the performance gap between model compounds and actual raw materials; iii) optimizing reaction processes to reduce the harshness of reaction conditions and realize mild, green, and large-scale production; iv) deepening the understanding of catalytic mechanisms through advanced characterization techniques to provide theoretical support for the rational design of catalysts. To promote the practical application of POM catalysis in biomass valorization, several concrete research directions are proposed. Future efforts should focus on the rational design of POM structures, in-depth mechanistic studies via operando characterization, and the development of stable and recyclable heterogeneous POM systems. The integration of POM catalysis with renewable energy inputs such as photocatalysis and electrocatalysis is highly promising for mild and green conversion. Further research should also address key bottlenecks including catalyst cost, scalability, and compatibility with industrial biorefineries, to advance sustainable biomass valorization. By systematically summarizing the catalytic roles of different POM families in reaction pathways, and structure-activity relationships across thermal, photocatalytic, and electrocatalytic systems, we hope this work provides a comprehensive reference for researchers in the field and inspires the rational design of next-generation POM-based catalysts for sustainable biomass valorization.

Acknowledgment

This work was financially supported by the National Natural Science Foundation of China (22571015 and 22271014).

References

[1] Zakzeski, J.; Bruijnincx, P. C. A.; Jongerius, A. L. and Weckhuysen, B. M. The Catalytic Valorization of Lignin for the Production of Renewable Chemicals. *Chem. Rev.* **2010**, *110*, 3552–3599.

[2] Li, H. R., A.; Saravanamurugan, S.; Pandey, A; Sangwan, R. S.; Yang, S. and Luque, R. Carbon-Increasing Catalytic Strategies for Upgrading Biomass into Energy-Intensive Fuels

and Chemicals. *ACS Catal.* **2018**, *8*, 148–187.

[3] Fan, Z.; Zhang, W.; Li, L.; Wang, Y.; Zou, Y.; Wang, S. and Chen, Z. Recent developments in electrode materials for the selective upgrade of biomass-derived platform molecules into high-value-added chemicals and fuels. *Green Chem.* **2022**, *24*, 7818–7868.

[4] Zakzeski, J.; Bruijnincx, P. C. A.; Jongerius, A. L. and Weckhuysen, B. M. The Catalytic Valorization of Lignin for the Production of Renewable Chemicals. *Chem. Rev.* **2010**, *110*, 3552–3599.

[5] Rinaldi, R.; Jastrzebski, R.; Clough, M. T.; Ralph, J.; Kennema, M.; Bruijnincx, P. C. A. and Weckhuysen, B. M. Paving the Way for Lignin Valorisation: Recent Advances in Bioengineering, Biorefining and Catalysis. *Angew. Chem. Int. Ed.* **2016**, *55*, 8164–8215.

[6] Wang, Y.; De, S. and Yan, N. Rational control of nano-scale metal-catalysts for biomass conversion. *Chem. Commun.* **2016**, *52*, 6210–6224.

[7] Zhang, C.; Shen, X.; Jin, Y.; Cheng, J.; Cai, C. and Wang, F. Catalytic Strategies and Mechanism Analysis Orbiting the Center of Critical Intermediates in Lignin Depolymerization. *Chem. Rev.* **2023**, *123*, 4510–4601.

[8] Kim, S.; Chmely, S. C.; Nimlos, M. R.; Bomble, Y. J.; Foust, T. D.; Paton, R. S. and Beckham, G. T. Computational Study of Bond Dissociation Enthalpies for a Large Range of Native and Modified Lignins. *J. Phys. Chem. Lett.* **2011**, *2*, 2846–2852.

[9] Hu, Y.; Yan, L.; Zhao, X.; Wang, C.; Li, S.; Zhang, X.; Ma, L. and Zhang, Q. Mild selective oxidative cleavage of lignin C–C bonds over a copper catalyst in water. *Green Chem.* **2021**, *23*, 7030–7040.

[10] Kleinert, M. and Barth, T. Towards a Lignincellulosic Biorefinery: Direct One-Step Conversion of Lignin to Hydrogen-Enriched Biofuel. *Energy Fuels* **2008**, *22*, 1371–1379.

[11] Kosa, M.; Ben, H.; Theliander, H. and Ragauskas, A. J. Pyrolysis oils from CO_2 precipitated Kraft lignin. *Green Chem.* **2011**, *13*, 3196–3202.

[12] Mukkamala, S.; Wheeler, M. C.; van Heiningen, A. R. P. and DeSisto, W. J. Formate-Assisted Fast Pyrolysis of Lignin. *Energy Fuels* **2012**, *26*, 1380–1384.

[13] Wang, S.; Ru, B.; Lin, H.; Sun, W. and Luo, Z. Pyrolysis behaviors of four lignin polymers isolated from the same pine wood. *Bioresour. Technol.* **2015**, *182*, 120–127.

[14] Wongsiriwan, U.; Noda, Y.; Song, C.; Prasassarakich, P. and Yeboah, Y. Lignocellulosic Biomass Conversion by Sequential Combination of Organic Acid and Base Treatments. *Energy Fuels* **2010**, *24*, 3232–3238.

[15] Yu, H.; Hu, J.; Fan, J. and Chang, J. One-Pot Conversion of Sugars and Lignin in Ionic Liquid and Recycling of Ionic Liquid. *Ind. Eng. Chem. Res.* **2012**, *51*, 3452–3457.

[16] Deepa, A. K. and Dhepe, P. L. Solid acid catalyzed depolymerization of lignin into value added aromatic monomers. *RSC Adv.* **2014**, *4*, 12625–12629.

[17] Deuss, P. J.; Scott, M.; Tran, F.; Westwood, N. J.; de Vries, J. G. and Barta, K. Aromatic Monomers by in Situ Conversion of Reactive Intermediates in the Acid-Catalyzed Depolymerization of Lignin. *J. Am. Chem. Soc.* **2015**, *137*, 7456–7467.

[18] Eom, H.-J.; Lee, D.-W.; Hong, Y.-K.; Chung, S.-H.; Seo, M.-g. and Lee, K.-Y. Effects of a sodium carbonate (Na_2CO_3) additive on the conversion of phenethyl phenyl ether (PPE) in high-temperature water. *Appl. Catal. A: Gen.* **2014**, *472*, 152–159.

[19] Chaudhary, R. and Dhepe, P. L. Solid base catalyzed depolymerization of lignin into low molecular weight products. *Green Chem.* **2017**, *19*, 778–788.

[20] Ding, Y.; Guo, T.; Li, Z.; Zhang, B.; Kühn, F. E.; Liu, C.; Zhang, J.; Xu, D.; Lei, M. and Zhang, T. Transition-metal-free synthesis of functionalized quinolines by direct conversion of β-O-4 model compounds. *Angew. Chem. Int. Ed.* **2022**, *134*, e202206284.

[21] Xu, W.; Miller, S. J.; Agrawal, P. K. and Jones, C. W. Depolymerization and Hydrodeoxygenation of Switchgrass Lignin with Formic Acid. *ChemSusChem* **2012**, *5*, 667–675.

[22] Wang, Y.-Y.; Ling, L.-L. and Jiang, H. Selective hydrogenation of lignin to produce chemical commodities by using a biochar supported Ni–Mo_2C catalyst obtained from biomass. *Green Chem.* **2016**, *18*, 4032–4041.

[23] McClelland, D. J.; Galebach, P. H.; Motagamwala, A. H.; Wittrig, A. M.; Karlen, S. D.; Buchanan, J. S.; Dumesic, J. A. and Huber, G. W. Supercritical methanol depolymerization and hydrodeoxygenation of lignin and biomass over reduced copper porous metal oxides. *Green Chem.* **2019**, *21*, 2988–3005.

[24] Wang, M.; Li, L. H.; Lu, J. M.; Li, H. J.; Zhang, X. C.; Liu, H. F.; Luo, N. C. and Wang, F. Acid promoted C–C bond oxidative cleavage of β-O-4 and β-1 lignin models to esters over a copper catalyst. *Green Chem.* **2017**, *19*, 702–706.

[25] Rafiee, M.; Alherech, M.; Karlen, S. D. and Stahl, S. S. Electrochemical Aminoxyl-Mediated Oxidation of Primary Alcohols in Lignin to Carboxylic Acids: Polymer Modification and Depolymerization. *J. Am. Chem. Soc.* **2019**, *141*, 15266–15276.

[26] Wu, X.; Xie, S.; Liu, C.; Zhou, C.; Lin, J.; Kang, J.; Zhang, Q.; Wang, Z. and Wang, Y. Ligand-Controlled Photocatalysis of CdS Quantum Dots for Lignin Valorization under Visible Light. *ACS Catal.* **2019**, *9*, 8443–8451.

[27] Gao, D.; Ouyang, D. and Zhao, X. Electro-oxidative depolymerization of lignin for production of value-added chemicals. *Green Chem.* **2022**, *24*, 8585–8605.

[28] Fang, Z.; Li, F.; Wang, M.; Li, F.; Wu, X.; Fan, K.; Tang, Q.; Sun, L. and Zhang, P. Selective electrocatalytic upgrading of lignin to aryl aldehydes and carboxylic acids over dodecyl sulfate-intercalated CoS nanocones. *Appl. Catal. B: Environ.* **2023**, *323*, 122149.

[29] Luo, Q.; Tian, S.; Qiang, Q.; song, F.; Su, W.; He, H.; An, Q. and Li, C. Copper-catalyzed C–C bond cleavage coupling with CN bond formation toward mild synthesis of lignin-based benzonitriles. *J. Environ. Sci.* **2025**, *151*, 505–515.

[30] Binder, J. B. and Raines, R. T. Simple Chemical Transformation of Lignocellulosic Biomass into Furans for Fuels and Chemicals. *J. Am. Chem. Soc.* **2009**, *131*, 1979–1985.

[31] Xing, R.; Qi, W. and Huber, G. W. Production of furfural and carboxylic acids from waste aqueous hemicellulose solutions from the pulp and paper and cellulosic ethanol industries. *Energy Environ. Sci.* **2011**, *4*, 2193–2205.

[32] Deng, W.; Zhang, Q. and Wang, Y. Polyoxometalates as efficient catalysts for transformations of cellulose into platform chemicals. *Dalton Trans.* **2012**, *41*, 9817–9831.

[33] Dutta, S.; De, S.; Alam, M. I.; Abu-Omar, M. M. and Saha, B. Direct conversion of cellulose and lignocellulosic biomass into chemicals and biofuel with metal chloride catalysts. *J. Catal.* **2012**, *288*, 8–15.

[34] Zhang, X.; Zhang, D.; Sun, Z.; Xue, L.; Wang, X. and Jiang, Z. Highly efficient preparation of HMF from cellulose using temperature-responsive heteropolyacid catalysts in cascade reaction. *Appl. Catal. B: Environ.* **2016**, *196*, 50–56.

[35] Yuan, B.; Guan, J.; Peng, J.; Zhu, G.-z. and Jiang, J.-h. Green hydrolysis of corncob cellulose into 5-hydroxymethylfurfural using hydrophobic imidazole ionic liquids with a recyclable, magnetic metalloporphyrin catalyst. *Chem. Eng. J.* **2017**, *330*, 109–119.

[36] Li, X.; Jia, P. and Wang, T. Furfural: A Promising Platform Compound for Sustainable Production of C4 and C5 Chemicals. *ACS Catal.* **2016**, *6*, 7621–7640.

[37] Chen, S.; Wojcieszak, R.; Dumeignil, F.; Marceau, E. and Royer, S. How Catalysts and Experimental Conditions Determine the Selective Hydroconversion of Furfural and 5-Hydroxymethylfurfural. *Chem. Rev.* **2018**, *118*, 11023–11117.

[38] Xu, C.; Paone, E.; Rodríguez-Padrón, D.; Luque, R. and Mauriello, F. Recent catalytic routes for the preparation and the upgrading of biomass derived furfural and 5-hydroxymethylfurfural. *Chem. Soc. Rev.* **2020**, *49*, 4273–4306.

[39] Li, S.; Dong, M.; Yang, J.; Cheng, X.; Shen, X.; Liu, S.; Wang, Z.-Q.; Gong, X.-Q.; Liu, H. and Han, B. Selective hydrogenation of 5-(hydroxymethyl)furfural to 5-methylfurfural over single atomic metals anchored on Nb_2O_5. *Nat. Commun.* **2021**, *12*, 584.

[40] Gao, Y.; Ge, L.; Xu, H.; Davey, K.; Zheng, Y. and Qiao, S.-Z. Electrocatalytic Refinery of Biomass-Based 5-Hydroxymethylfurfural to Fine Chemicals. *ACS Catal.* **2023**, *13*, 11204–11231.

[41] Gouzerh, P. and Proust, A. Main-Group Element, Organic, and Organometallic Derivatives of Polyoxometalates. *Chem. Rev.* **1998**, *98*, 77–112.

[42] Dolbecq, A.; Dumas, E.; Mayer, C. R. and Mialane, P. Hybrid Organic−Inorganic Polyoxometalate Compounds: From Structural Diversity to Applications. *Chem. Rev.* **2010**, *110*, 6009–6048.

[43] Hill, C. L. Introduction: PolyoxometalatessMulticomponent Molecular Vehicles To Probe Fundamental Issues and Practical Problems. *Chem. Rev.* *98*, 1–2.

[44] Santoni, M.-P.; Hanan, G. S. and Hasenknopf, B. Covalent multi-component systems of polyoxometalates and metal complexes: Toward multi-functional organic–inorganic hybrids in molecular and material sciences. *Coord. Chem. Rev.* **2014**, *281*, 64–85.

[45] Omwoma, S.; Gore, C. T.; Ji, Y.; Hu, C. and Song, Y.-F. Environmentally benign polyoxometalate materials. *Coord. Chem. Rev.* **2015**, *286*, 17–29.

[46] Dong, J.; Zhang, D.; Zhang, P.; Liu, C.; Li, J.; Bai, J.; Chi, Y. and Hu, C. Polyoxometalates for the decontamination of chemical warfare agents: From structure and composition

regulation to performance enhancement. *Coord. Chem. Rev.* **2024**, *517*, 215998.

[47] Xu, J.; Su, T.; Zhu, Z.; Chen, N.; Hao, D.; Wang, M.; Zhao, Y.; Ren, W. and Lü, H. Biomimetic oxygen activation and electron transfer for aerobic oxidative 5-hydroxymethylfurfural to 2,5-diformylfuran. *Chem. Eng. J.* **2020**, *396*, 125303.

[48] Zhang, S.-M.; Wang, Y.; Ma, Y.-Y.; Li, Z.-B.; Du, J. and Han, Z.-G. Three-Dimensional Silver-Containing Polyoxotungstate Frameworks for Photocatalytic Aerobic Oxidation of Benzyl Alcohol. *Inorg. Chem.* **2022**, *61*, 20596–20607.

[49] Geng, W.; Zhang, D.; Zhen, N.; Du, J.; Dong, J.; Liu, C.; Chen, S.-L.; Chi, Y. and Hu, C. Electroreductive C–C Coupling of Furfural to Jet Fuel Precursors in Neutral Media via Synergistic Catalysis of the Polyoxotungstate and Cu Complex. *ACS Catal.* **2024**, *14*, 10040–10052.

[50] Suzuki, K.; Mizuno, N. and Yamaguchi, K. Polyoxometalate Photocatalysis for Liquid-Phase Selective Organic Functional Group Transformations. *ACS Catal.* **2018**, *8*, 10809–10825.

[51] Li, N.; Liu, J.; Dong, B.-X. and Lan, Y.-Q. Polyoxometalate-Based Compounds for Photo- and Electrocatalytic Applications. *Angew. Chem. Int. Ed.* **2020**, *59*, 20779–20793.

[52] Chen, X.; Wu, H.; Shi, X. and Wu, L. Polyoxometalate-based frameworks for photocatalysis and photothermal catalysis. *Nanoscale* **2023**, *15*, 9242–9255.

[53] Yang, L.; Xu, M.; Wang, H.; Zhang, D. and Zhou, Z. Polyoxometalate-Based Frameworks: Construction Strategies and Photocatalytic Applications. *ChemCatChem* **2024**, *16*, e202400006.

[54] Zeb, Z.; Huang, Y.; Chen, L.; Zhou, W.; Liao, M.; Jiang, Y.; Li, H.; Wang, L.; Wang, L.; Wang, H.; Wei, T.; Zang, D.; Fan, Z. and Wei, Y. Comprehensive overview of polyoxometalates for electrocatalytic hydrogen evolution reaction. *Coord. Chem. Rev.* **2023**, *482*, 215058.

[55] Li, K.; Liu, T.; Ying, J.; Tian, A. and Wang, X. Recent research progress on polyoxometalate-based electrocatalysts in energy generation. *J. Mater. Chem. A* **2024**, *12*, 13576–13604.

[56] Ma, T.; Yan, R.; Wu, X.; Wang, M.; Yin, B.; Li, S.; Cheng, C. and Thomas, A. Polyoxometalate-Structured Materials: Molecular Fundamentals and Electrocatalytic Roles in Energy Conversion. *Adv. Mater.* **2024**, *36*, 2310283.

[57] Koley, P.; Shit, S. C.; Yoshida, T.; Ariga-Miwa, H.; Uruga, T.; Hosseinnejad, T.; Periasamy, S.; In, S.-I.; Mandaliya, D. D.; Gudi, R. D.; Iwasawa, Y. and Bhargava, S. K. Elucidation of Active Sites and Mechanistic Pathways of a Heteropolyacid/Cu-Metal-Organic Framework Catalyst for Selective Oxidation of 5-Hydroxymethylfurfural via Ex Situ X-ray Absorption Spectroscopy and In Situ Attenuated Total Reflection-Infrared Studies. *ACS Catal.* **2023**, *13*, 6076–6092.

[58] Zhang, H.; Yi, Z.; Fu, S.; Li, C.; Lucia, L. A. and Liu, Q. Pd nanocubes supported on SiW12 @Co-ZIF Nanosheets for High-efficiency rupture of ether bonds in model and actual lignin. *Appl. Catal. B: Environ.* **2023**, *322*, 122128.

[59] Cao, X.; Ding, Y.; Chen, D.; Ye, W.; Yang, W. and Sun, L. Cluster-Level Heterostructure of PMo_{12}/Cu for Efficient and Selective Electrocatalytic Hydrogenation of High-Concentration 5-Hydroxymethylfurfural. *J. Am. Chem. Soc.* **2024**, *146*, 25125–25136.

[60] Han, Y.-W.; Ye, L.; Gong, T.-J.; Lu, X.-B. and Fu, Y. Porous Composite-Mediated Bimetallic Cluster POMs/Zr-MOF for Catalytic Transfer Hydrogenation of Biomass-Derived Aldehydes and Ketones. *Adv. Funct. Mater.* **2024**, *34*, 2315044.

[61] Lan, J.; Lin, J.; Chen, Z. and Yin, G. Transformation of 5-Hydroxymethylfurfural (HMF) to Maleic Anhydride by Aerobic Oxidation with Heteropolyacid Catalysts. *ACS Catal.* **2015**, *5*, 2035–2041.

[62] Liu, D.; Chen, B.; Li, J.; Lin, Z.; Li, P.; Zhen, N.; Chi, Y. and Hu, C. Imidazole-Functionalized Polyoxometalate Catalysts for the Oxidation of 5-Hydroxymethylfurfural to 2,5-Diformylfuran Using Atmospheric O_2. *Inorg. Chem.* **2021**, *60*, 3909–3916.

[63] Li, Z.; Li, Y.; Chen, Y.; Wang, Q.; Jadoon, M.; Yi, X.; Duan, X. and Wang, X. Developing Dawson-Type Polyoxometalates Used as Highly Efficient Catalysts for Lignocellulose Transformation. *ACS Catal.* **2022**, *12*, 9213–9225.

[64] Wan, H.; Liu, Y.; Yu, C.; Cao, K.; Han, Y.; Sun, Z.; Shi, J. and Duan, X. Photo-promoted production of a new monophenolic compound from larch lignin with polyoxometalates supported on g-C_3N_4 under ambient conditions. *Green Chem.* **2025**, *27*, 5819–5831.

[65] Tian, H.-R.; Liu, Y.-W.; Zhang, Z.; Liu, S.-M.; Dang, T.-Y.; Li, X.-H.; Sun, X.-W.; Lu, Y. and Liu, S.-X. A multicentre synergistic polyoxometalate-based metal–organic framework for one-step selective oxidative cleavage of β-O-4

lignin model compounds. *Green Chem.* **2020**, *22*, 248–255.

[66] Gao, Z.; Yang, G.; Dong, J.; Liu, P.; Yu, F.; Li, Z.; Zhang, Y.; Zhang, M.; Huang, X. and Hu, C. Rational fabrication of three imidazole-functionalized ionic-type Pd-Polyoxovanadates for aerobic oxidation of 5-Hydroxymethulfurfural to 2,5-Diformylfuran. *J. Catal.* **2024**, *429*, 115261.

[67] Zhang, C.; Wang, M.; Zhao, C.; Wang, J.; Cao, Y.; Fan, L.; Liu, H. and Gao, G.-G. Enhanced selective oxidation of 5-Hydroxymethylfurfural with a recyclable V_{34}@Fe_3O_4/C catalyst Enriched with Mixed-valence polyoxovanadate active centers. *Fuel* **2025**, *397*, 135439.

[68] Li, J.; Li, Z.; Dong, J.; Fang, R.; Chi, Y. and Hu, C. Hexaniobate as a Recyclable Solid Base Catalyst to Activate C–H Bonds in Lignin Linkage Boosting the Production of Aromatic Monomers. *ACS Catal.* **2023**, *13*, 5272–5284.

[69] Li, J.; Shao, P.; Geng, W.; Lei, P.; Dong, J.; Chi, Y. and Hu, C. Highly efficient oxidative cleavage of lignin β-O-4 linkages via synergistic Co-CoO_x/N-doped carbon and recyclable hexaniobate catalysis. *Green Chem.* **2025**, *27*, 827–837.

[70] Li, J.; Shao, P.; Lei, P.; Zhang, D.; Liu, C.; Chen, S.; Chi, Y. and Hu, C. Polyoxoniobate as a Recyclable Proton Shuttle Enabling Efficient Lignin β-O-4 Linkage Cleavage: Experimental and Theoretical Insights. *ACS Catal.* **2026**, *16*, 2268–2279.

[71] Sun, Y.; Yang, K.; Zhu, Z.; Su, T.; Ren, W. and Lü, H. Deep eutectic solvents coupled with $(NH_4)_3H_6CoMo_6O_{24}$ trigger aerobic oxidation of 5-hydroxymethylfurfural to 5-formyl-2-furancarboxylic acid. *Chem. Commun.* **2022**, *58*, 8105–8108.

[72] Yang, D.; Xie, S.; Wu, D.; Ding, J.; Shi, E.; An, P.; Dai, S.; Guo, L. and Hou, Z. Efficient oxidative cleavage of β-O-4 linkage in lignin model compounds enabled by a simple Anderson-type polyoxometalate. *Green Chem.* **2025**, *27*, 14301–14316.

[73] Zhong, J.; Pérez-Ramírez, J. and Yan, N. Biomass valorisation over polyoxometalate-based catalysts. *Green Chem.* **2021**, *13*, 18–36.

[74] Yin, Q.; Wang, S.; Deng, H.; Shi, J.; Zhang, D. and Xu, W. The depolymerization of lignin over polyoxometalate catalysis: A review. *J. Environ. Chem. Eng.* **2024**, *12*, 114540.

[75] Zhang, H. and Fu, S. Polyoxometalate as an Effective Catalyst for Catalytic Lignin into Value-Added Molecules. *ChemCatChem* **2024**, *16*, e202301204.

[76] Deng, W.; Zhang, Q. and Wang, Y. Polyoxometalates as efficient catalysts for transformations of cellulose into platform chemicals. *Dalton Trans.* **2012**, *41*, 9817–9831.

[77] Yang, G.; Liu, Y. and Wei, Y. Application of polyoxometalates in biomass conversion. *Coord. Chem. Rev.* **2024**, *521*, 216272.

[78] Li, Z.; Liu, X.; Zhao, M.; Lv, H. and Yang, G.-Y. Recent advances in polyoxometalate-based catalysts for light-driven valorization of biomass derivatives. *Dalton Trans.* **2025**, *54*, 13851–13858.

[79] Yan, K.; Yu, Z.; Li, X.; Wang, Y.; Guo, M.; Xiong, J.; Zhang, R. and Lu, X. Polyoxometalates@Metal–Organic Frameworks: Synthesis Strategies, Nanostructure Modulation and Application in Biomass Conversion. *ChemSusChem* **2025**, *18*, e202401456

[80] Al-Hussaini, L.; Launay, F. and Galvez, E. Vanadium-Substituted Phosphomolybdic Acids for the Aerobic Cleavage of Lignin Models—Mechanistic Aspect and Extension to Lignin. *Materials* **2020**, *13*, 812–833.

[81] Al-Hussaini, L.; Valange, S.; Gálvez, M. E. and Launay, F. Alternative ball-milling synthesis of vanadium-substituted polyoxometalates as catalysts for the aerobic cleavage of C–C and C–O bonds. *Dalton Trans.* **2021**, *50*, 12850–12859.

[82] Díaz, J.; Pizzio, L. R.; Pecchi, G.; Campos, C. H.; Azócar, L.; Briones, R.; Romero, R.; Troncoso, E.; Méndez-Rivas, C.; Melín, V.; Murillo-Sierra, J. C. and Contreras, D. Catalytic Selective Oxidation of β-O-4 Bond in Phenethoxybenzene as a Lignin Model Using $(TBA)_5[PMo_{10}V_2O_{40}]$ Nanocatalyst: Optimization of Operational Conditions. *Molecules* **2023**, *28*, 6368–6381.

[83] Wang, Q.; Liu, Y.; Jiang, Y.; Chen, Y.; Li, Y.; Zhang, Y. and Wang, X. Full conversion of lignocellulose using polyoxometalate catalysts with redox sites and antagonistic acidity/basicity. *J. Colloid Interface Sci.* **2025**, *682*, 263–274.

[84] Xin, X.; Li, Z.; Chi, M.; Zhang, M.; Dong, Y.; Lv, H. and Yang, G.-Y. A recoverable polyoxometalate-ionic liquid catalyst for selective cleavage of lignin β-O-4 models under mild conditions. *Green Chem.* **2023**, *25*, 2815–2824.

[85] Du, X.; Tricker, A. W.; Yang, W.; Katahira, R.; Liu, W.; Kwok, T. T.; Gogoi, P. and Deng, Y. Oxidative Catalytic Fractionation and Depolymerization of Lignin in a One-Pot Single-Catalyst System. *ACS Sustainable Chem. Eng.* **2021**, *9*, 7719–7727.

[86] Zhang, J.; Zhu, X.; Xu, X.; Sun, Q.; Wei, L.; Li, K.; Zhai, S. and An, Q. Cooperative catalytic effects between aqueous

acidic ionic liquid solutions and polyoxometalate-ionic liquid in the oxidative depolymerization of alkali lignin. *J. Environ. Chem. Eng.* **2022**, *10*, 108260.

[87] Cao, K.; Yang, F.; Wan, H.; Duan, X.; Shi, J. and Sun, Z. A selective oxidative depolymerization of larch lignin to ethyl vanillate by multifunctional catalysts combining alkaline ionic liquid and polyoxometalates with hydrogen peroxide. *Int. J. Biol. Macromol.* **2025**, *295*, 139642.

[88] Zhang, Y.; Deng, H.; Li, M.; Zhao, L.; Xu, W. and Shi, J. Catalytic oxidative depolymerization of lignin to aromatic compounds using transition metal doped ionic Liquid-based polyoxometalate catalysts. *Sep. Purif. Technol.* **2025**, *359*, 130639.

[89] Cao, J.; Liu, Y.; Liu, H.; Liu, C.; Shi, J. and Li, N. Oxidative depolymerization of lignin enhanced by synergy of polyoxometalate and acetic acid. *Chin. J. Catal.* **2025**, *74*, 352–364.

[90] Zhang, Q.; Wang, S.; Jia, S.; Shi, J. and Xu, W. Solvent-mediated lignin depolymerization under oxidative conditions: Unveiling the role of solvents in the presence of polyoxometalates catalyst. *Mol. Catal.* **2025**, *574*, 114864.

[91] Gao, J. and Shi, J. Transition metal-substituted phosphomolybdic acid catalysts for selective oxidative depolymerization of lignin to aromatic monomers. *Int. J. Biol. Macromol.* **2025**, *317*, 144875.

[92] Zhang, A.; Ma, Y.; Mao, S.; Zhang, R.; Yuan, Y.; Wang, J.; Zhu, Y.; Wu, Z. and Sun, Y. Keggin-Type (Mo–V–P) Heteropolyacid-Catalyzed Selective Cleavage of β-O-4 Bond in Cotton Stalk Lignin for High Bio-Oil Yield. *ACS Sustainable Chem. Eng.* **2025**, *13*, 4623–4629.

[93] Guan, Y.; Wu, J.; Gao, Y.; Zheng, Y.; Zheng, J.; Xia, T.; Li, G.; Zhang, L.; Shi, Y.; Huo, M.; Yang, X. and Wang, X. Achieve full utilization of lignin, cellulose and hemicellulose from corn stover with amphiphilic polyoxometalate catalysts in a one-pot method. *Int. J. Biol. Macromol.* **2025**, *309*, 142892.

[94] Lee, H.-J. and Cho, E. S. Selective Photocatalytic C–C Bond Cleavage of Lignin Models and Conversion to High-Value Chemical by Polyoxometalate Under a Mild Water-Based Environment. *ACS Sustainable Chem. Eng.* **2023**, *11*, 7624–7632.

[95] Cui, M.; Liang, C.; Zhao, W.; Liu, X.; Dong, L.; Wang, D.; Fu, S.; Jiang, Z.; Wang, F. and Wei, X. Fabrication of Z-scheme $CdS/H_5PMo_{10}V_2O_{40}/g\text{-}C_3N_4$ for the photocatalytic depolymerization of lignin into aromatic monomers. *Fuel Process. Technol.* **2022**, *238*, 107481.

[96] Li, M.; Wang, T.; Zhao, M. and Wang, Y. Research on hydrogen production and degradation of corn straw by circular electrolysis with polyoxometalate (POM) catalyst. *Int. J. Hydrog. Energy* **2022**, *47*, 15357–15369.

[97] Li, M.; Wang, T.; Chen, X. and Ma, X. Conversion study from lignocellulosic biomass and electric energy to H_2 and chemicals. *Int. J. Hydrog. Energy* **2023**, *48*, 21004–21017.

[98] Xu, W.; Zhou, B.; Wang, Q.; Xu, G.; Li, N.; Liu, W. and Zhang, Z. C. Energy-efficient Electrochemical Hydrogen Production Combined with Biomass Oxidation Using Polyoxometalate and Metal Salts. *ChemCatChem* **2023**, *15*, e202300522

[99] Choi, Y.; Mehrotra, R.; Lee, S.-H.; Nguyen, T. V. T.; Lee, I.; Kim, J.; Yang, H.-Y.; Oh, H.; Kim, H.; Lee, J.-W.; Kim, Y. H.; Jang, S.-Y.; Jang, J.-W. and Ryu, J. Bias-free solar hydrogen production at 19.8 mA cm^{-2} using perovskite photocathode and lignocellulosic biomass. *Nat. Commun.* **2022**, *13*, 5709.

[100] Jiang, S.; Chu, Q.; Gao, J. and Shi, J. Study on the performance optimization and mechanism of Dawson-type P–W–V polyoxometalate catalyzed oxidative depolymerization of lignin to aromatic monomers. *Biomass Bioenergy* **2025**, *203*, 108337.

[101] Zhang, Y.; Jia, S.; Wang, X.; Deng, H.; Xu, W. and Shi, J. Bimetallic polyoxometalates catalysts for efficient lignin depolymerization: Unlocking valuable aromatic compounds from renewable feedstock. *Int. J. Biol. Macromol.* **2023**, *253*, 127363.

[102] Zhang, M.; Li, Z.; Feng, Y.; Xin, X.; Yang, G.-Y. and Lv, H. Highly selective hydrogenolysis of lignin β-O-4 models by a coupled polyoxometalate/CdS photocatalytic system. *Green Chem.* **2023**, *25*, 10091–10100.

[103] Shi, N.; Ding, Y.; Li, N.; Wen, F. and Liu, D. Polyoxometalates-modified and facets-engineered TiO_2 nanocomposites for selective photocatalytic cleavage of C–C bond of lignin models. *J. Environ. Chem. Eng.* **2023**, *11*, 110558.

[104] Shi, N.; Li, Y.; Li, N.; Wen, F. and Liu, D. Acidic-basic-redox trifunctional $Cu/P_2W_{17}V/\{001\}\text{-}TiO_2$ promotes photocatalytic lignin model conversion via tunable C-C/C-O cleavage. *Appl. Catal. A: Gen.* **2025**, *689*, 120030.

[105] Zhao, Q.; Zeng, Y.; Jiang, Z.; Huang, Z.; Long, D. L.; Cronin, L. and Xuan, W. High-Nuclearity

Polyoxometalate-Based Metal-Organic Frameworks for Photocatalytic Oxidative Cleavage of C−C Bond. *Angew. Chem. Int. Ed.* **2024**, *64*, e202421132.

[106] Flynn Jr, C. M. and Stucky, G. D. Heteropolyniobate complexes of manganese (IV) and nickel (IV). *Inorg. Chem.* **1969**, *8*, 332–334.

[107] Kinnan, M. K.; Creasy, W. R.; Fullmer, L. B.; Schreuder-Gibson, H. L. and Nyman, M. Nerve agent degradation with polyoxoniobates. *Eur. J. Inorg. Chem.* **2014**, *2014*, 2361–2367.

[108] Guo, W.; Lv, H.; Sullivan, K. P.; Gordon, W. O.; Balboa, A.; Wagner, G. W.; Musaev, D. G.; Bacsa, J. and Hill, C. L. Broad-Spectrum Liquid- and Gas-Phase Decontamination of Chemical Warfare Agents by One-Dimensional Heteropolyniobates. *Angew. Chem. Int. Ed.* **2016**, *55*, 7403–7407.

[109] Dong, J.; Hu, J.; Chi, Y.; Lin, Z.; Zou, B.; Yang, S.; Hill, C. L. and Hu, C. A Polyoxoniobate-Polyoxovanadate Double-Anion Catalyst for Simultaneous Oxidative and Hydrolytic Decontamination of Chemical Warfare Agent Simulants. *Angew. Chem. Int. Ed.* **2017**, *56*, 4473–4477.

[110] Hayashi, S.; Yamazoe, S.; Koyasu, K. and Tsukuda, T. Lewis Base Catalytic Properties of $[Nb_{10}O_{28}]^{6-}$ for CO_2 Fixation to Epoxide: Kinetic and Theoretical Studies. *Chem. – Asian J.* **2017**, *12*, 1635–1640.

[111] Dong, J.; Lv, H.; Sun, X.; Wang, Y.; Ni, Y.; Zou, B.; Zhang, N.; Yin, A.; Chi, Y. and Hu, C. A Versatile Self-Detoxifying Material Based on Immobilized Polyoxoniobate for Decontamination of Chemical Warfare Agent Simulants. *Chem. – Eur. J.* **2018**, *24*, 19208–19215.

[112] Li, X.; Dong, J.; Liu, H.; Sun, X.; Chi, Y. and Hu, C. Recoverable amphiphilic polyoxoniobates catalyzing oxidative and hydrolytic decontamination of chemical warfare agent simulants in emulsion. *J. Hazard. Mater.* **2018**, *344*, 994–999.

[113] Wu, Y.-L.; Li, X.-X.; Qi, Y.-J.; Yu, H.; Jin, L. and Zheng, S.-T. $\{Nb_{288}O_{768}(OH)_{48}(CO_3)_{12}\}$: A Macromolecular Polyoxometalate with Close to 300 Niobium Atoms. *Angew. Chem. Int. Ed.* **2018**, *57*, 8572–8576.

[114] Dong, J.; Sun, X.; Zhen, N.; Li, Z.; Liu, D.; Zou, B.; Dai, Q.; Chi, Y.; Chen, S.-L.; Poblet, J. M. and Hu, C. Oxidative detoxification of nerve agent VX simulant by polyoxoniobate: Experimental and theoretical insights. *J. Catal.* **2021**, *394*, 83–93.

[115] Zhu, G.; Shi, S.; Zhao, L.; Liu, M.; Gao, J. and Xu, J. Catalytic Activation of Carbon-Hydrogen Bonds in Lignin Linkages over Strong-Base-Modified Covalent Triazine Frameworks for Lignin Oxidative Cleavage. *ACS Catal.* **2020**, *10*, 7526–7534.

[116] Radhakrishnan, R.; Thiripuranthagan, S.; Devarajan, A.; Kumaravel, S.; Erusappan, E. and Kannan, K. Oxidative esterification of furfural by Au nanoparticles supported CMK-3 mesoporous catalysts. *Appl. Catal. A: Gen.* **2017**, *545*, 33–43.

[117] da Silva, M. J. and Rodrigues, A. A. Metal silicotungstate salts as catalysts in furfural oxidation reactions with hydrogen peroxide. *Mol. Catal.* **2020**, *493*, 111104.

[118] Desai, D. S. and Yadav, G. D. Solvent-free oxidative esterification of furfural to 2-methyl furoate using novel copper-exchanged tungstophosphoric acid supported on montmorillonite K-10 catalyst. *Mol. Catal.* **2022**, *524*, 112256.

[119] Guo, H. and Yin, G. Catalytic Aerobic Oxidation of Renewable Furfural with Phosphomolybdic Acid Catalyst: an Alternative Route to Maleic Acid. *J. Phys. Chem. C* **2011**, *115*, 17516–17522.

[120] Shi, S.; Guo, H. and Yin, G. Synthesis of maleic acid from renewable resources: Catalytic oxidation of furfural in liquid media with dioxygen. *Catal. Commun.* **2011**, *12*, 731–733.

[121] Lan, J.; Chen, Z.; Lin, J. and Yin, G. Catalytic aerobic oxidation of renewable furfural to maleic anhydride and furanone derivatives with their mechanistic studies. *Green Chem.* **2014**, *16*, 4351–4358.

[122] Lin, Y.; Ji, Y.; Zhang, Y.; An, H.; Zhao, Q.; Zhao, X. and Wang, Y. Highly selective oxidation of furfural to maleic acid with a Brønsted-Lewis dual-acid system. *J. Chem. Technol. Biotechnol.* **2025**, *100*, 1434–1443.

[123] Raabe, J.-C.; Esser, T.; Poller, M. J. and Albert, J. Synthesis and characterization of V substituted Anderson-type telluro-molybdates and tungstates for catalytic oxidation of furan derivatives to formic and maleic acid. *Catal. Today* **2024**, *441*, 114899.

[124] Esser, T.; Wassenberg, A.; Raabe, J.-C.; Voß, D. and Albert, J. Catalytic Valorization of Humins by Selective Oxidation Using Transition-Metal-Substituted Keggin-Type Polyoxometalate Catalysts. *ACS Sustainable Chem. Eng.* **2023**, *12*, 543–560.

[125] Rosatella, A. A.; Simeonov, S. P.; Frade, R. F. M. and Afonso, C. A. M. 5-Hydroxymethylfurfural (HMF) as a building block platform: Biological properties, synthesis and

synthetic applications. *Green Chem.* **2011**, *13*, 754–793.

[126] Lei, Q.; Li, J.; Cao, N.; Song, Z.; Liu, C.-L. and Dong, W.-S. Direct production of 2,5-diformylfuran from fructose catalysed by Mo-based composite oxides in static air. *Mol. Catal.* **2020**, *487*, 110892.

[127] Liu, B. and Zhang, Z. One-Pot Conversion of Carbohydrates into Furan Derivatives via Furfural and 5-Hydroxylmethylfurfural as Intermediates. *ChemSusChem* **2016**, *9*, 2015–2036.

[128] Pérez-Bustos, H. F.; Lucio-Ortiz, C. J.; de la Rosa, J. R.; de Haro del Río, D. A.; Sandoval-Rangel, L.; Martínez-Vargas, D. X.; Maldonado, C. S.; Rodriguez-González, V.; Garza-Navarro, M. A. and Morales-Leal, F. J. Synthesis and characterization of bimetallic catalysts Pd-Ru and Pt-Ru supported on γ-alumina and zeolite FAU for the catalytic transformation of HMF. *Fuel* **2019**, *239*, 191–201.

[129] Gong, M.; Mu, W.-X.; Cao, Y.-D.; Shao, Y.-W.; Hu, X.; Yin, D.; Liu, H.; Zhang, C.-H. and Gao, G.-G. A giant polyoxomolybdate molecular catalyst with unusual Mo^{6+}/Mo^{5+} synergistic mechanism for oxidation of hydroxyfurfural under atmospheric pressure. *Fuel Process. Technol.* **2023**, *242*, 107635.

[130] Ren, L.-K.; Yang, H.-Q. and Hu, C.-W. Theoretical study of the catalytic oxidation mechanism of 5-hydroxymethylfurfural to 2,5-diformylfuran by PMo-containing Keggin heteropolyacid. *Catal. Sci. Technol.* **2016**, *6*, 3776–3787.

[131] Liu, S.; Fu, X.; Dai, J.; Liu, Z.; Zhu, L. and Hu, C. One-Pot Synthesis of 2,5-Diformylfuran from Fructose by Bifunctional Polyaniline-Supported Heteropolyacid Hybrid Catalysts. *Catalysts* **2019**, *9*, 445.

[132] Cui, Y.; Zhang, Y.; Yu, F.; Fu, S.; Yao, Q.; Chen, Y.; Zhang, M.; Huang, X.; Shen, G. and Sun, D. In-situ self-assembly of two ultrastable bifunctional Keggin-type polyoxometalates-based zeolite-like frameworks for efficient cascade biomass chemicals conversion. *J. Catal.* **2024**, *429*, 115268.

[133] Yan, S.; Li, Y.; Li, P.; Jia, T.; Wang, S. and Wang, X. Fabrication of mesoporous POMs/SiO_2 nanofibers through electrospinning for oxidative conversion of biomass by H_2O_2 and oxygen. *RSC Adv.* **2018**, *8*, 3499–3511.

[134] Wu, J.; Yan, S.; Wang, C.; Lay, C.-H.; Wang, X.; Wang, X. and Huo, M. Fabrication of ordered mesoporous POMs/SiO_2–NH_2 nanofibers for production of DFF from 5-HMF for cellulose wastewater resource recovery. *Chemosphere* **2021**, *277*, 130316.

[135] Li, Y.; Li, Y.; Li, P.; Cao, P.; Wang, X. and Guan, H. POM@surf(n)/CeO_2 electrospun nanofibers for the facile oxidation of 5-HMF to DFF. *Appl. Catal. A: Gen.* **2019**, *583*, 117122.

[136] Li, Y.; Li, P.; Cao, P.; Li, Y.; Wang, X. and Wang, S. Fabrication of Trifunctional Polyoxometalate-Decorated Chitosan Nanofibers for Selective Production of 2,5-Diformylfuran. *ChemSusChem* **2019**, *12*, 3515–3523.

[137] Cao, P.; Li, Y.; Li, Y.; Zhang, X.; Wang, X. and Jiang, Z. Surfactant decorated hydrotalcite-supported polyoxometalates for aerobic oxidation of 5-hydroxymethylfurfural and monosaccharides. *Sustain. Energy Fuels* **2020**, *4*, 2236–2248.

[138] Gong, M.; Wang, X.-Y.; Li, M.-Q.; Mu, W.-X.; Cao, Y.-D.; Liu, H.; Lv, Y.-G.; Qi, X.-H. and Gao, G.-G. High-efficient and recoverable $Mo_{72}V_{30}$@Fe_3O_4/C catalyst for oxidation of hydroxyfurfural. *Fuel* **2023**, *332*, 126050.

[139] Cao, Y.-D.; Mu, W.-X.; Gong, M.; Fan, L.-L.; Han, J.; Liu, H.; Qi, B. and Gao, G.-G. Enhanced catalysis of a vanadium-substituted Keggin-type polyoxomolybdate supported on the M_3O_4/C (M = Fe or Co) surface enables efficient and recyclable oxidation of HMF to DFF. *Dalton Trans.* **2023**, *52*, 16303–16314.

[140] Wang, Q.; Li, Y.; Guan, H.; Yu, H. and Wang, X. Hydroxyapatite-Supported Polyoxometalates for the Highly Selective Aerobic Oxidation of 5-Hydroxymethylfurfural or Glucose to 2,5-Diformylfuran under Atmospheric Pressure. *ChemPlusChem* **2021**, *86*, 997–1005.

[141] Wang, Q.; Bu, W.; Li, Z.; Qi, Y. and Wang, X. PIC catalysis based on polyoxometalates promoting 5-HMF oxidation in H_2O/MIBK biphase. *Chin. Chem. Lett.* **2023**, *34*, 107548.

[142] Liu, R.; Chen, J.; Chen, L.; Guo, Y. and Zhong, J. One-Step Approach to 2,5-Diformylfuran from Fructose by Using a Bifunctional and Recyclable Acidic Polyoxometalate Catalyst. *ChemPlusChem* **2014**, *79*, 1448–1454.

[143] Rodikova, Y. and Zhizhina, E. Catalytic oxidation of 5-hydroxymethylfurfural into 2,5-diformylfuran using V-containing heteropoly acid catalysts. *React. Kinet. Mech. Catal.* **2020**, *130*, 403–415.

[144] Bai, J.; Dong, J.; Xiao, J.; Yang, T.; Wang, Y.; Chi, Y. and Hu, C. Catalytic Oxidative Valorization of Biobased 5-Hydroxymethylfurfural over Multi-ligand Functionalized

Polyoxovanadates. *Inorganic Chemistry* **2025**, *64*, 4630–4637.

[145] Zhou, H.; Dong, Y.; Xin, X.; Chi, M.; Song, T. and Lv, H. Electrocatalytic valorization of 5-hydroxymethylfurfural coupled with hydrogen production using tetraruthenium-containing polyoxometalate-based composites. *J. Mater. Chem. A* **2022**, *10*, 19963–19971.

[146] Xu, S.; Zhou, P.; Zhang, Z.; Yang, C.; Zhang, B.; Deng, K.; Bottle, S. and Zhu, H. Selective Oxidation of 5-Hydroxymethylfurfural to 2,5-Furandicarboxylic Acid Using O_2 and a Photocatalyst of Co-thioporphyrazine Bonded to g-C_3N_4. *J. Am. Chem. Soc.* **2017**, *139*, 14775–14782.

[147] Xu, J.; Zhu, Z.; Yuan, Z.; Su, T.; Zhao, Y.; Ren, W.; Zhang, Z. and Lü, H. Selective oxidation of 5-hydroxymethylfurfural to 5-formyl-2-furancar-boxylic acid over a Fe-Anderson type catalyst. *J. Taiwan Inst. Chem. Eng.* **2019**, *104*, 8–15.

[148] Gorbanev, Y. Y.; Klitgaard, S. K.; Woodley, J. M.; Christensen, C. H. and Riisager, A. Gold-Catalyzed Aerobic Oxidation of 5-Hydroxymethylfurfural in Water at Ambient Temperature. *ChemSusChem* **2009**, *2*, 672–675.

[149] Davis, S. E.; Houk, L. R.; Tamargo, E. C.; Datye, A. K. and Davis, R. J. Oxidation of 5-hydroxymethylfurfural over supported Pt, Pd and Au catalysts. *Catal. Today* **2011**, *160*, 55–60.

[150] Wang, F. and Zhang, Z. Cs-substituted tungstophosphate-supported ruthenium nanoparticles: An effective catalyst for the aerobic oxidation of 5-hydroxymethylfurfural into 5-hydroxymethyl-2-furancarboxylic acid. *J. Taiwan Inst. Chem. Eng.* **2017**, *70*, 1–6.

[151] Rabee, A. I. M.; Le, S. D.; Higashimine, K. and Nishimura, S. Aerobic Oxidation of 5-Hydroxymethylfurfural into 2,5-Furandicarboxylic Acid over Gold Stabilized on Zirconia-Based Supports. *ACS Sustain. Chem. Eng.* **2020**, *8*, 7150–7161.

[152] Chen, R.; Xin, J.; Yan, D.; Dong, H.; Lu, X. and Zhang, S. Highly Efficient Oxidation of 5-Hydroxymethylfurfural to 2,5-Furandicarboxylic Acid with Heteropoly Acids and Ionic Liquids. *ChemSusChem* **2019**, *12*, 2715–2724.

[153] Meng, F.; Zhao, Y.; Ma, Z.; Wang, Z.; Sun, P.; Zhang, X.; Wang, J. and Lyu, G. Construction of HPA-5 decorated lignin-assisted carbon defective engineering g-C_3N_4 for HMF selective conversion to maleic acid via photo-thermal and in situ self-Fenton processes. *Appl. Surf. Sci.* **2025**, *714*, 164412.

[154] Li, Z.; Zhang, M.; Xin, X. and Lv, H. Mechanistic Studies on the Photooxidation of 5-Hydroxymethylfurfural by Polyoxometalate Catalysts and Atmospheric Oxygen. *ChemCatChem* **2021**, *13*, 1389–1395.

[155] Gawade, A. B.; Tiwari, M. S. and Yadav, G. D. Biobased Green Process: Selective Hydrogenation of 5-Hydroxymethylfurfural to 2,5-Dimethyl Furan under Mild Conditions Using Pd-$Cs_{2.5}H_{0.5}PW_{12}O_{40}$/K-10 Clay. *ACS Sustain. Chem. Eng.* **2016**, *4*, 4113–4123.

[156] Han, Y. W.; Ye, L.; Gong, T. J.; Lu, X. B. and Fu, Y. Porous Composite-Mediated Bimetallic Cluster POMs/Zr-MOF for Catalytic Transfer Hydrogenation of Biomass-Derived Aldehydes and Ketones. *Adv. Funct. Mater.* **2024**, *34*, 2315044.

[157] Nandiwale, K. Y.; Vishwakarma, M.; Rathod, S.; Simakova, I. and Bokade, V. V. One-Pot Cascade Conversion of Renewable Furfural to Levulinic Acid over a Bifunctional $H_3PW_{12}O_{40}/SiO_2$ Catalyst in the Absence of External H_2. *Energy Fuels* **2020**, *35*, 539–545.

[158] Zhu, S.; Cen, Y.; Guo, J.; Chai, J.; Wang, J. and Fan, W. One-pot conversion of furfural to alkyl levulinate over bifunctional Au-$H_4SiW_{12}O_{40}/ZrO_2$ without external H_2. *Green Chem.* **2016**, *18*, 5667–5675.

[159] Peng, L.; Gao, X.; Liu, Y.; Zhang, J. and He, L. Coupled Transfer Hydrogenation and Alcoholysis of Furfural To Yield Alkyl Levulinate over Multifunctional Zirconia-Zeolite-Supported Heteropoly Acid. *Energy Fuels* **2021**, *35*, 4182–4190.

[160] Liu, Y.; Song, D.; Huang, Z.; Liu, X.; Yang, X. and Guo, Y. Dual-acidic Sn(IV)-based polyoxometalates for one-pot catalytic transfer hydrogenation−alcoholysis cascade reactions. *J. Colloid Interface Sci.* **2025**, *699*, 138247.

[161] Fábos, V.; Lui, M. Y.; Mui, Y. F.; Wong, Y. Y.; Mika, L. T.; Qi, L.; Cséfalvay, E.; Kovács, V.; Szűcs, T. and Horváth, I. T. Use of Gamma-Valerolactone as an Illuminating Liquid and Lighter Fluid. *ACS Sustain. Chem. Eng.* **2015**, *3*, 1899–1904.

[162] Winoto, H. P.; Fikri, Z. A.; Ha, J.-M.; Park, Y.-K.; Lee, H.; Suh, D. J. and Jae, J. Heteropolyacid supported on Zr-Beta zeolite as an active catalyst for one-pot transformation of furfural to γ-valerolactone. *Appl. Catal. B: Environ.* **2019**, *241*, 588–597.

[163] Srinivasa Rao, B.; Yogita; Dhana Lakshmi, D.; Kumari, P. K. and Lingaiah, N. Influence of metal oxide and heteropoly tungstate location in mesoporous silica towards catalytic transfer hydrogenation of furfural to γ-valerolactone. *Sustain.*

Energy Fuels **2021**, *5*, 3719–3728.

[164] Mutlu, B.; Unal, B. and Unlu, D. A novel and clean technique for the one-pot production of green chemical γ-valerolactone from furfural using bifunctional $H_3PW_{12}O_4$/UiO-66 catalyst: Pervaporation membrane reactor. *J. Environ. Chem. Eng.* **2024**, *12*, 112665.

[165] Ma, M.; Hou, P.; Zhang, P.; Guo, Q.; Yue, H.; Huang, J.; Tian, G. and Feng, S. Tandem catalysis of furfural to γ-valerolactone over polyoxometalate-based metal-organic frameworks: Exploring the role of confinement in the catalytic process. *Renew. Energy* **2024**, *227*, 120474.

[166] Liu, Z.; Zhu, X.; Cai, C.; Zheng, J.; Yan, B.; Ning, L.; Yang, D. and Xue, B. Hf-SBA-15 supported heteropolyacid: An efficient catalyst for one-pot production of γ-valerolactone from furfural. *Biomass Bioenergy* **2025**, *203*, 108295.

[167] Su, J.; Yang, X.; Shi, H.; Yao, S. and Zhou, M. Heteropolyacid promoted lignin-MOF derived spherical catalyst for catalytic hydrogen transfer of 5-hydroxymethylfurfural. *J. Colloid Interface Sci.* **2024**, *669*, 336–348.

[168] Moore, G. W. K.; Howell, S. E. L.; Brady, M.; Xu, X. and McNeil, K. Anomalous collapses of Nares Strait ice arches leads to enhanced export of Arctic sea ice. *Nat. Commun.* **2021**, *12*, 1.

[169] Akhade, S. A.; Singh, N.; Gutiérrez, O. Y.; Lopez-Ruiz, J.; Wang, H.; Holladay, J. D.; Liu, Y.; Karkamkar, A.; Weber, R. S.; Padmaperuma, A. B.; Lee, M.-S.; Whyatt, G. A.; Elliott, M.; Holladay, J. E.; Male, J. L.; Lercher, J. A.; Rousseau, R. and Glezakou, V.-A. Electrocatalytic Hydrogenation of Biomass-Derived Organics: A Review. *Chem. Rev.* **2020**, *120*, 11370–11419.

[170] Ali, T.; Wang, H.; Iqbal, W.; Bashir, T.; Shah, R. and Hu, Y. Electro-Synthesis of Organic Compounds with Heterogeneous Catalysis. *Adv. Sci.* **2023**, *10*, 2205077.

[171] Zhang, Y. and Shen, Y. Electrochemical hydrogenation of levulinic acid, furfural and 5-hydroxymethylfurfural. *Appl. Catal. B: Environ.* **2024**, *343*, 123576.

[172] Páez, A.; Rojas, H. A.; Portilla, O.; Sathicq, G.; Afonso, C. A. M.; Romanelli, G. P. and Martínez, J. J. Preyssler Heteropolyacids in the Self-Etherification of 5-Hydroxymethylfurfural to 5,5′-[Oxybis(methylene)]bis-2-furfural Under Mild Reaction Conditions. *ChemCatChem* **2017**, *9*, 3322–3329.

[173] Yang, H.; Qi, T.; Xiang, B.; Xie, H.; Liu, L.; Huang, Z.; Yang, H.-Q. and Hu, C. Theoretical Insights into the Cooperative Catalytic Mechanism of a PW-Containing Keggin Heteropolyacid Anion and Ethanol toward Conversion of Fructose into 5-Ethoxymethylfurfural in Ethanol Solution. *ACS Sustain. Chem. Eng.* **2021**, *9*, 14789–14799.

[174] da Silva, M. J.; Lopes, N. P. G. and Bruziquesi, C. G. O. Furfural acetalization over Keggin heteropolyacid salts at room temperature: effect of cesium doping. *React. Kinet. Mech. Catal.* **2021**, *133*, 913–931.

[175] da Silva, M. J.; de Andrade da Silva, P. H.; Ferreira, S. O.; da Silva, R. C. and Brusiquezi, C. G. O. How the Cobalt Position in the Keggin Anion Impacts the Activity of Tungstate Catalysts in the Furfural Acetalization with Alkyl Alcohols. *ChemistrySelect* **2022**, *7*, e202104174.

[176] Che, P.; Lu, F.; Zhang, J.; Huang, Y.; Nie, X.; Gao, J. and Xu, J. Catalytic selective etherification of hydroxyl groups in 5-hydroxymethylfurfural over $H_4SiW_{12}O_{40}$/MCM-41 nanospheres for liquid fuel production. *Bioresour. Technol.* **2012**, *119*, 433–436.

[177] Wang, S.; Zhang, Z.; Liu, B. and Li, J. Silica coated magnetic Fe3O4 nanoparticles supported phosphotungstic acid: a novel environmentally friendly catalyst for the synthesis of 5-ethoxymethylfurfural from 5-hydroxymethylfurfural and fructose. *Catal. Sci. Technol.* **2013**, *3*, 2104–2112.

[178] Liu, A.; Liu, B.; Wang, Y.; Ren, R. and Zhang, Z. Efficient one-pot synthesis of 5-ethoxymethylfurfural from fructose catalyzed by heteropolyacid supported on K-10 clay. *Fuel* **2014**, *117*, 68–73.

[179] Liu, A.; Zhang, Z.; Fang, Z.; Liu, B. and Huang, K. Synthesis of 5-ethoxymethylfurfural from 5-hydroxymethylfurfural and fructose in ethanol catalyzed by MCM-41 supported phosphotungstic acid. *J. Ind. Eng. Chem.* **2014**, *20*, 1977–1984.

[180] Ren, Y.; Liu, B.; Zhang, Z. and Lin, J. Silver-exchanged heteropolyacid catalyst (Ag_1H_2PW): An efficient heterogeneous catalyst for the synthesis of 5-ethoxymethylfurfural from 5-hydroxymethylfurfural and fructose. *J. Ind. Eng. Chem.* **2015**, *21*, 1127–1131.

[181] Raveendra, G.; Rajasekhar, A.; Srinivas, M.; Sai Prasad, P. S. and Lingaiah, N. Selective etherification of hydroxymethylfurfural to biofuel additives over Cs containing silicotungstic acid catalysts. *Appl. Catal. A: Gen.* **2016**, *520*, 105–113.

[182] Wang, Z. and Chen, Q. Conversion of

5-hydroxymethylfurfural into 5-ethoxymethylfurfural and ethyl levulinate catalyzed by MOF-based heteropolyacid materials. *Green Chem.* **2016**, *18*, 5884–5889.

[183] Wang, Z.; Li, H.; Fang, C.; Zhao, W.; Yang, T. and Yang, S. Simply Assembly of Acidic Nanospheres for Efficient Production of 5-Ethoxymethylfurfural from 5-Hydromethylfurfural and Fructose. *Energy Technol.* **2017**, *5*, 2046–2054.

[184] Kumari, P. K.; Rao, B. S.; Padmakar, D.; Pasha, N. and Lingaiah, N. Lewis acidity induced heteropoly tungustate catalysts for the synthesis of 5-ethoxymethyl furfural from fructose and 5-hydroxymethylfurfural. *Mol. Catal.* **2018**, *448*, 108–115.

[185] Kumari, P. K.; Rao, B. S.; Dhana Lakshmi, D.; Sai Paramesh, N. R.; Sumana, C. and Lingaiah, N. Tungstophosphoric acid supported on mesoporouus niobiumoxophosphate: an efficient solid acid catalyst for etherification of 5-hydroxymethylfurfural to 5-ethoxymethylfurfural. *Catal. Today* **2019**, *325*, 53–60.

[186] Portilla-Zuñiga, O. M.; Martínez, J. J.; Casella, M.; Lick, D. I.; Sathicq, Á. G.; Luque, R. and Romanelli, G. P. Etherification of 5-hydroxymethylfurfural using a heteropolyacid supported on a silica matrix. *Mol. Catal.* **2020**, *494*, 111125.

[187] Hafizi, H.; Walker, G. and Collins, M. N. Efficient production of 5-ethoxymethylfurfural from 5-hydroxymethylfurfural and carbohydrates over lewis/brønsted hybrid magnetic dendritic fibrous silica core-shell catalyst. *Renew. Energy* **2022**, *183*, 459–471.

[188] Lu, F.; Wu, S.-H.; Hung, Y. and Mou, C.-Y. Size Effect on Cell Uptake in Well-Suspended, Uniform Mesoporous Silica Nanoparticles. *Small* **2009**, *5*, 1408–1413.